Melanie Krüger

Alternatives to animal research:

from *in vitro* to *ex vivo* liver models

Alternatives to animal research:
from *in vitro* to *ex vivo* liver models

Melanie Krüger

2024

Melanie Krüger - **Alternatives to animal research: from *in vitro* to *ex vivo* liver models.**
PhD thesis, Faculty of Veterinary Medicine, Utrecht University, 2024

Coverdesign and layout: Bettina Zajonc and Melanie Krüger

Alternatives to animal research: from *in vitro* to *ex vivo* liver models

Alternatieven voor proefdieronderzoek: van *in vitro* naar *ex vivo* levermodellen

(met een samenvatting in het Nederlands)

Proefschrift

ter verkrijging van de graad van doctor aan de
Universiteit Utrecht
op gezag van de
rector magnificus, prof. dr. H.R.B.M. Kummeling,
ingevolge het besluit van het College voor Promoties
in het openbaar te verdedigen op

dinsdag 8 oktober 2024 des middags te 12.15 uur

door

Melanie Krüger

geboren op 29 mei 1985
te Hildesheim, Duitsland

Promotoren:
Prof. dr. H.S. Kooistra
Dr. B. Spee

Copromotor:
Dr. L. Kock

Beoordelingscommissie:
Prof. dr. A. de Bruin
Dr. ir. R. Levato
Prof. M. Rasponi
Prof. dr. J. Ritskes - Hoitinga
Prof. dr. D. Salvatori

1 CONTENTS

2 Introduction

Liver disease is the cause for 4% of deaths worldwide, with an estimated 2 million deaths annually[1,2]. The liver performs essential functions, such as detoxification, metabolism, and synthesis of proteins, and its dysfunction can be due to a range of disorders, including cirrhosis, hepatitis, and liver cancer. Chronic liver disease is a significant global health issue with a high prevalence and increasing burden. Apart from mortality, morbidity is also very high, leading to an even further increased clinical burden and quality of life is impaired tremendously by liver diseases. In addition, liver diseases lead to a major economic burden with, for example, higher health care expenditures by average $9,505 ± $2,028 per year for chronic liver diseases, which increases as the diseases progress[3]. There are four major causes of chronic liver disease: hepatitis C (CHC; globally 58 million infected according to WHO), hepatitis B (CHB; globally 296 million infected according to WHO), alcohol-related liver disease (ALD; estimated 50% of chronic liver disease related deaths) and nonalcoholic fatty liver disease (NAFLD; up to 38% of prevalence and most common cause of chronic liver disease)[3]. It should be noted that the new consensus nomenclature for the NAFLD is now metabolic dysfunction-associated steatotic liver disease (MASLD)[4],

but for consistency with published data NAFLD is further used in this thesis. The prevalence is distributed unequally across the world (see Figure 1), with CHC and CHB being most prevalent in the Middle East, Northern Africa, and Asia. NAFLD is most commonly found in the Middle East and Northern Africa as well, whereas ALD on the other hand is impacting all regions to a similar degree [1–3].
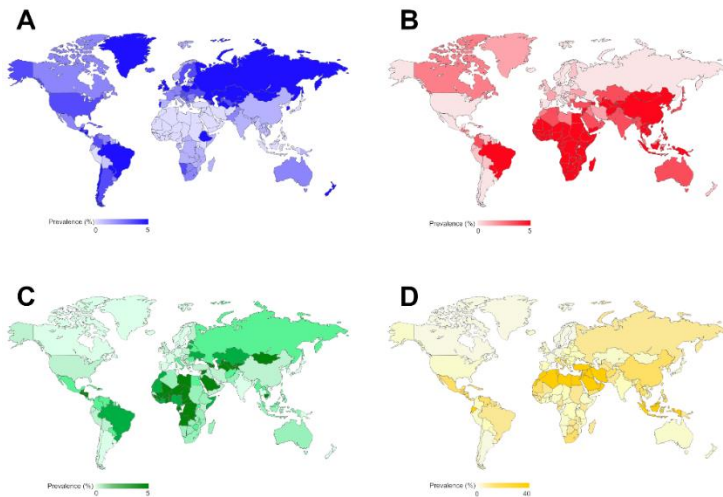
Figure 1: Adapted from Younossi et al., 2023[3] :(A)Prevalence of hepatitis C virus (global prevalence 5.5%), (B) prevalence of hepatitis B virus (global prevalence 2.0%), (C)prevalence of alcohol-related liver disease (global prevalence 1.8%), and (D)prevalence of nonalcoholic fatty liver disease (in adults age ≥ 20 years) (global prevalence 23.7%).

Depending on the region, prevalence for NFLD is increasing at different rates (total increase of 126% from 1990 to 2017[3], worldwide prevalence 32%[5], and ALD shows a total increase of 78% from 1990 to 2017[3]. Another common and challenging cause for acute liver failure (ALF) is drug-induced liver injury (DILI), which can result in the hospitalization of approximately 23% of those impacted by idiosyncratic DILI, contributing to around 11% of cases of ALF in developed countries. Notably, in advanced economies, cases of acetaminophen (paracetamol) overdose are a classic illustration of inherent and foreseeable DILI which account for half of all identifiable ALF instances[6].

2.1 Liver diseases; causes, diagnosis and treatment

Liver disease refers to any condition that affects and/or damages the liver. There are many types of liver disease which can be caused by toxic substances[6], inflammation[7], inherited conditions[8], autoimmune disease[9], cholestasis[10], obesity[11] and misuse of alcohol[12]. Liver disease can also occur in acute or chronic stages with the latter leading to scaring or cirrhosis when the damage is retained[13]. Signs and symptoms of liver disease include jaundice, hepatic encephalopathy, and coagulopathy. The

mechanisms behind the development of liver diseases include reactive oxygen species, for instance due to viral infections[14] or toxic metabolites of drugs[15], which in turn can lead to DNA damage. Other mechanisms include apoptosis, alteration of the gut microbiota, mitochondrial injury[11], immune-mediated injury[11,16], insulin resistance[17], gut microbial translocation, systemic inflammation, senescence, and nodular regenerative hyperplasia[16]. Diagnosis is usually through liver function tests such as elevated levels of liver specific enzymes in the blood.[18] Additional diagnostic methods include imaging studies such as ultrasound, computed tomography (CT), elastography and magnetic resonance imaging (MRI) to assess the liver's structure and identify abnormalities[17,19]. Liver biopsy is the golden standard for many diagnoses such as NAFLD[20]. Treatment is highly dependent on the type and stage of the disease. For viral hepatitis, if available, vaccines or antiviral medications may be prescribed to prevent or control the infection, respectively[21]. In cases of fatty liver disease, lifestyle changes like weight loss, exercise, and dietary modifications are essential[17]. There is no reliable pharmacological treatment for drug induced liver injury (DILI) yet, but steroids have been proven useful[6,22]. Unfortunately, for end-stage liver disease patients or

those with an acute loss of hepatic parenchyma, acute or fulminant hepatitis, liver transplantation is the only curative option. Liver transplantation is a complex and expensive procedure with potential challenges such as finding a suitable donor, risk of organ rejection, and the need for lifelong immunosuppressive medications to prevent rejection[23].

2.2 Liver during health and disease

The liver is the largest gland in the human body, accounting for 2-3% of average body weight and, in humans, can be divided into four anatomical lobes. Hepatic lobules are the smaller divisions of the liver lobes and are arranged in a portal area with a capillary network, where blood enters the lobule, a parenchymal area, and a central vein, where the blood exits the lobule[24]. Within the parenchymal area we find two major epithelial cells, hepatocytes and cholangiocytes. Hepatocytes are the main functional cells of the liver and play a crucial role in various metabolic functions. They are for example involved in the synthesis of proteins[25], carbohydrate and lipid metabolism, and detoxification[26]. Cholangiocytes form a diverse and constantly changing group of epithelial cells that make up a complex network of bile ducts called the biliary tree. Their primary role involves modifying

hepatic canalicular bile, also known as primary bile, as it travels along the biliary tree. This modification process is achieved by orchestrating the transport of different ions, solutes, and water across the apical and basolateral plasma membranes of cholangiocytes. It is influenced and regulated by a variety of factors, such as hormones, peptides, nucleotides, neurotransmitters, and bile acids, which act through intracellular signaling pathways and regulatory cascades. This coordinated activity allows cholangiocytes to finely tune the composition of bile as it progresses through the biliary tree[27]. Other cell types include hepatic stellate cells (that have a role in regeneration and fibrosis), Kupffer cells, and liver sinusoidal endothelial cells[28,29].

The polarization of these cells is vital for liver homeostasis, and disruptions in this process can have significant implications for liver function and health. Polarization involves the establishment of distinct cellular domains with specialized functions and distinct molecular compositions. Hepatocytes exhibit apicobasal polarization, characterized by the formation of apical and basolateral plasma membrane domains (see Figure 2). This polarization is essential for the vectorial transport of molecules such as bile acids and nutrients. Additionally, bile canaliculi, which are formed by adjacent hepatocytes,

represent another level of cellular polarization crucial for bile secretion[30]. Furthermore, non-parenchymal cells within the liver, such as Kupffer cells and hepatic stellate cells, also display polarization in response to various stimuli, contributing to immune responses and tissue remodeling[31].
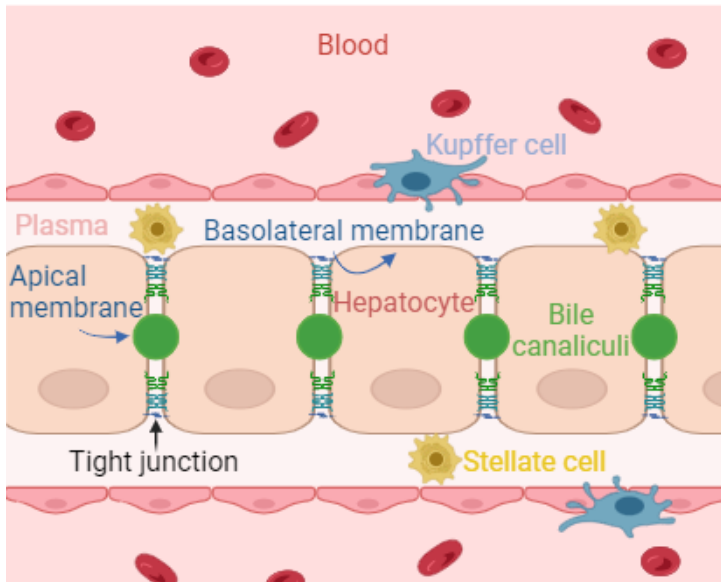
Figure 2: Adapted after Gissen et al.[30] Hepatocytes form bile canaliculi where their domains connect (apical membrane) and can have two basal domains that face the sinusoids with blood. Tight junctions strengthen the lumen of the bile canaliculi, Kupffer cells reside in the sinusoids, whereas stellate cells can be found in the Space of Disse in the plasma.

Not only the cell type and polarization determine the function of the cells within the liver, but also the spatial heterogeneity of metabolic and functional activities within

the hepatic lobule, referred to as liver zonation. This phenomenon arises from the differential distribution of oxygen, nutrients, and signaling molecules along the portal-central axis of the lobule[32]. Hepatocytes in distinct zones exhibit varying enzymatic profiles and specialized functions, with periportal hepatocytes primarily engaged in gluconeogenesis, beta-oxidation, ureagenesis, and protein synthesis, whereas pericentral hepatocytes specialize in processes like glycolysis, lipogenesis, and drug metabolism[32,33]. This zonal organization is crucial for the efficient regulation of hepatic functions and plays a pivotal role in maintaining metabolic homeostasis in response to physiological and pathological challenges as well as for regeneration (see Figure 3). Therefore, understanding liver zonation is vital for elucidating liver pathophysiology and developing targeted therapeutic interventions[32].
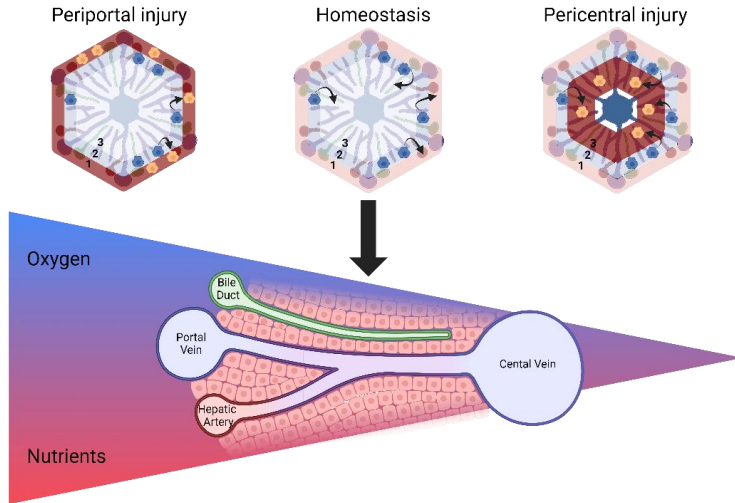
Figure 3: Adapted from Paris et al., 2022[32]: Hepatocyte zonation is evident in both the maintenance of normal liver function and during the process of regeneration. Innovative and separate lineage tracing models have revealed that all hepatocytes possess the capacity to proliferate. However, in the context of maintaining liver equilibrium, it is primarily the midzonal hepatocytes that play a central role in proliferation, whereas in response to injury, hepatocyte proliferation tends to be regional or diffuse in nature.

The liver has a large capacity to regenerate. Liver regeneration is a complex process controlled by multiple extracellular signals, which directly promote hepatocyte proliferation and delay or even prevent regeneration when absent[34]. Intracellular signaling pathways in hepatocytes are rapidly activated within minutes after partial hepatectomy, although the triggering mechanisms remain unclear[34]. All hepatic cell types participate in cell proliferation during liver regeneration, and no distinct

17

stem cells are involved. Notably, in cases of serious impairment of hepatocyte or cholangiocyte proliferation, these cell types can transdifferentiate into each other, acting as facultative stem cells[35]. In chronic liver diseases, compensatory proliferation of surviving hepatocytes occurs in response to the loss of hepatocytes, exposing them to potential genotoxic injury that could lead to neoplasia[34]. Overall, while the liver possesses a significant capacity for regeneration following injury, this regenerative capability is limited, particularly in instances where underlying inflammatory responses[36] or excessive scarring[37] are present. This limitation is a key reason why liver diseases are prevalent and can advance to end-stage liver disease, where transplantation remains the sole curative option.

2.3 Liver models

The development of reliable and predictive models to study liver disease is critical for understanding the underlying mechanisms and developing effective therapies. Various *in vitro* and *in vivo* models have been developed to study liver disease, including 2D and 3D cell models[38,39], decellularized liver scaffolds[38,40], normothermic perfused *ex vivo* liver models[41], and animal models[42].

2.3.1 Research animal models for liver disease

Animal models have played a significant role in the study of liver disease, providing crucial insights into the underlying mechanisms and potential treatments. However, their use has been a subject of ethical controversy due to concerns about animal welfare. Additionally, the extent to which findings from animal studies can be directly translated to human conditions has been a point of debate[43]. Various research animal models have been employed in liver disease research, ranging from small animals like mice and rats to larger ones like pigs and non-human primates.

Small animal models offer advantages in terms of ease of handling, lower costs, and shorter reproductive cycles, allowing for a more rapid assessment of potential interventions. Rodents have been extensively used due to the availability of genetically modified strains that can mimic certain human liver diseases. In Germany alone, a total of 31,675 mice and 1,156 rats were used in 2020 for research regarding the gastrointestinal system including the liver[44]. Examples for application are genetic mouse models that can aid in understanding hepatic lipid homeostasis and lipid-associated pathologies by targeting hepatic lipid mobilization[45] or in studying

cholestasis[10] and autoimmune hepatitis[46,47]. Other models are based on diets for example to study primary sclerosing cholangitis, NAFLD, or ALD, chemically inducing liver damage by repeatedly administering toxins, surgical manipulation (e.g., by ligation of the bile duct to induce secondary biliary fibrosis), infection of mice with parasites (to study schistosomiasis/Malaria for example), and many others[46]. However, the differences in physiology and metabolism between rodents and humans can limit the direct applicability of results to human disease. The comparison between human and rodent livers reveals interesting differences in their structure and blood supply. One anatomical difference for example is that larger livers consist of a greater number of lobules rather than having larger lobules. This distinction suggests that liver size in different species is determined more by the overall quantity of functional units (lobules) rather than their individual size[48]. This knowledge sheds light on the liver's adaptability and efficiency in scaling its functional capacity to suit the needs of the organism. Moreover, in larger livers, the blood supply is characterized by a higher proportion of arterial blood and a relatively reduced amount of portal blood. This unique vascular distribution indicates a variation in nutrient and oxygen delivery, potentially influencing metabolic

processes within the liver[48]. For NAFLD for example, no ideal mouse model exists that can mimic the most relevant metabolic changes observed in humans (i.e., obesity, insulin resistance/hyperglycemia and hyperlipidemia)[49]. In an extensive study involving over 2,000 drugs and utilizing rat, mouse, and rabbit models to investigate toxic responses, the results revealed that the positive predictive value did not surpass that of random chance[50,51]. These findings underscore the limitations of using research animal models to predict human outcomes. Specifically, they highlight that the absence of toxicity in these animal models cannot reliably forecast the absence of adverse events in humans. Conversely, the presence of toxicity in these models does not consistently correlate with toxicity in humans[50]. These discrepancies both hinder the clinical development of otherwise promising drugs and lead to high numbers of failed drug trials[51]. One of the reasons for these discrepancies can lie in cross-species differences in cytochrome P450 (CYP) enzyme and transport protein expression, which play a crucial role in toxicity prediction during drug development. These variations in expression levels and substrate specificities among different species can significantly impact drug metabolism, disposition, and ultimately, toxicity outcomes. For instance, CYP2B6 and CYP3A4

were highly expressed in primary human hepatocytes in an extensive study compared to different rat and mouse models[52].

Large research animal models, such as pigs and non-human primates, provide advantages in terms of their physiological similarities to humans, enabling researchers to study liver disease in a more contextually relevant setting. The liver of pigs, for instance, shares numerous similarities with human liver anatomy[53], and is therefore highly preferred in experimental medicine as a large research animal model for investigating acute liver disease and liver failure[54]. For example, porcine models are applied in studying regeneration after partial hepatectomy[55] due to its suitability for extracorporeal circulation, repetitive blood sampling, and training in surgical techniques applicable to humans[54]. Also, acetaminophen-induced liver failure[56,57] and non-alcoholic steatohepatitis (NASH)[58] were studied in pig models and due to their close physiology porcine livers and hepatocytes have even been used for xenotransplantations[59]. This is despite the fact that the histology of porcine livers is different to humans. Pig liver exhibits irregular, pentagonal hepatic lobules that are clearly defined by connective tissue septa. It is important to exercise caution when interpreting porcine liver

histology, as it can resemble fibrotic changes observed in the human liver, especially in males with a higher presence of connective tissue[54]. In contrast, human liver presents roughly hexagonal hepatic lobules without interlobular septa, and connective tissue is typically found within the interlobular space[60]. These distinct microscopic characteristics highlight the need for careful consideration of species-specific liver histology when conducting comparative studies but while these differences exist, they do not render the pig model irrelevant for fibrosis research purposes as quantitative assessment and sex of the animal can be taken into account during the histological analysis[54].

Non-human primates offer even closer genetic homology to humans, providing insights into complex diseases that are challenging to replicate in smaller research animals but are very contentious, highly regulated and raise major ethical concerns[61]. Furthermore, working with large research animal models, including pigs, also comes with technical complexities and higher financial costs, leading to smaller experimental cohorts. The significant interindividual variability within these cohorts makes it more challenging to statistically evaluate and interpret the research findings[54].

Therefore, alternative models have been developed to study liver disease, each with its advantages and limitations. These alternatives to research animal models have the potential to reduce the number of animals used in liver disease research, address ethical concerns, and reduce costs associated with animal research[62].

Additionally, the regulatory landscape, both in the US and Europe, has changed in order to encourage the move towards avoiding research animal models and allowing alternative models to be used for drug approval pathways instead. The FDA Modernization Act 2.0, signed into law by President Biden on December 29, 2022, brings about a significant change in clinical trials. Clinical trial leaders can now opt for alternatives to animal trials before conducting human trials, following the updated section 505 of the Federal Food, Drug, and Cosmetics Act[63]. These alternatives include cell-based assays and computer models, reducing the reliance on research animal models in drug development. Pharmaceutical companies can request exemptions from animal trials, and the FDA will assess if skipping these trials would impact drug safety and efficacy. The European Medicines Agency (EMA) is also committed to promoting ethical practices regarding animals in medicine testing. The agency supports the 3Rs principles (replace, reduce, and

refine) across the European Union (EU). These principles encourage the adoption of alternative methods to animal testing while maintaining scientific quality and improving animal welfare. Directive 2010/63/EU further emphasizes the integration of 3Rs principles and animal welfare standards throughout drug development and testing. Its ultimate goal is to replace animal research with non-animal methods, ensuring better protection for animals used in scientific research. To advance these goals, EMA's Innovation Task Force (ITF) is providing special support to developers in replacing, reducing, and refining the use of animals for drug development and testing. This includes promoting the implementation of New Approach Methodologies (NAMs) that adhere to EU legislation on animal protection in scientific research. By adopting these measures, drug development can become more ethical, innovative, and efficient, with reduced reliance on animal-based research[64].

2.3.2   Cell models for liver disease

2D and 3D cell models involve the culture of liver cells in a monolayer or in three-dimensional structures, respectively. 2D models are simple and cost-effective, but they do not accurately mimic the complex microenvironment of the liver, such as the extracellular

matrix (ECM) and cell-cell interactions[65] and static monolayers can lead to changes in morphology and gene expression[38]. In contrast, 3D models provide a more physiologically relevant environment, allowing for the study of liver disease pathogenesis and drug toxicity[66]. 3D liver models can be created using different techniques such as self-assembling methods, microfluidic systems, and 3D printing[39]. In recent years, biomaterials have emerged as suitable tools to enhance the physiological relevance of these models. The use of biomaterials in liver models has shown improvement in cell survival and function and enhancing liver disease modeling[67]. Biomaterials, such as hydrogels, micro- and nanofibers, and electrospun scaffolds, have been used to mimic the ECM in these models[67]. It is known that the use of biomimetic ECM hydrogels improve the survival and function of primary human liver cells in a 3D model compared to their 2D counterparts[66]. One promising hydrogel, nanofibrillar cellulose, has been developed as a degradable scaffold for three-dimensional tissue engineering (see **chapter 3**), and the cellulose nanofibril hydrogel has further been shown to promote hepatic differentiation of human liver organoids (see **chapter 4**).

2.3.3 *Ex vivo* models for liver disease

Several *ex vivo* models have been developed to study liver disease, including decellularized liver scaffolds and normothermic machine perfusion. Decellularized liver scaffolds are a promising model for studying liver disease. They involve the removal of the cellular components from a liver, leaving behind the ECM, which can then be repopulated with liver cells. This approach provides an environment that more closely resembles the native liver, allowing for the study of liver regeneration, disease progression, and drug screening[68]. Decellularized liver scaffolds have been used to generate functional liver tissue in vitro and in vivo, making them a promising tool for future liver tissue engineering[40]. This approach is specifically interesting for whole organ engineering, as not only the ECM can be preserved, but also the vascular network and biliary tree[69]. To engineer a fully functional and recellularized scaffold, suitable for applications like transplantation [70] or disease research, it is imperative to repopulate the scaffold with a combination of both parenchymal and nonparenchymal cell types. In the context of the liver, employing stem cells (e.g., embryonic stem cells (ESCs), induced pluripotent stem cells (iPSCs), or mesenchymal stem cells (MSCs)), which can differentiate into hepatic and biliary lineages, offers

distinct advantages over primary cells with limited viability[71]. Furthermore, the reseeding of nonparenchymal cells such as endothelial cells[70], cholangiocytes, Kupffer cells, and stellate cells is essential for achieving sustained and efficient functionality over the long term[71].

In this thesis we investigated the potential of using porcine intrahepatic cholangiocyte organoids for engraftment in decellularized liver scaffolds, aiming to provide insights into the use of decellularized liver scaffolds for tissue engineering purposes. The level of polarized engraftment achieved by these organoids is reported, which refers to the successful integration and positioning of the cholangiocyte organoids within the liver scaffolds. This approach holds promise for liver disease modeling as it allows for the observation of how cholangiocytes behave and function in a three-dimensional liver-like environment, thereby offering crucial insights into potential disease mechanisms and therapeutic strategies (see **chapter 5**).

Normothermic perfused *ex vivo* liver models involve the perfusion of a whole liver with a nutrient-rich solution at body temperature, mimicking the *in vivo* conditions of the liver. This model is capable of sustaining liver function for an extended duration, with functionality lasting up to three days[72]. While predominantly employed in transplantation

contexts and liver regeneration efforts[73], it also proves valuable in research, enabling investigations into liver disease mechanisms when configured as disease models[74] and facilitating drug research[75]. Furthermore, this model exhibits potential for studying reperfusion injury prevention, a critical concern in clinical transplantation[73,76,77]. Additionally, it has found application in diverse therapeutic interventions, encompassing defatting of steatotic livers, gene therapy, and immunomodulation[78]. However, it is expensive, technically very challenging, and further requires a constant supply of healthy livers from the chosen species, which usually entails the use of research animals[41,72,79,80]. In this thesis we developed an accessible slaughterhouse-based normothermic perfusion model and, as a proof-of`-concept, investigated its potential to function as a disease model for fatty liver disease and acetaminophen toxicity (see **chapter 6**).

2.4 Summary and outline of the thesis

In summary, the burden of liver disease is significant, and the development of reliable and predictive liver disease models is crucial for understanding the underlying mechanisms and developing effective therapies. Various *in vitro*, *in vivo* and *ex vivo* models have been developed,

each with their advantages and limitations. Biomaterials have emerged as a promising approach to enhance the physiological relevance of 3D cell-based models, providing a more accurate representation of the native liver microenvironment and approaches such as decellularized liver scaffolds and whole perfused livers can complete the picture. Future research in this area holds promise in improving our understanding of liver disease and developing effective therapies to address this global health issue.

The research presented in this thesis focuses on modeling various aspects of liver function by using promising cell sources, bioreactors and biomaterials. These technologies combined have vastly improved liver characteristics which can impact the field of hepatology by providing the most relevant and tailored models which can be used for a multitude of research purposes to better understand diseases and develop treatments. In **part I** we will show novel *in vitro* approaches using hydrogels, organoids and bioreactors. In **part II** we tested two *ex vivo* models, one using decellularized liver tissue and one whole organ perfusion system. In **chapter 3**, the focus is primarily on biomaterials introducing a novel hydrogel which can be used in conjunction with microfluidic devices. This plant-based hydrogel called nanocellulose

is then applied to a primary cell source in **chapter 4** which, when combined with organoids, could be a viable alternative to the animal-derived hydrogels such as Matrigel. The same primary cell source but from pigs instead of humans is grafted onto a decellularized liver scaffold in **chapter 5**, which presents an even more relevant environment that could pave the way to whole organ engineering. In **chapter 6** we have developed a simple normothermic *ex vivo* liver platform using porcine slaughterhouse livers for disease modeling. This platform has the potential to reduce the number of animals used in research, as it uses livers that would otherwise be discarded, and it showed the further potential to study fat and drug metabolism in the model. The overall aim of this thesis is to provide further insight into several alternative approaches and advance the research in the field to reach the goal of providing ethically and physiologically sound models to study liver disease (see Figure 4 below).

In **part I**, *in vitro* approaches, we identified several (sub)aims:

1. Determine if plant-based hydrogels in flow culture devices can be used for tissue engineering.
2. Provide insight into the use of plant-based hydrogels as alternatives for animal-derived hydrogels for hepatic organoid culture.
3. Determine the proliferation and differentiation capacity of liver derived organoids in plant-based hydrogels.

In **part II**, *ex vivo* models, we also identified several (sub)aims:

4. Provide insight into the use of decellularized pig livers for tissue engineering purposes.
5. Determine the efficacy of recellularization in same species decellularized liver with liver derived organoids.
6. Create a normothermic perfusion system that sustains liver function in livers from slaughterhouse pigs and can function as a disease model.
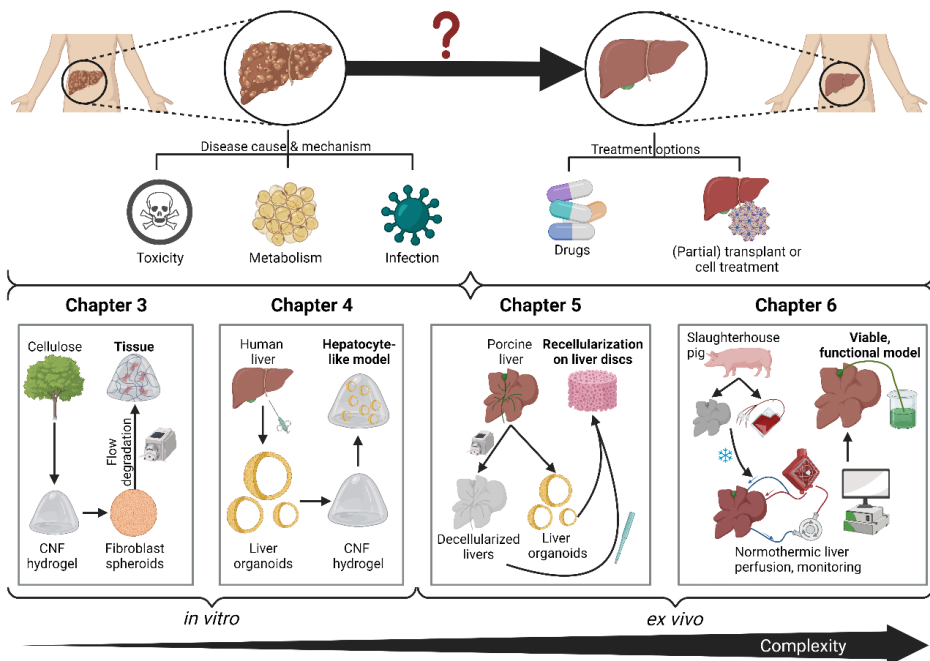
Figure 4: The schematic Figure illustrates the different aspects of liver modeling presented in this thesis. Chapter 3 focuses on the hydrogel called nanocellulose for use with microfluidic devices. Chapter 4 combines nanocellulose with organoids as a potential animal-free alternative to Matrigel. Chapter 5 grafts the same primary cell source but from pigs onto a decellularized liver scaffold. In Chapter 6, a simple normothermic ex vivo liver platform using porcine slaughterhouse livers is developed for disease modeling. This comprehensive research aims to provide ethically and physiologically sound liver disease models, advancing the field of hepatology and supporting various research purposes for better disease understanding and treatment development.

2.5 References

1. Asrani SK, Devarbhavi H, Eaton J, Kamath PS. Burden of liver diseases in the world. J Hepatol. 2019;70(1):151-171. doi:10.1016/j.jhep.2018.09.014

2. Devarbhavi H, Asrani SK, Arab JP, Nartey YA, Pose E, Kamath PS. Global burden of liver disease: 2023 update. J Hepatol. Published online August 2023. doi:10.1016/j.jhep.2023.03.017

3. Younossi ZM, Wong G, Anstee QM, Henry L. The Global Burden of Liver Disease. Clinical Gastroenterology and Hepatology. 2023;21(8):1978-1991. doi:10.1016/j.cgh.2023.04.015

4. Rinella ME, Lazarus J V., Ratziu V, et al. A multisociety Delphi consensus statement on new fatty liver disease nomenclature. Hepatology. 2023;78(6):1966-1986. doi:10.1097/HEP.0000000000000520

5. Riazi K, Azhari H, Charette JH, et al. The prevalence and incidence of NAFLD worldwide: a systematic review and meta-analysis. Lancet Gastroenterol Hepatol. 2022;7(9):851-861. doi:10.1016/S2468-1253(22)00165-0

6. Fernandez-Checa JC, Bagnaninchi P, Ye H, et al. Advanced preclinical models for evaluation of drug-induced liver injury – consensus statement by the European Drug-Induced Liver Injury Network [PRO-EURO-DILI-NET]. J Hepatol. 2021;75(4):935-959. doi:10.1016/j.jhep.2021.06.021

7. Moreau R, Tonon M, Krag A, et al. EASL Clinical Practice Guidelines on acute-on-chronic liver failure. J Hepatol. Published online August 2023.

doi:10.1016/j.jhep.2023.04.021

8. Karlsen TH, Lammert F, Thompson RJ. Review Genetics of liver disease : From pathophysiology to clinical practice. J Hepatol. 2015;62(1):S6-S14. doi:10.1016/j.jhep.2015.02.025

9. Ricciuto A, Kamath BM, Hirschfield GM, Trivedi PJ. Primary sclerosing cholangitis and overlap features of autoimmune hepatitis: A coming of age or an age-ist problem? J Hepatol. Published online August 1, 2023. doi:10.1016/j.jhep.2023.02.030

10. Mariotti V, Cadamuro M, Spirli C, Fiorotto R, Strazzabosco M, Fabris L. Animal models of cholestasis: An update on inflammatory cholangiopathies. Biochim Biophys Acta Mol Basis Dis. 2019;1865(5):954-964. doi:10.1016/j.bbadis.2018.07.025

11. Vetrano E, Rinaldi L, Mormone A, et al. Non-alcoholic Fatty Liver Disease (NAFLD), Type 2 Diabetes, and Non-viral Hepatocarcinoma: Pathophysiological Mechanisms and New Therapeutic Strategies. Biomedicines. 2023;11(2). doi:10.3390/biomedicines11020468

12. Mitra S, De A, Chowdhury A. Epidemiology of non-alcoholic and alcoholic fatty liver diseases. Transl Gastroenterol Hepatol. 2020;5. doi:10.21037/TGH.2019.09.08

13. Moon AM, Singal AG, Tapper EB. Contemporary Epidemiology of Chronic Liver Disease and Cirrhosis. Clinical Gastroenterology and Hepatology. 2020;18(12):2650-2666. doi:10.1016/j.cgh.2019.07.060

14. Talwani R, Gilliam BL, Howell C. Infectious Diseases and the Liver. Clinical Liver Diseases. 2011;15(1):111-130.

doi:10.1016/j.cld.2010.09.002

15. Bhakuni GS, Bedi O, Bariwal J, Deshmukh R, Kumar P. Animal models of hepatotoxicity. Inflammation Research. 2016;65(1):13-24. doi:10.1007/s00011-015-0883-0

16. Kaspar MB, Sterling RK. Mechanisms of liver disease in patients infected with HIV. BMJ Open Gastroenterol. 2017;4(1). doi:10.1136/bmjgast-2017-000166

17. Adams LA, Angulo P. Treatment of non-alcoholic fatty liver disease. Postgrad Med J. 2006;82(967):315-322. doi:10.1136/pgmj.2005.042200

18. Agrawal S, Dhiman RK, Limdi JK. Evaluation of abnormal liver function tests. Postgrad Med J. 2016;92(1086):223-234. doi:10.1136/postgradmedj-2015-133715

19. Decharatanachart P, Chaiteerakij R, Tiyarattanachai T, Treeprasertsuk S. Application of artificial intelligence in chronic liver diseases: a systematic review and meta-analysis. BMC Gastroenterol. 2021;21(1). doi:10.1186/s12876-020-01585-5

20. Rockey DC, Caldwell SH, Goodman ZD, Nelson RC, Smith AD. Liver biopsy. Hepatology. 2009;49(3):1017-1044. doi:10.1002/hep.22742

21. Castaneda D, Gonzalez AJ, Alomari M, Tandon K, Zervos XB. From hepatitis A to E: A critical review of viral hepatitis. World J Gastroenterol. 2021;27(16):1691-1715. doi:10.3748/wjg.v27.i16.1691

22. Andrade RJ, Chalasani N, Björnsson ES, et al. Drug-induced liver injury. Nat Rev Dis Primers.

2019;5(1). doi:10.1038/s41572-019-0105-0

23. Terrault NA, Francoz C, Berenguer M, Charlton M, Heimbach J. Liver Transplantation 2023: Status Report, Current and Future Challenges. Clinical Gastroenterology and Hepatology. 2023;21(8):2150-2166. doi:10.1016/j.cgh.2023.04.005

24. Abdel-Misih SRZ, Bloomston M. Liver Anatomy. Surgical Clinics of North America. 2010;90(4):643-653. doi:10.1016/j.suc.2010.04.017

25. Zhou Z, Xu MJ, Gao B. Hepatocytes: a key cell type for innate immunity. Published online 2016. doi:10.1038/cmi.2015.97;published

26. Huang P, Chen Q. Generation of hepatocytes by transdifferentiation. In: Stem Cells and Cancer in Hepatology: From the Essentials to Application. Elsevier; 2018:103-114. doi:10.1016/B978-0-12-812301-0.00006-2

27. Tabibian JH, Masyuk AI, Masyuk T V, Hara SPO, Larusso NF. Physiology of Cholangiocytes. Compr Physiol. 2013;3(1):1-49. doi:10.1002/cphy.c120019.Physiology

28. Damania A, Jain E, Kumar A. Advancements in in vitro hepatic models: Application for drug screening and therapeutics. Hepatol Int. 2014;8(1):23-38. doi:10.1007/s12072-013-9490-8

29. Yu W, Wang S, Wang Y, et al. MicroRNA: role in macrophage polarization and the pathogenesis of the liver fibrosis. Front Immunol. 2023;14. doi:10.3389/fimmu.2023.1147710

30. Gissen P, Arias IM. Structural and functional hepatocyte polarity and liver disease. J Hepatol. 2015;63(4):1023-1037.

doi:10.1016/j.jhep.2015.06.015

31. Chen J, Deng X, Liu Y, et al. Kupffer cells in non-alcoholic fatty liver disease: Friend or foe? Int J Biol Sci. 2020;16(13):2367-2378. doi:10.7150/ijbs.47143

32. Paris J, Henderson NC. Liver zonation, revisited. Hepatology. 2022;76(4):1219-1230. doi:10.1002/hep.32408

33. Jungermann K, Keitzmann T. Zonation of Parenchymal and Nonparenchymal Metabolism in Liver. Annu Rev Nutr. 1996;16(1):179-203. doi:10.1146/annurev.nu.16.070196.001143

34. Michalopoulos GK, Bhushan B. Liver regeneration: biological and pathological mechanisms and implications. Nat Rev Gastroenterol Hepatol. 2021;18(1):40-55. doi:10.1038/s41575-020-0342-4

35. Campana L, Esser H, Huch M, Forbes S. Liver regeneration and inflammation: from fundamental science to clinical applications. Nat Rev Mol Cell Biol. 2021;22(9):608-624. doi:10.1038/s41580-021-00373-7

36. Starlinger P, Brunnthaler L, McCabe C, et al. Transcriptomic landscapes of effective and failed liver regeneration in humans. JHEP Reports. 2023;5(4). doi:10.1016/j.jhepr.2023.100683

37. Jindal A, Jagdish RK, Kumar A. Hepatic Regeneration in Cirrhosis. J Clin Exp Hepatol. 2022;12(2):603-616. doi:10.1016/j.jceh.2021.08.029

38. Wang J, Huang D, Yu H, Cheng Y, Ren H, Zhao Y. Developing tissue engineering strategies for liver regeneration. Engineered Regeneration.

2022;3(1):80-91.
doi:10.1016/j.engreg.2022.02.003

39. Polidoro MA, Ferrari E, Marzorati S, Lleo A, Rasponi M. Experimental liver models: From cell culture techniques to microfluidic organs-on-chip. Liver International. 2021;41(8):1744-1761. doi:10.1111/liv.14942

40. Dai Q, Jiang W, Huang F, Song F, Zhang J, Zhao H. Recent Advances in Liver Engineering With Decellularized Scaffold. Front Bioeng Biotechnol. 2022;10. doi:10.3389/fbioe.2022.831477

41. Lascaris B, de Meijer VE, Porte RJ. Normothermic liver machine perfusion as a dynamic platform for regenerative purposes: What does the future have in store for us? J Hepatol. 2022;77(3):825-836. doi:10.1016/j.jhep.2022.04.033

42. Nevzorova YA, Boyer-Diaz Z, Cubero FJ, Gracia-Sancho J. Animal models for liver disease – A practical approach for translational research. J Hepatol. 2020;73(2):423-440. doi:10.1016/j.jhep.2020.04.011

43. McGonigle P, Ruggeri B. Animal models of human disease: Challenges in enabling translation. Biochem Pharmacol. 2014;87(1):162-171. doi:10.1016/j.bcp.2013.08.006

44. Verwendung von Versuchstieren im Jahr 2020. Accessed July 29, 2023. https://www.bf3r.de/de/verwendung_von_versuch stieren_im_jahr_2020-288932.html

45. Haemmerle G, Lass A. Genetically modified mouse models to study hepatic neutral lipid mobilization. Biochim Biophys Acta Mol Basis Dis. 2019;1865(5):879-894. doi:10.1016/j.bbadis.2018.06.001

46. Liu Y, Meyer C, Xu C, et al. Animal models of chronic liver diseases. Am J Physiol Gastrointest Liver Physiol. 2013;304(5). doi:10.1152/ajpgi.00199.2012

47. Christen U. Animal models of autoimmune hepatitis. Biochim Biophys Acta Mol Basis Dis. 2019;1865(5):970-981. doi:10.1016/j.bbadis.2018.05.017

48. Kruepunga N, Hakvoort TBM, Hikspoors JPJM, Köhler SE, Lamers WH. Anatomy of rodent and human livers: What are the differences? Biochim Biophys Acta Mol Basis Dis. 2019;1865(5):869-878. doi:10.1016/j.bbadis.2018.05.019

49. Jahn D, Kircher S, Hermanns HM, Geier A. Animal models of NAFLD from a hepatologist's point of view. Biochim Biophys Acta Mol Basis Dis. 2019;1865(5):943-953. doi:10.1016/j.bbadis.2018.06.023

50. Bailey J, Thew M, Balls M. An Analysis of the Use of Animal Models in Predicting Human Toxicology and Drug Safety. Alternatives to Laboratory Animals. 2014;42(3):181-199. doi:10.1177/026119291404200306

51. Van Norman GA. Limitations of Animal Studies for Predicting Toxicity in Clinical Trials: Is it Time to Rethink Our Current Approach? JACC Basic Transl Sci. 2019;4(7):845-854. doi:10.1016/j.jacbts.2019.10.008

52. Hammer H, Schmidt F, Marx-Stoelting P, Pötz O, Braeuning A. Cross-species analysis of hepatic cytochrome P450 and transport protein expression. Arch Toxicol. 2021;95(1):117-133. doi:10.1007/s00204-020-02939-4

53. Olayanju A, Jones L, Greco K, Goldring CE, Ansari

T. Application of porcine gastrointestinal organoid units as a potential in vitro tool for drug discovery and development. Journal of Applied Toxicology. 2019;39(1):4-15. doi:10.1002/jat.3641

54. Eberlova L, Maleckova A, Mik P, et al. Porcine Liver Anatomy Applied to Biomedicine. Journal of Surgical Research. 2020;250:70-79. doi:10.1016/j.jss.2019.12.038

55. Wittauer EM, Oldhafer F, Augstein E, et al. Porcine model for the study of liver regeneration enhanced by non-invasive 13C-methacetin breath test (LiMAx test) and permanent portal venous access. PLoS One. 2019;14(5). doi:10.1371/journal.pone.0217488

56. Newsome PN, Henderson NC, Nelson LJ, et al. Development of an invasively monitored porcine model of acetaminophen-induced acute liver failure. BMC Gastroenterol. Published online 2010:10-34. doi:10.1186/1471-230x-10-34

57. Thiel C, Thiel K, Etspueler A, et al. A Reproducible Porcine Model of Acute Liver Failure Induced by Intrajejunal Acetaminophen Administration. European Surgical Research. 2011;46(3):118-126. doi:10.1159/000323411

58. Panasevich MR, Meers GM, Linden MA, et al. High-fat, high-fructose, high-cholesterol feeding causes severe NASH and cecal microbiota dysbiosis in juvenile Ossabaw swine. Am J Physiol Endocrinol Metab. 2018;314:78-92. doi:10.1152/ajpendo

59. Li X, Wang Y, Yang H, Dai Y. Liver and Hepatocyte Transplantation: What Can Pigs Contribute? Front Immunol. 2022;12. doi:10.3389/fimmu.2021.802692

60. Saxena R. Practical Hepatic Pathology: A Diagnostic Approach: Second Edition.; 2017.

61. Chatfield K, Morton D. The Use of Non-human Primates in Research. In: ; 2018:81-90. doi:10.1007/978-3-319-64731-9_10

62. Ribitsch I, Baptista PM, Lange-Consiglio A, et al. Large Animal Models in Regenerative Medicine and Tissue Engineering: To Do or Not to Do. Front Bioeng Biotechnol. 2020;8:972:1-28. doi:10.3389/fbioe.2020.00972

63. Text - S.5002 - 117th Congress (2021-2022): FDA Modernization Act 2.0 | Congress.gov | Library of Congress. Accessed July 29, 2023. https://www.congress.gov/bill/117th-congress/senate-bill/5002/text

64. Ethical use of animals in medicine testing | European Medicines Agency. Accessed July 29, 2023. https://www.ema.europa.eu/en/human-regulatory/research-development/ethical-use-animals-medicine-testing

65. Milner E, Ainsworth M, McDonough M, et al. Emerging Three-Dimensional Hepatic Models in Relation to Traditional Two-Dimensional In Vitro Assays for Evaluating Drug Metabolism and Hepatoxicity. Med Drug Discov. 2020;8:100060. doi:10.1016/j.medidd.2020.100060

66. Booij TH, Price LS, Danen EHJ. 3D Cell-Based Assays for Drug Screens: Challenges in Imaging, Image Analysis, and High-Content Analysis. SLAS Discovery. 2019;24(6):615-627. doi:10.1177/2472555219830087

67. Yang W, Wang X, Wang Z. Engineered liver tissue in vitro to mimic liver functions and its biomedical applications. Mater Adv. 2022;3(10):4132-4154.

doi:10.1039/d2ma00144f

68. Olgasi C, Cucci A, Follenzi A. Ipsc-derived liver organoids: A journey from drug screening, to disease modeling, arriving to regenerative medicine. Int J Mol Sci. 2020;21(17):1-30. doi:10.3390/ijms21176215

69. Zhang X, Chen X, Hong H, Hu R, Liu J, Liu C. Decellularized extracellular matrix scaffolds: Recent trends and emerging strategies in tissue engineering. Bioact Mater. 2022;10:15-31. doi:10.1016/j.bioactmat.2021.09.014

70. Uygun BE and S gutierrez A and YH and IM louisa and G a and SC and MJ and KN and TA and HM and NY and YML. Organ reengineering through development of a transplantable recellularized. National Institutes of health. 2011;16(7):814-820. doi:10.1038/nm.2170.Organ

71. Zhou Q, Li L, Li J. Stem cells with decellularized liver scaffolds in liver regeneration and their potential clinical applications. Liver International. 2015;35(3):687-694. doi:10.1111/liv.12581

72. Clavien PA, Dutkowski P, Mueller M, et al. Transplantation of a human liver following 3 days of ex situ normothermic preservation. Nature Biotechnology 2022 40:11. 2022;40(11):1610-1616. doi:10.1038/s41587-022-01354-7

73. Eshmuminov D, Becker D, Borrego LB, et al. An integrated perfusion machine preserves injured human livers for 1 week. Nat Biotechnol. 2020;38:189-198. doi:10.1038/s41587-019-0374-x

74. Maione F, Gilbo N, Lazzaro S, et al. Porcine Isolated Liver Perfusion for the Study of Ischemia Reperfusion Injury: A Systematic Review. Vol 102.; 2018. doi:10.1097/TP.0000000000002156

75. Stevens LJ, Donkers JM, Dubbeld J, et al. Towards human ex vivo organ perfusion models to elucidate drug pharmacokinetics in health and disease. Drug Metab Rev. 2020;52(3):438-454. doi:10.1080/03602532.2020.1772280

76. Mendes-Braz M, Elias-Miró M, Jiménez-Castro MB, Casillas-Ramírez A, Ramalho FS, Peralta C. The current state of knowledge of hepatic ischemia-reperfusion injury based on its study in experimental models. J Biomed Biotechnol. 2012;2012. doi:10.1155/2012/298657

77. Siniscalchi A, Gamberini L, Laici C, et al. Post reperfusion syndrome during liver transplantation: From pathophysiology to therapy and preventive strategies. World J Gastroenterol. 2016;22(4):1551-1569. doi:10.3748/wjg.v22.i4.1551

78. Ceresa CDL, Nasralla D, Pollok JM, Friend PJ. Machine perfusion of the liver: applications in transplantation and beyond. Nat Rev Gastroenterol Hepatol. 2022;19(3). doi:10.1038/s41575-021-00557-8

79. Eshmuminov D, Leoni F, Schneider MA, et al. Perfusion settings and additives in liver normothermic machine perfusion with red blood cells as oxygen carrier. A systematic review of human and porcine perfusion protocols. Transplant International. 2018;31(9):956-969. doi:10.1111/tri.13306

80. Vogel T, Brockmann JG, Friend PJ. Ex-vivo normothermic liver perfusion: An update. Curr Opin Organ Transplant. 2010;15(2):167-172. doi:10.1097/MOT.0b013e328337349d

Part I. Novel *In vitro* Models and Hydrogels

3 Nanofibrillar Cellulose as an Enzymatically and Flow Driven Degradable Scaffold for 3D Tissue Engineering

Melanie Krüger[1,2]*, Bart Spee[2], Andreas Walther[3], Laura De Laporte[4,5], Linda M. Kock[1]

[1]LifeTec Group BV
Kennedyplein 10-11; 5611 ZS Eindhoven; the Netherlands;

[2]Universiteit Utrecht; Veterinary Medicine
Uppsalalaan 8; 3584 CT Utrecht; the Netherlands;

[3]Albert-Ludwigs-Universität Freiburg; Institute for Macromolecular Chemistry

Stefan-Meier-Strasse 3; Hermann Staudinger Building; 79104 Freiburg; Germany;

[4]DWI – Leibniz-Institut für Interaktive Materialien e.V.; Advanced Materials for Biomedicine

[5]ITMC – Institute of Technical and Macromolecular Chemistry; RWTH University Aachen Forckenbeckstr. 50; 52056 Aachen; Germany

*Corresponding author

3.1 Abstract

Nanofibrillar cellulose as a naturally biocompatible scaffold material is very promising for tissue engineering. It is shear thinning but has the downside of not being degradable in animals, it can only be degraded by cellulase enzymes. In this study, a newly developed bioreactor was used to culture fibroblast spheroids under flow conditions inside nanocellulose hydrogels with and without the presence of cellulase. The aim was to control the tissue size and ideally find a match between degradation and tissue formation within this promising material. Both the concentration of cellulase and the flow rate were varied and their influence on the activity and growth of fibroblast clusters was assessed. Cluster diameters, degradation, metabolic activity and tissue production increase with higher cellulase concentration, although concentrations above 1 g/L do not have additional benefit. Flow leads to more viable cells, more proliferation and migration, leading to overall larger tissue constructs compared to static conditions. This is most likely due to the shear thinning effect of flow on cellulose nanofibrils in addition to the increased nutrient supply through perfusion. At a constant cellulase concentration

of 1 g/L, a flow of 2 mL/min proved to be to optimal for tissue production. Therefore, degradation in combination with flow leads to more effective tissue production in cellulose nanofibril hydrogels, which is a very potent scaffold material for tissue engineering.

3.2 Introduction

In tissue engineering, biomaterials replace native tissue partly or completely. The materials hereby serve as a 3D scaffold that permits maintenance of the cells and their signaling and allows for proliferation, differentiation and extracellular matrix (ECM) production to enable the development of new tissue with the desired function[1,2]

One obvious choice of scaffold material for this application are hydrogels due to their properties similar to tissue[3]. Some of the most commonly used hydrogels in tissue engineering are composed of synthetic aliphatic polymers as copolymers such as poly(lactic acid) and poly(glycolic acid)[1], poly(ethylene glycol)[3]or natural molecules, such as alginate, elastin, fibrinogen, collagen or hyaluronic acid[3].

Additionally, the development of bioreactors that create physiologically relevant culture conditions is essential for successful tissue engineering[1,4]. Bioreactors in this field

aim at mimicking *in vivo* conditions as closely as possible to examine and understand physiology on a cellular or molecular level and supply the cells with nutrients and oxygen, as well as mechanical and chemical stimuli[5,6].

It is of utmost importance for *in vitro* engineered tissues to receive sufficient nutrient and oxygen supply, which is *in vivo* perceived by vascularization[6–8]. In every tissue *in vivo*, except for skin, cartilage or cornea, the cells are not further away from blood supply than 200 µm, which correlates with the maximum distance of oxygen diffusion inside three-dimensional (3D) tissue[9]. If blood supply through vessels is not present, the success of tissue engineered constructs, also after implantation, is dependent on the diffusion of nutrients and oxygen, which is only possible for very small constructs[7]. Consequently, to achieve optimal tissue viability, it is essential to either control the tissue size in a way to avoid dead cores or to provide means of perfusion into the tissue as for example by vascularization[2].

Most of the above-mentioned conventional hydrogels used as scaffolds to engineer tissues show either a limited range in mechanical properties, do not exhibit topographical features, such as nanoscale cues for cell alignment or migration, and are difficult to engineer with

respect to biocompatibility and degradability[3]. Natural hydrogels have the advantage to contain many biological signals, gel at relevant low concentrations, and mainly form fibrous structures with micro-scale pores, which nicely mimic the natural ECM. However, biological gels usually suffer from poor mechanical properties. For example, collagen usually has an elastic modulus of 1 kPa, alginate which loses 40% of its mechanical stability within 9 days in culture due to loss of calcium alginate bonds[10], and fibrin is completely degraded within 2 weeks if no inhibitors are added [11]. Furthermore, depending on the source, natural materials can cause immunogenic responses[12]. Conventional synthetic polymeric hydrogels can overcome such limitations[12] but are expensive and crosslink at higher concentrations, which results in nanomesh pores. Cellulose has proven to be an emerging biomaterial in the field of cell culture. It is biocompatible and cell adhesive, has tunable mechanical properties[3,13,14], is shear-thinning[15], which is interesting for many scaffold fabrication techniques, and is not degradable without the addition of cellulase[16,17]. Cellulose is widely available as it is the most abundant biopolymer on earth[18], which is directly isolated from wood and is mainly found in the cell walls of plants[19], where it is organized into highly crystalline microfibrils[19] and can be

chemically modified to form stable hydrogels [3, 14]. Initially, cellulose fibril agglomerations have diameters between 2 and 20 µm, depending on its source[19]. They are very tightly bound through numerous hydrogen bonds and entanglement, which makes it very difficult to extract them[19]. Classical methods either use harsh mechanical treatment with a high energy consumption or chemical treatment that result in a much-reduced fibril length[19]. Through the method of 2,2,6,6-tetramethylpiperidinyl-1-oxyl (TEMPO) mediated oxidation of native cellulose, the oxidation of primary alcohol groups in aqueous media is catalyzed[19]. The oxidation process is limited to the surface of the fibers[19], where aldehyde and carboxyl groups are introduced[20], resulting in a negative surface charge[19]. Due to the anionic character, it is possible to separate the fibrils in a subsequent mechanical treatment[20] with a pressure homogenizer[15]. The resulting nonocellulose fibrils (CNFs) have a high crystalline character with a diameter of 2.5 ± 2 nm and large apect ratio[3,15]. They belong to the stiffest natural biomaterials ($E_{cellulose.I}$ = 138 GPa) and thereby give the CNF hydrogels remarkable mechanical properties, similar to the classical polymer gels[3,15].

The extracted CNFs, made of β-D glycopyranose polysaccharide chains[21], gel at a low solid content of 1 wt-

%[15] and form reversible CNF hydrogels[20] with an apparent viscosity degree of polymerization (DP_v) of 600 and 0.85 mmol/g carboxyl group content[15]. The hydrogel holds together through entanglements and hydrogen bonds[20], which results in shear-thinning and self-healing behavior[15]. As CNFs are highly biocompatible[22,23], it's hydrogels have shown promising results in tissue engineering applications such as culturing of stem cells[23], 3D liver cell culture[21] and as a sacrificial template for the engineering of tubular fibroblast constructs[3]. Furthermore, CNFs exhibit stable functionality and fabrications costs are very low compared to other biomaterials[22].

As an interesting property, CNFs are not degradable within animals due to the lack of appropriate enzymes[17,18,24]. Only the enzyme cellulase can degrade cellulose into glucose and it has been shown that this degradation and its degradation products do harm animal cells *in vitro*[17,24]. This means that cells can be cultured undisturbed on CNF substrates until confluency, after which the material can be degraded on demand by the addition of cellulase[3]. However, to culture cells inside a CNF gel or enable cell infiltration in the body, gradual degradation is required.

Therefore, in order to fully exploit the potential of CNF hydrogels as tissue engineering scaffolds it is essential to gain insight into how to induce and control their degradation kinetics. It is important that the rate of degradation matches the tissue formation, so that the mechanical support of the CNF scaffold persists as long as it is required. Here, we aim to achieve a better understanding of the conditions needed to grow cells inside 3D CNF hydrogels with the use of a custom-made bioreactor. Additional to enzymatic degradation, we hypothesize that fluid flow can aid degradation due to the shear thinning properties of the CNF hydrogel.

To the best of our knowledge, there has been no research to date investigating the potential of 3D cell growth inside CNF hydrogels for tissue engineering under flow culture in combination with enzymatic degradation. The newly developed dynamic and modular bioreactor enables the creation of a fluid/medium flow that can aid in degradation of the material and provide nutrient supply deeper into the tissue compared to pure diffusion. The cellulase concentration and flow rates are systematically varied to study cell migration and proliferation, while the bioreactor allows for online assessment of various parameters such as metabolic activity and microscopic imaging.

3.3 Materials and Methods

The present study is divided into two main parts. In study I, the flow rate is kept constant, while the cellulase concentration in the medium is varied in order to determine the effect of the enzymatic degradation onto the cells, their viability, proliferation, migration and ECM formation. In study II, the cellulase concentration is kept constant, while the flow is varied to examine the influence of flow onto the above-mentioned parameters.

3.3.1 Bioreactor

The bioreactor was designed using the 3D CAD software NX (Version 8.0, Siemens PLM Software) and was manufactured in polyether ether ketone (PEEK) as a modular system to accommodate different needs in flow, chamber size, and online imaging. More specifically, the modular system provides the option to switch between static cultures and cultures including flow, the latter can be supplied in precisely determined rates through perfusion channels in the main chamber (Figure 1), driven by an external pump. Furthermore, options for cell seeding from top-seeding to bioprinting are possible due to a removable lid that allows full access to the culture chamber and construct. Both 2D and 3D cultures can be executed in different construct sizes as the insert, which

is 3D printed in nylon, can be tailored to the individual experiment (between 10 µl and 2.4 mL hydrogel volume). In this present study it was designed to hold a volume of 100 µl and provide channels facing the perfusion channels that allow some active diffusion into the hydrogel, but not a direct and complete perfusion of the total medium stream through the hydrogel to not exert an excessive shear stress, due to the shear thinning properties of the CNF hydrogel.

Finally, to monitor micro- and macroscopic changes of the biomaterial and cells over time under an inverted microscope, a microscope coverslip (24 x 24 mm, 0.2 mm thickness, Menzel, Thermo Scientific) is incorporated in the bottom and sealed towards the bioreactor parts. The materials of the bioreactor (PEEK, glass) and 3D printed insert (nylon) are biocompatible (data not shown).
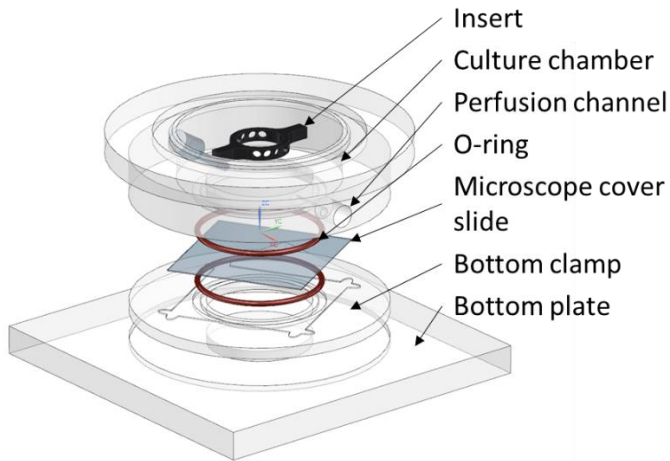
Figure 1: Bioreactor design in exploded view with components from top to bottom: insert, chamber, o-ring, microscope cover slide, o-ring, bottom clamp, bottom plate

3.3.2   CNF preparation

The CNFs were produced by oxidizing paper pulp using the TEMPO method[13–15] with subsequent dispersion in water and high-pressure homogenization. After autoclaving at 121°C for 20 min, the gel has a pH of 6 and consists of 0.62 wt-% of cellulose.

3.3.3   Fibroblast cluster formation

In order to introduce cells into the CNF hydrogel, clusters consisting of murine connective tissue fibroblasts (L929 cell line, Leibniz Institut DSMZ GmbH) are produced with

the hanging drop method. This is necessary, because the CNF cannot be mixed with salty solutions as it tends to coagulate and loses its self-healing ability. To execute the hanging drop method, a solution of 12 g/L methyl cellulose (high viscosity, Sigma) in RPMI medium (Roswell Park Memorial Institute, 1640, Life Technologies™) is produced to increase the viscosity and enhance droplet formation. Afterwards a cell suspension with 250,000 cells/mL is made in medium containing 20% v/v of 12 g/L methyl cellulose solution in RPMI medium with 10% fetal bovine serum (FBS, HyClone, LOT number RYK35913, GE Healthcare) and 1% v/v Penicillin/Streptomycin (Lonza) (RPMI+). The cell clusters are formed by hanging drops of medium from the inverted bottom of a petri dish, where the dispersed cells sink to bottom of the hanging drop and form a cluster there. The cell suspension is divided into droplets of 30 µL, resulting in a cluster size of 7,500 cells each. Clusters are formed during incubation overnight at 37°C and 5% CO_2 in air under humidified atmosphere.

Next day, the cell clusters are collected with fresh RPMI medium by flushing them off the petri dish and they are subsequently included into the gels in the bioreactor. This is achieved by first pipetting 50 µL of 0.62 wt-% CNF hydrogel into the bioreactor insert and then, with tweezers

and needles, placing the clusters from the medium suspension on top of the gel. Immediately afterwards another 50 µL of CNF gel is pipetted on top of the cluster, to prevent it from drying out. Due to the self-healing properties of the gel, the clusters are now exactly center in 100 µL of gel. Subsequently, 200 µL RPMI+ medium is pipetted on top of the gels.

3.3.4 Study I

In this study, 100 µL of CNF gel per bioreactor with an included fibroblast cluster of 7,500 cells is cultured for 14 days at 37°C and 5% CO_2. During this time, 10 mL RPMI+ medium with cellulase (*Trichoderma reseei*, Sigma) concentrations of 2, 1, 0.5, 0.25, 0 g/L (n=6 for each concentration) are pumped through each bioreactor circuit with a flow of 1 mL/min by a cartridge pump (Masterflex and Masterflex Puri-Flex tubing L/S 13). After 7 days a complete medium change is performed.

3.3.5 Study II

In this study flows are varied while cellulase concentrations remain constant and the set-up is similar to study I with n = 6 per condition. The difference is that in this case cellulase concentration is fixed to 1 g/L based on preliminary outcomes of study I and the flow rate is

varied between 0.25, 0.75, 1 and 2 mL/min respectively. As a control, cultures without flow are executed.

3.3.6 Analyses

Cluster Area

The maximum 2D projection of the cluster area of each sample at each timepoint (day 0, 3, 7, 10, and 14; n=6 for each timepoint) is determined by removing the bioreactor temporarily from the pumping circuit and incubator and placing it under a microscope (Nikon Eclipse TE 300). Without impairing sterility, brightfield images are taken at 4X magnification and processed in the software Image J (National Institute of Health and Laboratory for Optical and Computational Instrumentation, University of Wisconsin).

Migration and proliferation

At the start of each culture, 1 µL of CellBrite red cytoplasmic membrane online staining (Biotium) is added to the RPMI+ medium of half of the samples per condition (n=3). After 24 h of circulation of the medium, the fluorescent images (555 nm) are taken (Nikon Eclipse TE 300) at 4X magnification on day 3, 7, 10, and 14. After the medium change on day 7, no additional staining is added.

This way the already stained cells which sustain their fluorescent staining can be monitored with regard to their migration and proliferation outwards during the entire culture period.

Viability

RPMI+ medium containing 4 µM/mL Calcein AM (Life Technologies™) and 2 µM/mL Propidium iodide (Life Technologies™) is prepared. On day 0 and 14, the medium of 3 samples per condition (n=3) is replaced with 100 µL of staining solution and incubated at 37°C and 5% CO_2 for 20 minutes. Subsequently the medium is removed, and samples are washed 3 times with 100 µL of fresh RPMI+ medium for 5 min each. Finally, visualization is achieved under a fluorescent microscope (Nikon Eclipse TE 300) at 555 nm (dead cells) and 470 nm (living cells) at a 4X magnification. Images are combined and processed in Image J (NIH) afterwards.

Metabolic Activity

On day 0, 7, and 14 Presto Blue (Invitrogen) is added at a concentration of 10% v/v to RPMI+ medium and 300 µL are added to each sample within the bioreactor (n=3 for each condition). After incubation of 4 h at 37°C and 5% CO_2, 100 µL of medium is removed and pipetted into a

black 96 well plate (Costar). The fluorescent intensity at an excitation wavelength of 535 nm and emission wavelength of 615 nm is then analyzed with a plate reader (Clariostar, BMG Lifetech). If the sample is cultured further, the remaining staining medium is removed and replaced by fresh RPMI+ medium.

Degradation

On days 0, 3, 7, 10, and 14 medium samples of 1 µL from the running culture (n=6 per condition) are analyzed for their glucose content utilizing a diabetes blood analyzer (ONE TOUCH Vita), as glucose is the degradation product of cellulose when the enzyme cellulase is used.

Histology

On day 14, 3 samples from each condition (n=3) are fixed in 3.7% formaldehyde (Sigma) for 1 h and subsequently processed for paraffin embedding. All samples are cut in 5 µm sections. To visualize ECM components, Mayer's Hematoxylin (nuclear counterstain) and Eosin staining (Sigma) is performed. Slides are imaged by light microscopy (Nikon Eclipse TE 300) to identify the slides with cell clusters present (data not shown). These slides are then stained for fibronectin and with immunostaining. For this purpose, the slides are blocked to prevent non-

specific staining with 4% w/v bovine serum albumin (BSA, Sigma) in PBS (Sigma) for 2 hours at room temperature after dewaxing and rehydration. The primary antibody anti-fibronectin in rabbit (F3648, Sigma) in a 1:200 solution of 4% BSA in PBS is incubated over night at 37°C. As a negative control, incubation with only the BSA/PBS buffer without primary antibody is executed. After washing the slides 3 times for 30 min with PBS, the secondary antibody anti-rabbit IgG (H+L) – CF 568 (Sigma) in a 1:100 solution of 4% BSA/PBS buffer is incubated protected from light for four hours at 37°C. Subsequently, a 1:500 solution of DAPI (Sigma) in PBS is incubated on the slides for 2h, which are then washed 3 times for 30 minutes with PBS before being embedded in Roti-Histokitt (Carl-Roth). Visualization is achieved under a fluorescent microscope (Nikon Eclipse TE 300) at 568 nm (fibronectin) and 454 nm (DAPI). Images are combined in Image J (NIH) afterwards and the software is used to determine the total area of the cluster on a slide by measuring the outline of the DAPI stained section. Within this area, the total area of fibronectin staining is determined to result into a percentage of fibronectin inside of the cell cluster without taking the production of fibronectin on the outer perimeter into account. For each

experimental condition, two different clusters were analyzed.

Statistics

The quantitative data (cluster size, glucose concentration and metabolic activity) is analyzed for statistical significance between groups with SPSS (IBM). The approach of a mixed model analysis with the maximum likelihood method is applied with fixed (study I: cellulase concentration, days and a factorial term of the two; for study II: flow, days and the factorial term) and random effects (bioreactor, within one condition). Results are reparametrized and if a logarithmic transformation is applied, results are back transformed for reporting. Normality is tested by examining the normal Q-Q plot of residuals and linearity and constant variance are tested by examining the scatter plots of residuals over predicted values. In the cases of study II readouts of metabolic activity and glucose concentration, no variance between bioreactors could be found, therefore the random effect was eliminated.

3.4 Results and Discussion

3.4.1 Proliferation, degradation and migration

Due to its shear-thinning properties, we hypothesize that the CNF hydrogel will be affected by the flow applied in the bioreactor. As has been seen in previously conducted pilot experiments (results not shown), if the flow is too high (4 mL/min or higher), the hydrogel converts to a liquid state and is flushed out of the bioreactor. A flow of 1 mL/min does not affect the integrity of the CNF hydrogel and is used as a basis in study I. We have equally seen that a cellulase concentration of 4 g/L in flow conditions destroys the gel to rapidly within a few days. Therefore, concentrations between 0 and 2 g/L are tested in study I.

As depicted in Figure 2A, cluster sizes increase over time in all samples of study I. When no cellulase is added, the increase from day 0 to day 14 is 31% ($p \leq 0.001$), whereas the highest increase of 59% ($p \leq 0.001$) over the culture period is achieved at a cellulase concentration in the medium of 0.5 g/L, with significant differences compared to day 0 starting on day 7. At the highest concentration of 2 g/L cellulase, the increase compared to day 0 is only 15% on day 14 ($p = 0.005$), with significant differences only starting at day 10. Compared to no added cellulase, the cluster size for 2 g/L cellulase even starts to decrease

from day 3 onwards (22% lower on day 3 (p = 0.005), 34 % on day 7 (p ≤ 0.001), 33 % on day 10 (p ≤ 0.001) and 29 % on day 14 (p ≤ 0.001)). Therefore, the cluster sizes grow less without the addition of cellulase and are even smaller with a high concentration of cellulase (2 g/L), indicating that those conditions limit migration and proliferation of cells. The fact that the clusters grow without cellulase is likely due to the presence of flow causing reorganization in the nanocellulose, giving the cells space to grow. At the opposite end, the small clusters after addition of a high amount of enzyme (2 g/L) in combination with a flow of 1 mL/min suggests that degradation is very high and reduces the presence of scaffold to support cluster expansion. This confirms previous findings that, under optimal conditions and at cellulase concentrations of 2 g/L, a scaffold made of bacterial cellulose hydrogel (chemically similar to plant derived CNF[24]) is nearly completely degraded within one week[17].

The results of cluster size measurements in function of the flow rate in study II are shown in Figure 2B. Differently to study I, the first significant differences compared to a static culture (no flow) can be observed only from day 10 onwards. On that day, the cluster size increased 36% compared to the static culture for a flow of 0.25 mL/min,

26% for a flow of 1 mL/min and 29% for 2 mL/min with p ≤ 0.001 for each case. The largest increase in cluster size is observed on day 14 with 88% compared to day 0 for a flow of 2 mL/min (p ≤ 0.001), which is higher than the largest increase for study I with 59%. Also notable is that on day 14, all cluster sizes under flow are higher than the static control, except for a flow of 1 mL/min (25% for a flow of 0.25 mL/min, 37% for 1 mL/min flow and 52% for 2 mL/min). This means that the highest flow rate utilized in this study leads to the largest clusters and that the hypothesis of flow having a major influence on the proliferation and migration of cells is confirmed. However, it is equally true that the onset of influence of flow in the chosen range occurs later than in the case of enzymatic degradation. Furthermore, the finding of the highest flow rate having the biggest impact on the cell cluster size indicates that there are more benefits of adding flow to the culture than pure degradation. Also in study I, we demonstrate that higher degradation can lead to a decrease in cluster size due to a lack of scaffold support. Therefore, the beneficial effect of flow is thought to be due to creation of space through the shear thinning effect that leaves the remaining structure intact rather than inducing a complete degradation around the cells, thereby allowing cells to move further outwards from the cluster as fluid

flow also stimulates migration of cells[25]. Furthermore, in the case of flow, more nutrients can be flushed into the hydrogel and cluster so that cells are more viable and active. Additionally, the degradation product of the CNF hydrogel, glucose, is flushed out of the scaffold, which prevents any kind of product inhibition, which is, however, not a particularly critical issue for highly efficient cellulases.

Figure 2C shows the glucose concentration measured in mmol/l over the 14 days of culture for study I. Note that the medium is changed at day 7, so that the glucose values after the measurements of day 7 are again the initial ones of day 0. Within the first week of culture, no significant differences in glucose concentration are found compared to day 0 for any of the cellulase concentrations. In fact, the only significant differences are found after the second week of culture, on day 14, compared to the values on day 0 (or day 7 after refreshing respectively). For a cellulase concentration of 2 g/L, there is a decrease of 2.4 mmol/l ($p \leq 0.001$), whereas the glucose concentration increased about 1.3 mmol/l for 0 g/L cellulase ($p = 0.005$). On day 10, both the glucose concentrations for 2 g/L and 1 g/L of cellulase are higher than that of no added enzyme ($p \leq 0.001$ for each condition), however, after 4 additional days, the values

decrease significantly. As glucose is the degradation product of CNF but is also taken up by the cells, there is a twofold effect at play. The increase at day 10 compared to 0 g/L cellulase and overall increase over time for no added cellulase can be explained by glucose being liberated by enzymatic degradation into the medium at a higher rate than it is taken up by the cells. As this cellulase has an optimal working condition in acidic environments (pH 5.0) and could be inhibited at a pH above 6[17], it is further hypothesized that degradation mostly takes place in the direct vicinity of the cells, where they acidify the extracellular environment through release of waste products[26]. Under optimal conditions, the material can be degraded completely within 7 days[3], but as pH in the present study is higher than optimal working conditions, more cells could also mean a potentially higher degradation but also more glucose uptake. As we saw previously, the cluster size was the smallest for a cellulase concentration of 2 g/L. This correlates to the lower glucose concentration for those conditions, which would mean that the effects of a potential high liberation through the high enzyme concentration is hindered by low amounts of acidic environments due to low number of cells. However, it must also be said that the glucose measured is also subject to different amounts of medium

evaporation over time caused by the system set-up, which could potentially influence the values. In future studies, different cellulases could be tested that operate at different optimal pH ranges to find an optimal fit for the cells employed[17].

Similar to the results of cluster sizes, changes in glucose concentrations in the medium for study II are not as high as in study I, as can be seen in Figure 2D. There is no significant change in glucose concentration from day 0 to day 14 for either a static culture or cultures with flow. The significant differences found between flow cultures compared to the static culture on each day are also not very high. This was to be expected, as flow probably does not significantly increase degradation as mentioned above but only solubilizes the CNF without breaking it down to its glucose components that could be picked up in the measurement. As the cellulase concentration is the same for all the conditions, differences in medium glucose concentration may mostly be assigned to consumption by the cells. This also manifests in the fact that there was no variance found between the bioreactors within one study and, therefore, no random effect should be calculated in the statistical analysis.
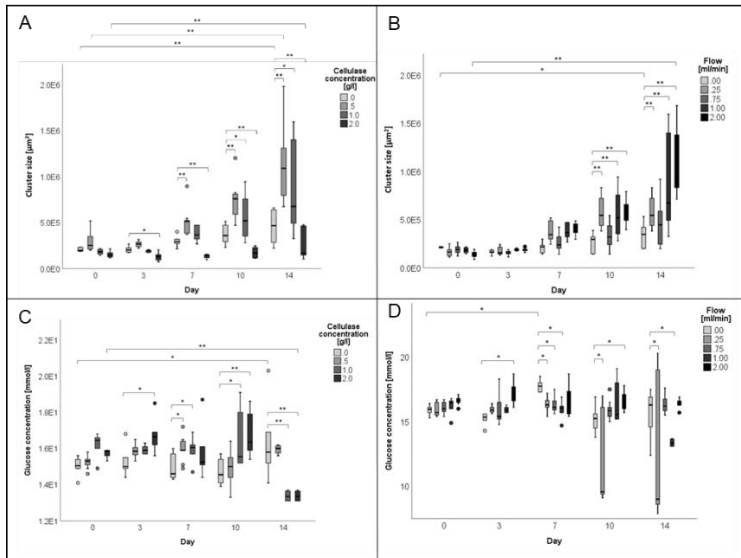
Figure 2: A+B: Effect on cluster size over 14 days (n=6). A: Effect of cellulase concentrations under flow conditions of 1 mL/min (study I). B: Effect of flow rates under fixed cellulase concentration of 1 g/L (study II). C+D: Effect on glucose concentration over 14 days (n=3). C: Effect of cellulase concentrations under flow conditions of 1 mL/min (study I). D: Effect of flow rated under fixed cellulase concentration of 1 g/L (study II). A-D: *: $p \leq 0.05$, **: $p \leq 0.001$.

The hypothesis that cells are enabled to proliferate and migrate within the gel with increased degradation and aided by flow is further indicated by the online CellBrite red stain, which enables long-term cell and cluster tracking (Figure 3A and Figure 3B). The stain was only added the first 7 days, after which it was removed. The stain allows visualizing the growth of the clusters over time. As stained cells are observed beyond the cluster diameter at 7 days, this demonstrates that cells are

migrating outwards. In Figure 3A, it is also visible that the cluster without addition of any cellulase remains very round with a sharp edge and increases only slightly in size. This is due to the still very dense CNF matrix surrounding the cluster. In contrast to that, a ragged edge of the cluster is visible for 0.5 g/L and 1 g/L of cellulase. In the case of 1 g/L enzyme, a spike outward from the original cluster is visible as the cells migrated into the direction of the flow. If 2 g/L of cellulase is added to the medium, the cluster remains in its original form or even decreases in size. As mentioned above, this is probably because the degradation is too rapid such that the migrating cells cannot find enough support anymore.

Figure 3B shows a similar trend for clusters in study II. Here, a clear effect of the flow direction (from right to left) is visible. The cluster edge facing the flow is rather round and condensed, whereas the migration of the fibroblasts is visible on the opposite side, which points in the direction of the flow. This proves that flow does have a direct influence on migration and cluster growth, as has been seen in other studies as well[25]. Flow is known to induce adhesion activation and cell polarization, which lead to migration through directional protrusion extension[25].

3.4.2 Viability and Tissue Formation

In order for cells to produce ECM and finally form a functional tissue, a prerequisite is the viability of cells. In both studies, the cells are incorporated into the gel in the form of a cluster. Most likely, this handling process causes the outer cell layers to die, as can be seen in the red color in the image of day 0 in Figure 3C. However, the core stays viable and after static culturing for 14 days, the expanding outside is viable, but the core is dead as this initial study does not yet address the formation of blood vessels to keep the inner core of the formed tissue alive. For all conditions, except for the cultures without cellulase at 1 mL/min flow and 1 g/L cellulase with 2 mL/min of flow, resulting in small clusters, the clusters show a red core and green outer layers. The conditions with the largest clusters (0.5 and 1 g/L cellulase and 1 mL/min flow) show a very large dead core, which is most likely due to diffusion limitations of nutrients into the cluster. At higher flow, the dead cores for the cellulase concentration of 1g/L become smaller while live and dead cells are equally distributed over the cluster without a clear core structure. This can be explained by the fact that flow increases diffusion of nutrients that can enter the cluster more effectively to sustain the cells.

The measured metabolic activity (Figure 4A and Figure 4B) gives further insight into the cell clusters viability and number of cells present. For study I (Figure 4A), the absence of cellulase decreases the mean activity by 1.479 FI units from day 0 to day 14 ($p \leq 0.001$), whereas there is no change between day 0 and day 14 for a cellulase concentration of 2 g/L. This is interesting as we have seen before that the cluster size is much reduced for the latter condition which means that the metabolic activity stays constant, despite a smaller cluster size. The reason for this can possibly be found in the comparatively higher viability of the remaining cells (Figure 3C). In fact, with a flow of 1 mL/min on day 14, only the metabolic activity of condition 1 g/L cellulase is significantly higher (3.820 FI units, $p \leq 0.001$) compared to no cellulose, which is again interesting as the cluster size for this enzyme concentration is smaller than in the case of 0.5 g/L cellulase. This can mean that the cells are more active when there is more enzymatic degradation.
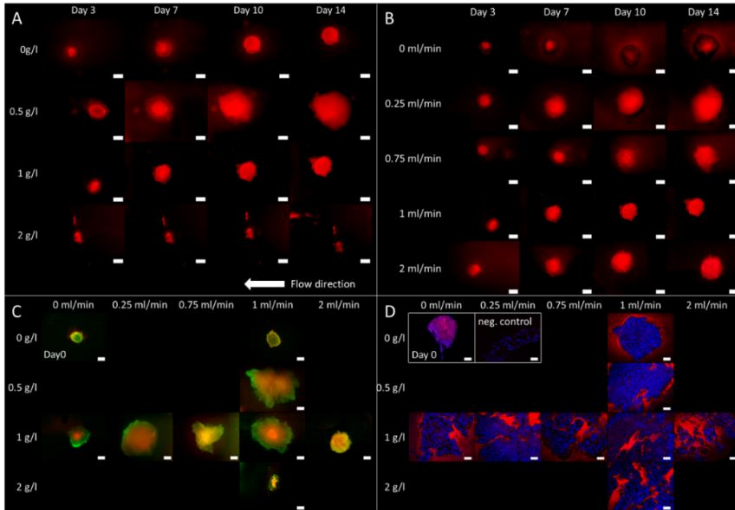
Figure 3: A+B: Effect on migration and proliferation into the biodegradable scaffold by representative images of CellBrite red staining. Cells are incubated with the stain in the first week and then maintain the staining in the second week of culture after a medium change, images are taken every 3-4 days, scale bars: 250 µm, arrow indicates direction of flow through the scaffold (n=3 per condition). A: Effect of cellulase concentrations at a flow rate of 1 mL/min (study I). B: Effect of flow rates at a fixed cellulase concentration of 1 g/L. C: Representative images of viability staining for all conditions of study I and II. Viable cells are stained green and dead cells in red after 14 days of culture and Day 0 respectively, scale bar: 250 µm (n=3 per condition). D: Representative images of immunohistochemical samples of all conditions stained for the nucleus (blue) and fibronectin (red) after the culture of 14 days, scale bar: 50 µm (n=3 per condition).

The metabolic activity for study II (Figure 4B) shows a surprisingly high increase for the static culture from day 0 to day 14, even though we see a small dead core in this case (Figure 3C). As opposed to study I, the metabolic activity increases over time for all flow conditions in study II in the presence of 1 g/L cellulase, which indicates that

flow has a large influence on the activity of the cells. For example, for a flow of 2 mL/min, there is an increase in activity of 7.291 FI units from day 0 to day 14 (p ≤ 0.001), which is high, especially with respect to the cluster size. This illustrates that flow aids in maintaining a high level of metabolic activity, which can be due to improved nutrient supply and removal of waste products[26,27]. It has been reported before that small particles can penetrate deeper into a 3D matrix and cell clusters under the influence of flow compared to static conditions[28].
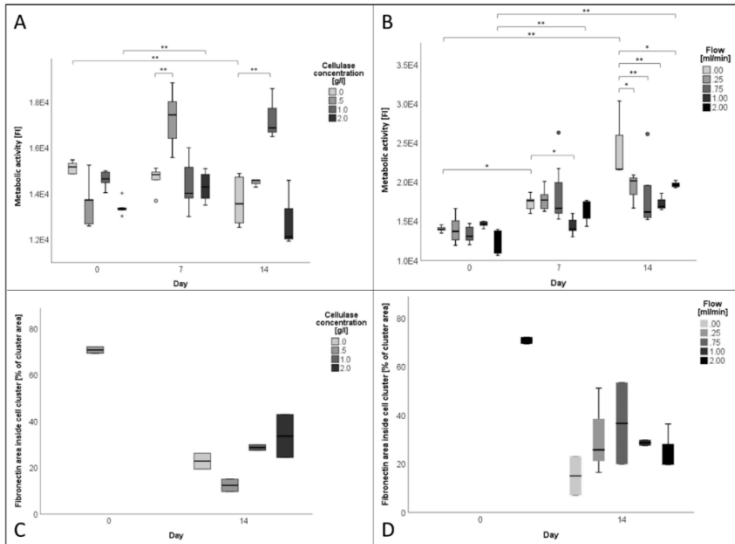
Figure 4: A+B: Effect on metabolic activity measured in Fluorescent Intensity (FI) over 14 days (n=3 per condition) (*: p ≤ 0.05, **: p ≤ 0.001). A: Effect of cellulase concentrations under flow conditions of 1 mL/min (study I). B: Effect of flow rates under fixed cellulase concentration of 1 g/L (study II). C+D: Quantitative determination of percentage of fibronectin that has been produced inside the cell cluster during the culture of 14 days (n=3 per condition). C: Effect of cellulase concentrations under flow conditions of 1 mL/min (study I). D: Effect of flow rates under fixed cellulase concentration of 1 g/L (study II).

To evaluate tissue formation, histology samples are compared. In Figure 3D, representative images of the immunohistological staining against fibronectin, the ECM protein produced by fibroblasts, are shown. On day 0, the nuclei in blue and fibronectin in red are equally distributed. The fibronectin in this case has been produced by the cells when they were hanging freely in medium drops overnight without any constraining hydrogel scaffold

surrounding them. After 14 days of culturing inside a CNF hydrogel without cellulase, the clusters are still dense and fibronectin has only been produced on the perimeter without any infiltration. With increasing cellulase concentration, more space within the clusters can be observed being filled with fibronectin. This is also represented in Figure 4C, where the percentage area of fibronectin within the cell clusters is plotted for different cellulase concentrations. The percentage on day 0 is the highest, due to the homogeneous spread but after 14 days most fibronectin production is within the cluster for 2 g/L, which is in agreement with the higher metabolic activity of the cells being exposed to higher enzyme concentrations. A similar trend is apparent for study II (Figure 4D). With increasing flow, more fibronectin can be found inside the cluster as space is made available for the ECM production by shear thinning of the CNF and the cells were more active in the presence of flow. At 2 mL/min of flow and 1 g/L cellulase concentration, a higher percentage of fibronectin is produced compared to the highest cellulase concentration of 2 g/L and 1 mL/min of flow. This indicates that flow seems to play a larger role than enzymatic degradation with regard to fibronectin production, which was also the case of metabolic activity.

Importantly, in most cases, fibronectin seems to be present at higher amounts at the edges of the cluster.

The condition with the largest cluster size that is most viable and presents the highest ECM production at the same time is with 1 g/L of added cellulase at a flow of 2 mL/min. Changes in the hydrogel structure through flow, as the CNF hydrogel is shear thinning, has hereby shown to have a beneficial influence on cell proliferation and migration by creating space without causing the growth of clusters to arrest due to insufficient scaffold support. We have further demonstrated that although larger clusters inadvertently lead to dead cell cores without the addition of further perfusion modalities, flow can remedy this effect by introducing more nutrients deeper into the tissue, leading to larger viable cell clusters with higher metabolic activity and more ECM production within the cluster.

Further studies aim to further study the degradation kinetics of the CNF hydrogels as glucose is both the degradation product and a nutrient taken up by the cells. In addition, co-cultures to enable blood vessel formation will extent culture durations and give deeper insights into the potential of this hydrogel to tissue regenerative purposes.

Nevertheless, the CNF hydrogel is clearly suitable as a natural biocompatible 3D tissue engineering scaffold and we have demonstrated a way towards controlling the size and viability of cell spheroids by tuning enzyme concentration and flow. The material has no adverse effects onto the cells nor has the degradation enzyme cellulase or its breakdown product glucose. If a controlled delivery of cellulase would be included into the hydrogel, degradation even within the human body could be achieved for regenerative applications[17]. Due to its shear thinning character, CNF hydrogels have a very high potential to be used as injectable materials *in vivo*[29] or in bioprinting technologies to make *ex vivo* tissue models for drug testing. For the latter, the tissue can be kept small to not impair viability, whereas tissue regeneration applications call for large tissue sizes.

3.5 Conclusion

The aim of this study was to determine if a CNF hydrogel is suitable as a tissue engineering scaffold and if we can control the tissue production of cell clusters inside the hydrogel by means of a newly developed flow bioreactor with online assessment possibilities. By using our bioreactor, we have not only proven its working principle but also that the size, viability, activity and ECM

production of a fibroblast cell cluster is influenced by the interplay between enzymatic degradation and flow. There is a balance between a low degradation that leaves the cells no room for proliferation and migration and a very high degradation that removes the scaffold support to quickly, leading to small cluster sizes as well. Importantly, the addition of flow changes the internal structure around the cells, locally helping the cells to grow, while increasing their metabolic activity and ability to produce and deposit extracellular fibronectin. The shear-thinning effect through flow enables nutrients to diffuse deeper into the tissue, resulting in larger, viable mini-tissues.

3.6 Funding Data

3.7 References

1. Iqbal N, Khan AS, Asif A, Yar M, Haycock JW, Rehman IU. Recent concepts in biodegradable polymers for tissue engineering paradigms: a critical review. Int Mater Rev. 2019;64(2):91-126. doi:10.1080/09506608.2018.1460943

2. Salehi-Nik N, Ghassem Amoabediny BP, Tabesh H, et al. Engineering parameters in bioreactor's design: a critical aspect in tissue engineering. Biomed Res Int. 2013;2013(Article ID 762132):15. doi:10.1155/2013/762132

3. Torres-Rendon JG, Köpf M, Gehlen D, et al. Cellulose Nanofibril Hydrogel Tubes as Sacrificial Templates for Freestanding Tubular Cell Constructs. Biomacromolecules. 2016;17(3):905-913. doi:10.1021/acs.biomac.5b01593

4. Figallo E, Flaibani M, Zavan B, Abatangelo G, Elvassore N. Micropatterned biopolymer 3D scaffold for static and dynamic culture of human fibroblasts. Biotechnol Prog. 2007;23(1):210-216. doi:10.1021/bp0602092

5. Selden C, Fuller B. Role of bioreactor technology in tissue engineering for clinical use and therapeutic target design. Bioengineering. 2018;5(2):1-10.
    doi:10.3390/bioengineering5020032

6. Lawrence BJ, Devarapalli M, Madihally S V. Flow dynamics in bioreactors containing tissue engineering scaffolds. Biotechnol Bioeng. 2009;102(3):935-947. doi:10.1002/bit.22106

7. Kannan RY, Sales K, Butler P, Seifalian AM, Salacinski HJ. The roles of tissue engineering and vascularisation in the development of micro-vascular networks: a review. Biomaterials.

2004;26(14):1857-1875.
doi:10.1016/j.biomaterials.2004.07.006

8. Neumann T, Nicholson BS, Sanders JE. Tissue engineering of perfused microvessels. Microvasc Res. 2003;66(1):59-67. doi:10.1016/S0026-2862(03)00040-2

9. Novosel EC, Kleinhans C, Kluger PJ. Vascularization is the key challenge in tissue engineering. Adv Drug Deliv Rev. 2011;63(4):300-311. doi:10.1016/j.addr.2011.03.004

10. Shoichet MS, Li RH, White ML, Winn SR. Stability of hydrogels used in cell encapsulation: An in vitro comparison of alginate and agarose. Biotechnol Bioeng. 1996;50(4):374-381. doi:10.1002/(SICI)1097-0290(19960520)50:4<374::AID-BIT4>3.0.CO;2-I

11. Jungst T, Smolan W, Schacht K, Scheibel T, Groll J. Strategies and Molecular Design Criteria for 3D Printable Hydrogels. Chem Rev. 2016;116(3):1496-1539. doi:10.1021/acs.chemrev.5b00303

12. Li Y, Rodrigues J, Tomás H. Injectable and biodegradable hydrogels: Gelation, biodegradation and biomedical applications. Chem Soc Rev. 2012;41(6):2193-2221. doi:10.1039/c1cs15203c

13. Benítez AJ, Torres-Rendon J, Poutanen M, Walther A. Humidity and multiscale structure govern mechanical properties and deformation modes in films of native cellulose nanofibrils. Biomacromolecules. 2013;14(12):4497-4506. doi:10.1021/bm401451m

14. Benítez AJ, Walther A. Cellulose nanofibril nanopapers and bioinspired nanocomposites: A review to understand the mechanical property

space. J Mater Chem A. 2017;5(31):16003-16024. doi:10.1039/c7ta02006f

15. Torres-Rendon JG, Femmer T, De Laporte L, et al. Bioactive gyroid scaffolds formed by sacrificial templating of nanocellulose and nanochitin hydrogels as instructive platforms for biomimetic tissue engineering. Adv Mater. 2015;27(19):2989-2995. doi:10.1002/adma.201405873

16. Pooyan P, Tannenbaum R, Garmestani H. Mechanical behavior of a cellulose-reinforced scaffold in vascular tissue engineering. J Mech Behav Biomed Mater. 2012;7:50-59. doi:10.1016/j.jmbbm.2011.09.009

17. Hu Y, Catchmark JM. Integration of cellulases into bacterial cellulose: Toward bioabsorbable cellulose composites. J Biomed Mater Res - Part B Appl Biomater. 2011;97 B(1):114-123. doi:10.1002/jbm.b.31792

18. Bačáková L, Novotná K, Pařzek M. Polysaccharides as cell carriers for tissue engineering: The use of cellulose in vascular wall reconstruction. Physiol Res. 2014;63(SUPPL.).

19. Saito T, Nishiyama Y, Putaux J-L, Vignon M, Isogai A. Homogeneous Suspensions of Individualized Microfibrils from TEMPO-Catalyzed Oxidation of Native Cellulose. Biomacromolecules. 2006;7(6):1687-1691. doi:10.1021/bm060154s

20. Syverud K, Pettersen SR, Draget K, Chinga-Carrasco G. Controlling the elastic modulus of cellulose nanofibril hydrogels—scaffolds with potential in tissue engineering. Cellulose. 2015;22(1):473-481. doi:10.1007/s10570-014-0470-5

21. Bhattacharya M, Malinen MM, Lauren P, et al.

Nanofibrillar cellulose hydrogel promotes three-dimensional liver cell culture. J Control Release. 2012;164(3):291-298. doi:10.1016/j.jconrel.2012.06.039

22. Pooyan P, Kim IT, Jacob KI, Tannenbaum R, Garmestani H. Design of a cellulose-based nanocomposite as a potential polymeric scaffold in tissue engineering. Polymer (Guildf). 2013;54(8):2105-2114. doi:10.1016/j.polymer.2013.01.030

23. Lou Y-R, Kanninen L, Kuisma T, et al. The Use of Nanofibrillar Cellulose Hydrogel As a Flexible Three-Dimensional Model to Culture Human Pluripotent Stem Cells. Stem Cells Dev. 2013;23(4):380-392. doi:10.1089/scd.2013.0314

24. Sannino A, Demitri C, Madaghiele M. Biodegradable cellulose-based hydrogels: Design and applications. Materials (Basel). 2009;2(2):353-373. doi:10.3390/ma2020353

25. Polacheck WJ, German AE, Kamm RD, Ingber DE, Mammoto A. Mechanotransduction of fluid stresses governs 3D cell migration. Proc Natl Acad Sci. 2014;111(7):2447-2452. doi:10.1073/pnas.1316848111

26. Alexander FA, Wiest J. Online, label-free monitoring of organ-on-a-chip models: The case for microphysiometry. Proc Annu Int Conf IEEE Eng Med Biol Soc EMBS. 2015;2015-Novem:7091-7094. doi:10.1109/EMBC.2015.7320026

27. van Duinen V, Trietsch SJ, Joore J, Vulto P, Hankemeier T. Microfluidic 3D cell culture: From tools to tissue models. Curr Opin Biotechnol. 2015;35:118-126. doi:10.1016/j.copbio.2015.05.002

28. Chee PN, Pun SH. A perfusable 3D cell-matrix tissue culture chamber for in situ evaluation of nanoparticle vehicle penetration and transport. Biotechnol Bioeng. 2008;99(6):1490-1501. doi:10.1002/bit.21698

29. Gaffey AC, Chen MH, Venkataraman CM, et al. Injectable shear-thinning hydrogels used to deliver endothelial progenitor cells, enhance cell engraftment, and improve ischemic myocardium. J Thorac Cardiovasc Surg. 2015;150(5):1268-1277. doi:10.1016/j.jtcvs.2015.07.035

4 Cellulose Nanofibril Hydrogel Promotes Hepatic Differentiation of Human Liver Organoids

Melanie Krüger[1,2], Loes A. Oosterhoff[1], Monique E. van Wolferen[1], Simon A. Schiele[3], Andreas Walther[4], Niels Geijsen[1,5], Laura De Laporte[3], Luc J.W. van der Laan[6], Linda M[2]. Kock, Bart Spee[1]*

[1]Department of Clinical Sciences of Companion Animals, Faculty of Veterinary Medicine, Utrecht University, Uppsalalaan 8, 3584 CT Utrecht, The Netherlands

[2]LifeTec Group BV, Kennedyplein 10-11, 5611 ZS Eindhoven, The Netherlands

[3]DWI – Leibniz-Institut für Interaktive Materialien e.V.; Advanced Materials for Biomedicine, ITMC – Institute of Technical and Macromolecular Chemistry, RWTH University Aachen Forckenbeckstr. 50, 52056 Aachen, Germany

[4]Albert-Ludwigs-Universität Freiburg, Institute for Macromolecular Chemistry, Stefan-Meier-Strasse 3, Hermann Staudinger Building, 79104 Freiburg, Germany

[5]Hubrecht Institute for Developmental Biology and Stem Cell Research, University Medical Center Utrecht, Uppsalalaan 8, 3584 CT Utrecht, The Netherlands

[6]Department of Surgery, Erasmus MC, Postbus 2040, 3000 CA Rotterdam, the Netherlands

*Corresponding author

4.1 Abstract

To replicate functional liver tissue *in vitro* for drug testing or transplantation, 3D tissue engineering requires representative cell models as well as scaffolds that not only promote tissue production but also are applicable in a clinical setting. Recently, adult liver-derived liver organoids are found to be of much interest due to their genetic stability, expansion potential, and ability to differentiate toward a hepatocyte-like fate. The current standard for culturing these organoids is a basement membrane hydrogel like Matrigel (MG), which is derived from murine tumor material and apart from its variability and high costs, possesses an undefined composition and is therefore not clinically applicable. Here, a cellulose nanofibril (CNF) hydrogel is investigated with regard to its potential to serve as an alternative clinical grade scaffold to differentiate liver organoids. The results show that its mechanical properties are suitable for differentiation with overall, either equal or improved, functionality of the hepatocyte-like cells compared to MG. Therefore, and because of its defined and tunable chemical definition, the CNF hydrogel presents a viable alternative to MG for liver tissue engineering with the option for clinical use.

4.2 Introduction

Liver diseases were the 12th leading cause of death in the United States in 2015 and the numbers are increasing.[1] Reasons for this high mortality include a lack of good treatments, a shortage of donor livers for transplantation and a lack of knowledge about underlying pathologies.[2] The aim of liver tissue engineering is to develop three-dimensional (3D) liver tissues that replicate the *in vivo* liver functions as close as possible.[3] Successful liver constructs can on one hand side serve as a testing platform for xenobiotics, toxins, or as disease models.[4] On the other side, they can be used *in vivo* as an alternative for donor organs and as a basis for stimulating liver regeneration through cell delivery.[4]

Considering that one of the most significant causes for an acute liver failure (ALF) are drug induced liver injuries (DILI) (11% of all ALF cases in the United States),[5] there is a clear need for preclinical drug testing models that can accurately predict the effect of drugs on the liver tissue and improve the success rate of only 10% in clinical drug testing.[6] Current tissue engineered liver models have significant disadvantages that hamper their use. Presently, the gold standard to test toxicity and metabolism consists of primary human hepatocyte

cultures in 2D. However, 2D cultures fail to represent the complex 3D structure of native liver tissue[7] and further problems associated with primary hepatocytes are limited availability, restricted lifespan, rapid dedifferentiation, functional variability and a limit in drug transporter activity.[8] Moreover, despite their large replication capacity *in vivo*, hepatocytes cannot be expanded in culture.[9] A predictive cell model, therefore, needs to have a stable hepatic signature and the potential to expand in order to be readily available,[9] and should be three-dimensional.[8] For stem cell-derived hepatocyte like cells or even adult hepatocytes, it is known that a three-dimensional structure leads to an improved survival rate and functional phenotype.[10]

One of the potential solutions is using liver-derived adult stem cells cultured as organoids. These organoids create structures that resemble their organ of origin by assembling themselves into a 3D structure and growing and expanding *in vitro*.[11] Adult stem cells isolated from human liver biopsies can be cultured in a 3D extracellular matrix (ECM) mimicking the microenvironment of these cells *in vivo*.[11] Liver organoids allow for an almost infinite and genetically stable expansion of adult stem cells *in vitro* and can be differentiated into hepatocyte-like cells.[9] These organoids are maintained in Matrigel™, which is a

thermosensitive hydrogel prepared from a basement membrane-rich sarcoma, the Engelbreth-Holm-Swarm (EHS) murine tumor, which must be propagated in mice.[12] Therefore Matrigel[TM] is a material of undefined murine origin with a high batch-to-batch variability of up to 50%[13] and high purchase costs.[12] In order for the liver organoids to be used in *in vitro* models or in the clinic, new hydrogels need to be tested that 1) allow for a better hepatic differentiation, and 2) provide a scaffold that can be applied clinically. For clinical application it is essential for the material to have the potential for approval by the FDA or other regulatory bodies and comply with good manufacturing practices, which is not possible for Matrigel[TM], due to the animal origin and undefined composition.[3]

One potential alternative biomaterial for Matrigel[TM] that is shear thinning, swellable in water, and enables 3D cell culture is cellulose, which is the most abundant biopolymer on earth with its main source being cell walls of plants.[14,15] In nature, cellulose is formed by micron-sized fibril agglomerations of diameters between 2 and 20 μm, depending on its source.[16] Extraction can be achieved through oxidation mediated by 2,2,6,6-tetramethylpiperidinyl-1-oxyl (TEMPO), which catalyzes the oxidation of primary alcohol groups in the presence of

water.[16] In this way, aldehyde and carboxyl groups are introduced[17] on to the surface of the fibers[16] resulting in a negative surface charge which enables the subsequent separation of the fibrils[17] with a pressure homogenizer.[18] This results in nanofibrils with a thickness of 2.5 ± 2 nm that are very crystalline and have a high aspect ratio.[18] These fibrils, consisting of β-D glycopyranose polysaccharide chains[6] are one of the stiffest natural biomaterials with $E_{cellulose.I} = 138$ GPa and they are the underlying reason for the remarkable mechanical properties of the hydrogel.[18] When mixed with water, they form reversible cellulose nanofibril hydrogels (CNF)[17] already at very low solid contents[18] of approximately 0.2%. The nanoscale network within this hydrogel can be seen in SEM images of the material.[19] The shear-thinning and self-healing behavior associated with this hydrogel[18] is due to the entanglement, hydrogen bonds and ionic interactions that keep it together,[17] which also prevent degradation in aqueous environments.[20] The CNF is naturally biocompatible[12,21] and has therefore been used for different tissue engineering applications. Among those with promising results are cultures in CNF hydrogel of stem cells,[12] culture[6] and differentiation[8] of liver cell lines such as HepaRG and HepG2 or progenitor cell thereof and as a sacrificial template for the engineering of tubular

cell constructs.[19] The hydrogel is very stable in the long-term and fabrication costs are much lower compared to other materials, such as Matrigel[TM].[20] CNFs are not degradable in humans,[14,22,23] but controlled degradation can be achieved by either adding the enzyme cellulase[12,22] or making use of the shear thinning properties and reaching degradation through medium flow[24] if desired.

To our knowledge cellulose nanofibril hydrogels have only been tested in combination with cell lines, which are associated with the above-mentioned drawbacks. Cellulose as a natural polymer in combination with human liver organoids would fulfil most of the significant characteristics necessary for successful liver tissue engineering mentioned in a recent review on the specific demands of hydrogels for this purpose[3]. These are namely the human autologous cell source, the potential to include vasculature, possible additions of bioactive substrates, biocompatibility, bioprintability, chemical definition, mechanical properties in the range of 0.2 – 1 kPa and the possibility to be degradable. Therefore, the aim of this study is to test the potential of CNF hydrogels as a scaffold for liver tissue engineering. For that purpose, human liver organoids from several donors were differentiated in CNF hydrogels and examined with

respect to their metabolic activity, maturation level, functionality, and polarization in comparison to Matrigel™ to assess the potential of CNF as a scaffold for differentiation of human liver organoids into functional hepatocytes for toxicity testing and regenerative medicine.

4.3 Materials and Methods

4.3.1 Cellulose Nanofibril Hydrogel

The cellulose nanofibril hydrogel was produced with the TEMPO method, where paper pulp (Papiertechnische Stiftung, Heidenau, Germany) is oxidized, then dispersed in water and homogenized under high pressure.[18,44,45] Sterility was achieved by autoclaving the gel at 121°C for 20 min. The stock concentration of cellulose (CNF) after this procedure is 0.6 % w/v (CNF 0.6) at a pH of 6. The 0.6 % w/v CNF hydrogel was diluted with sterile demineralized water to 0.4 % w/v (CNF 0.4) and 0.2 % w/v (CNF 0.2).

4.3.2 Organoid Expansion and Differentiation

Human liver organoid cultures were generated from three independent, anonymized adult organ donors. Tissue samples (<0.5 cm^3) of donor liver biopsies were collected during liver transplantation at the Erasmus Medical Center

Rotterdam are routinely taken to test for any liver pathology. Use of these tissues for research purposes was approved by the Medical Ethical Council of the Erasmus MC and informed consent was given by recipients (MEC-2014-060). Biopsies were stored in ice cold organ preservation fluid (University of Wisconsin Solution, Bridge of Life Ltd, London, UK) for transportation and processed for organoid-initiation as described previously [8]. In short, cells were cultured in Matrigel™ (Corning, New York, NY, USA) droplets in 24-well plates in EM for up to 13 passages. EM consisted of Advanced DMEM/F12 supplemented with 1% (v/v) penicillin-streptomycin (ThermoFisher, Waltham, Massachusetts, USA), 1% (v/v) GlutaMax (ThermoFisher), 10 mM HEPES (ThermoFisher), 2% (v/v) B27 supplement without vitamin A (Invitrogen, Carlsbad, CA, USA), 1% N2 supplement (Invitrogen), 10×10^{-3} M nicotinamide (Sigma-Aldrich, Zwijndrecht, the Netherlands), 1.25×10^{-3} M N-acetylcysteine (Sigma-Aldrich), 10% (v/v) R-spondin-1 conditioned medium (the Rspo1-Fc-expressing cell line was a kind gift from Calvin J. Kuo), 10×10^{-6} M forskolin (Sigma-Aldrich), 5×10^{-6} M A83-01 (Tocris Bioscience, Bristol, UK), 50 ng mL^{-1} EGF (Invitrogen), 25 ng mL^{-1} HGF (Peprotech, London, UK), 0.1 mg mL^{-1} FGF10 (Peprotech), 10×10^{-9} M recombinant human (Leu15)-

gastrin I (Sigma-Aldrich), and 0.1 mg mL^{-1} Noggin (Peprotech).

In order to assess the possibility to expand liver organoids in CNF hydrogel, organoids cultured in Matrigel^{TM} (Corning) were reseeded into either 50 µl fresh Matrigel^{TM}, CNF 0.4 or CNF 0.6 (n=3 for each condition) and cultured with 500 µl EM medium for 7 days with medium changes on day 2 and 4.

For the differentiation experiments, EM was supplemented with 25 ng mL^{-1} BMP-7 (Peprotech) four days prior to organoid transfer and the start of differentiation. At the start of differentiation, the organoids were reseeded into 50 µL Matrigel^{TM} or CNF hydrogels (CNF 0.2, CNF 0.4, CNF 0.6) and differentiation medium (DM) was added. DM consisted of EM without R-spondin-1 and nicotinamide but with the addition of 25 ng mL^{-1} BMP7 (Peprotech), 10×10^{-6} M DAPT (γ-secretase inhibitor, Selleckchem, Houston, TX, USA), 100 ng mL^{-1} FGF19 (R&D Systems, Minneapolis, MN, USA), and 30×10^{-6} M dexamethasone (Sigma-Aldrich). Media was refreshed on day 4 and day 6 until the culture was terminated on day 7. In the case of Matrigel^{TM}, EM was added as a control.

4.3.3 Analyses

Hydrogel characterization

Rheological tests to characterize the material (n = 1) were performed on the stock concentration of 0.6 % w/v CNF hydrogel with a 1HR-3 DHR-3 rheometer in combination with a SST ST 20 mm 2° smart-sweep cone plate and analyzed with Texas Instrument TRIOS software (Texas Instruments, Dallas, TX, USA). The protocol for characterization of a hydrogel was applied as described by Zuidema et al. [27] and adopted according to Rowland et al. [26]. For all measurements 400 µL of CNF hydrogel was used, the gap between plates was set to 0.5 mm, and temperature was constant at 20°C. The gel was soaked for 60 sec in order to allow the gels to swell after compression and equilibrate to the temperature. Dynamic oscillatory amplitude sweep measurements were taken at 1 rad/s and oscillatory frequency sweep measurements were conducted at 0.5 % oscillating strain. For altering strain experiments, the strain was altered between 1 and 500 % in periods of 30 sec and flow sweeps were conducted with 5 sec equilibration time and 30 sec averaging time. The Young's modulus (E) was calculated by determining the plateau value of the frequency sweep

(G'_e) and with an assumed Poisson's ratio (v) of 0.5 of incompressible materials according to Equation (1):

$$E = 2 * G'_e (1+ v) \qquad (1)$$

Swelling of the prepared gel was measured by submerging 0.5 of the 0.6 % w/v CNF hydrogel in 2 mL demineralized water and 1x PBS for 30 min, 1h, and 4h and the liquid is renewed after 2 min, 20 min and then every hour (n=3). For each timepoint the swelling ratio is calculated by measuring the wet weight of the swollen gels with the cellulose concentrations before and after swelling.

Morphology

The morphology of the organoids was followed over time for all conditions and brightfield images were taken at day 1 and day 7 after the start of differentiation with an Olympus Color CCD microscope (CKX41, Tokyo, Japan), Leica DFC425C camera, and accompanying Leica-suite software (Wetzlar, Germany), and postprocessed with Image-J software (NIH, Madison, Wisconsin, USA).

Metabolic activity

Metabolic activity of the organoids in all conditions was measured on day 1, 4, 6, and 7 (day 2, 4, and 7 for the expansion experiment) with the Alamar Blue assay (Invitrogen) with n = 3 per condition. The Alamar Blue solution was diluted to 10% (v/v) with Advanced DMEM/F12 medium (Gibco) and incubated in three wells for each hydrogel condition and donor, and wells with gel but without organoids (n = 3 per condition) for 2 hours. Fluorescence was measured at 540/590 nm with a DxC-600 Beckman plate reader (Beckman Coulter, Brea, CA, USA) and the levels of the wells without organoids were subtracted from the read-outs for background correction. All values were compared to day 1, which was set to 100 % of metabolic activity.

Gene expression

Gene expression analysis on all conditions (MG, CNF 0.2, CNF 0.4, CNF 0.6) and respective medium condition (DM, EM) were used to assess the differentiation status of the organoids (n = 6 per condition). The samples were lysed with 350 µL RLT buffer (Qiagen, Hilden, Germany) containing 1% (v/v) 2-Mercaptoethanol (Sigma-Aldrich). Isolation of mRNA was done according to the

manufacturer's instructions with a RNeasy micro-kit (Qiagen) and the total mRNA was measured with a NanoDrop ND-1000 spectrophotometer (Thermo Fisher Scientific, Breda, The Netherlands) at 260/280 nm. For the synthesis of complementary DNA (cDNA) from 500 ng mRNA, the manufacturer's protocol for the used iScript cDNA Synthesis Kit (Bio-Rad, Hercules, CA, USA) was applied. Quantitative PCR (qPCR) was performed using a Bio-Rad CFX384 Real-Time PCR Detection System (Bio-Rad) with 10 ng cDNA per reaction and iQ™ SYBR® Green Supermix (Bio-Rad). Primers are listed in Table 1. Data was analyzed with BioRad CFX manager software (CFX Maestro, Bio-Rad, Hercules, CA, USA), relative gene expression was calculated according to the $2^{-\Delta CT}$ formula and normalized to the reference genes GAPDH and RPL19. As reference, samples from hepatocytes pooled from 10 donors (mixed gender, LiverPool™ Cryoplateable Hepatocytes, BioreclamationIVT, Brussels, Belgium) and a whole liver sample from one donor were added to the analysis.

Table 1: Primers used for qPCR analysis.

Gene	Forward	Reverse
RPL19	ATGAGTATGCTCAGGCTTCAG	GATCAGCCCATCTTTGATGAG
GAPDH	TGCACCACCAACTGCTTAGC	GGCATGGACTGTGGTCATGAG
LGR5	GCAGTGTTCACCTTCCC	GGTCCACACCCAATTCTG
KRT19	CTTCCGAACCAAGTTTGAGAC	AGCGTACTGATTTCCTCCTC
ALB	GTTCGTTACACCAAGAAAGTACC	GACCACGGATAGATAGTCTTCTG
HNF4A	GTACTCCTGCAGATTTAGCC	CTGTCCTCATAGCTTGACCT
CYP3A4	TGATGGTCAACAGCCTGTGCTGG	CCACTGGACCAAAAGGCCTCCG
CYP1A2	CCCAGAATGCCCTCAACA	CCACTGACACCACCACCTGAT
CYP2D6	GAGGTGCTGAATGCTGTC	AGGTCATCCTGTGCTCAG
CYP2C19	GGGACAGAGACAACAAGCA	CCTGGACTTTAGCTGTGACC
UGT	AATACTCGGCTGTATGATTGG	CATAGATCCCATTCATTCCACC
SULT	TTCCTTGAGTTCAAAGCCC	TGTCTTCAGGAGTCGTGG
MRP2	GCCAACTTGTGGCTGTGATAGG	ATCCAGGACTGCTGTGGGACAT
BSEP	TTGAGACAATAGACAGGAAACC	TCTGGAAGGATAATGGAAGGT

Hepatic function

To measure the enzyme activity, the same samples that have been used for metabolic activity analysis (n = 3 per condition) were lysed with Milli-Q water (Merck, Millipore, Burlington, MA, USA). Subsequently, ALAT, ASAT, Albumin, GLDH, as well as total protein, were measured with the clinical chemistry analyzer Beckman AU680 (Beckman Coulter, Brea, CA, USA) using standard protocols. Finally, albumin values were corrected for total protein levels and all enzyme values were divided by the metabolic activity values to correct for the number of viable cells.

Histology

Hydrogel samples from each condition (n = 2 per condition) were fixed with 4% paraformaldehyde and embedded in paraffin. For stainings, 5 µm sections were cut and sections were deparaffinized and rehydrated.

For immunohistochemistry, the slides were blocked in 10% v/v normal goat serum (Bio-Rad), after antigens were retrieved. Antigen retrieval for albumin and HNF4a staining was achieved with a 10 mM Tris/1 mM EDTA solution (both Sigma-Aldrich) with 0.5% Tween 20 (Merck KGaA, Darmstadt, Germany) at pH 9.0 for 30 min at 98°C. For MRP2 antigen retrieval was performed with a 10 mM citrate buffer (Merck) at pH 6 for 30 min at 98°C and ZO1 antigen retrieval was performed with 0.4 % w/v pepsin (Dako, Santa Clara, CA, USA) in 0.2 N HCl (Merck) for 20 minutes at 37 °C. The primary antibody for albumin (A6684, Sigma), was incubated in a 1:1,000 dilution; HNF4a (sc8987, Santa Cruz, Dallas, TX, USA) in a 1:300 dilution; MRP2 (Mon9027, Monosan, Uden, the Netherlands) in a 1:75 dilution; and ZO1 (40-2300, Invitrogen) in a 1:250 dilution, all incubations were performed overnight at 4°C. The wash buffer for albumin, HNF4a, MRP2 and ZO1 was PBS + 0.1 % (v/v) Tween 20. Envisioning of the antibodies was achieved with goat-

anti-mouse/rabbit HRP (ImmunoLogic, Amsterdam, the Netherlands) and DAB/metal (ImmunoLogic, Amsterdam, the Netherlands) concentrate. As a counterstain hematoxylin (Dako, Glostrup, Denmark) was applied and slides were mounted with Vectamount (Vector Laboratories, Peterborough, United Kingdom) after dehydration. Images were taken on the Olympus BX60 microscope (Olympus, Leiderdorp, the Netherlands) and processed with Image-J software (NIH, Madison, Wisconsin, USA).

The PAS staining was performed by the Veterinary Pathology Diagnostics Centre in Utrecht according to the standardized procedures.

Statistical analysis

Extreme outliers with values more than three times the interquartile range are identified for each outcome parameter and excluded from further analysis using SPSS Statistics 25 (IBM, Armonk, USA). Statistical analysis for all data was performed with Graphpad Prism 8 (San Diego, CA, USA).

For the metabolic activity studies with averaged CNF hydrogel concentrations, a two-way ANOVA analysis was performed followed by a Tukey post-hoc test. For the

metabolic activity study comparing different CNF hydrogel conditions, multiple t-tests using the Holm-Sidak method were executed. After careful investigation of all data, no significant differences between the different CNF hydrogel concentrations were found (see Figures S2, S3, S4). Therefore, data for each read-out of all CNF hydrogel concentrations were averaged in further analysis. Data of transaminase activity and gene expression averaged over CNF hydrogel concentrations has been log transformed and then a one-way ANOVA was performed with Tukey's post-hoc test. Data of transaminase activity and gene expression comparing different CNF hydrogel concentration has been log transformed and then a mixed- effects analysis was performed to account for missing values followed by Tukey's post-hoc test All transformed data was back transformed for reporting. All analyzed data was normally distributed and had equal variances as tested by examining the normal Q-Q plot of residuals and by examining the scatter plots of residuals over predicted values respectively. Differences were considered statistically significant for $p < 0.05$ and p-values are depicted in the figures, where asterisks represent the statistical significance (*$p < 0.05$, **$p < 0.01$ ***$p < 0.001$, ****$p < 0.0001$, ns: not significant). Furthermore, n refers to the sample size for each

statistical analysis. Data is presented as a box diagram with median and 25th and 75th percentiles and whiskers from min to max for metabolic activity (DM conditions) data and bar graphs with mean and standard deviation for all other data sets.

4.4 Results

4.4.1 Hydrogel characterization

In order to examine the mechanical characteristics of the hydrogel, we have performed a rheological analysis by conducting an amplitude sweep measurement (Figure 1A), frequency sweep (Figure 1B), altering strain measurement (Figure 1C), and dynamic viscosity measurement (Figure 1D). As is visualized in Figure 1A, CNF hydrogel exhibits highly elastic behavior with *G'* (84.1 ± 4.2 Pa) roughly 10 times that of *G''* (8 ± 0.4 Pa) before the critical strain point of about 100% strain. From the frequency sweep in Figure 1B it can be seen that *G'* and *G''* are nearly constant over the range of frequencies between 0.1 to 10 rad/s with *G'* > *G''*. Rapid self-healing is demonstrated by the altering strain experiment shown in Figure 1C. At high strains *G''* is higher than *G'*, but by altering back to low strain, the storage modulus *G'* recovers quickly, restoring the original viscoelastic property. Complete recyclability is shown by repeating this

process over 5 cycles without a change in property. The CNF hydrogel also demonstrates shear-thinning behavior as can be seen in Figure 1D with a viscosity decrease for increasing shear rates. The Young's modulus (E) is calculated to be approximately 255 Pa with a plateau value of G' of 85 Pa of the frequency sweep.
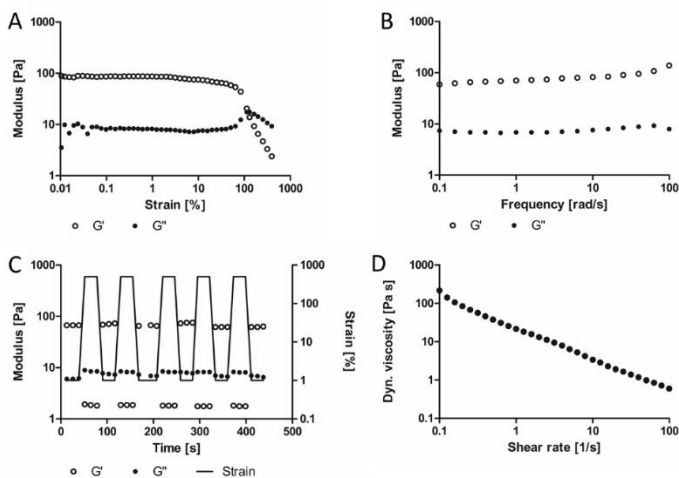
Figure 1: Rheological data of 0.4 mL of 0.6 % (w/v) CNF hydrogel at 20°C and a plate gap of 0.5 mm. A) Dynamic oscillatory amplitude sweep measurement at 1 rad*sec^{-1}, B) Frequency sweep measurements at 0.5% oscillating strain,) Altering strain measurement between 1 and 500 % in periods of 30 sec, D) Dynamic viscosity measurement with 5 sec equilibrium time and 30 sec averaging time

As can be seen in Figure 2, the swelling ratio of the CNF hydrogel in demineralized water increases by 17% (±7.5) after only 30 min, which reduces the cellulose concentration from 0.6 % (w/v) to 0.54 % (w/v) (±0.04) and

there is no equilibrium reached after 4h. This is also the reason for the high standard deviations, as differentiation between the hydrogel and water is hardly possible after extended swelling times. This effect is not observed for swelling in PBS, where an equilibrium is reached after only 30 min. Morphology and metabolic activity
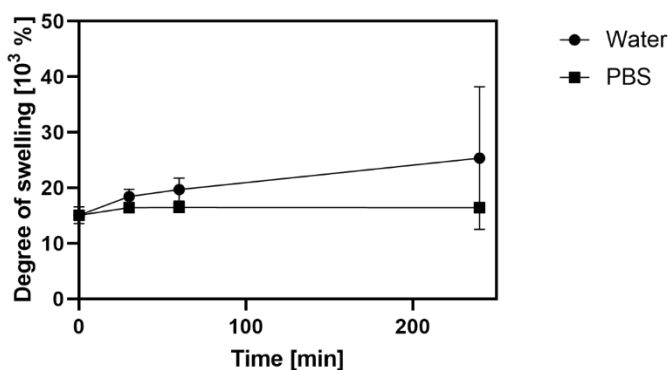
Figure 2: Degree of swelling for 0.5 mL 0.6 % (w/v) CNF hydrogel in 2 mL demineralized water and 1X PBS over 4 hours, data depicted as mean ± SD (n=3)

To test the potential of human liver organoids to expand within the cellulose nanofibril hydrogel (CNF) hydrogel, the organoids were reseeded into Matrigel™ (MG) and CNF hydrogels and cultured for 7 days with expansion medium (EM). The Alamar Blue staining (Figure S1) shows that there is no significant increase in metabolic activity over the culture period within the CNF hydrogel, whereas the metabolic activity increases by 73% (p =

0.0011) in MG, which indicated that organoids cannot be propagated in CNF.

For assessing the differentiation potential, human liver organoids from three donors were expanded in Matrigel™ before being transferred to another Matrigel™ or to CNF. In Matrigel™, two different media conditions were compared: EMand differentiation medium (DM). In CNF hydrogel, only DM was used to show the differentiation potential of the biomaterial. In Figure S2, it is shown that the metabolic activity within each day is not significantly different between any of the CNF hydrogel concentrations, therefore the data was averaged over all donors and CNF hydrogel concentrations and representative images are shown for morphology. When comparing CNF hydrogels to Matrigel™, more condensed, smaller and darker human liver organoids were observed (Figure 3A). In the case of DM, the organoids did not appear to be proliferating in both MG and CNF hydrogel, while control samples cultured in MG with EM continued to grow over these 7 days. This was confirmed by the Alamar blue staining, indicating that the total metabolic activity increases over time for organoids cultured in Matrigel™ in EM up to 120 % (p = 0.0011) on day 7 (Figure 3B). The organoids in MG and DM show no significant change in metabolic activity. In CNF hydrogel,

an initial reduction of metabolic activity was observed for all donors with an average decrease of 23 % ($p < 0.0001$) from day 1 to day 4 but no significant difference between day 4 and day 7.
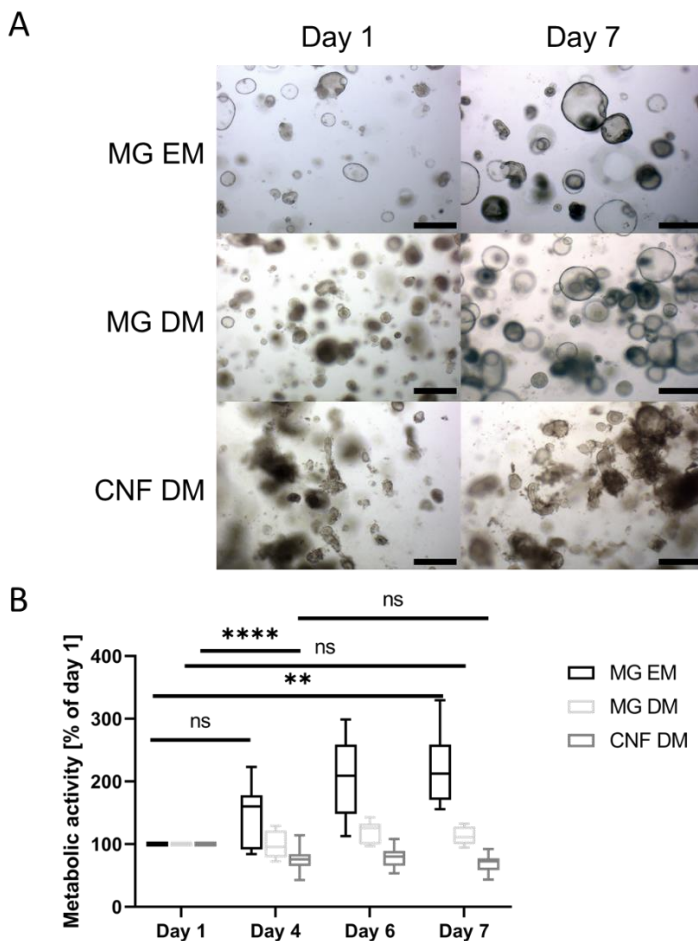
Figure 3: A) Representative brightfield images showing liver organoid morphology on day 1 and day 7 after transfer into Matrigel^{TM} under EM or DM conditions, or into CNF hydrogel 0.4% (w/v) under DM conditions, scale bar 500 µm; B) Metabolic activity at day 4, 6, and 7 relative to values at day 1 (n= 9 for MG EM and DM, n=24 for CNF DM); data depicted as box with median and 25th and 75th percentile and whiskers from min to max, (**p < 0.01, ****p < 0.0001, ns: not significant), ANOVA with Tukey's post-hoc test.

4.4.2 Gene expression

To determine the maturation level and fate of the hepatocyte-like cells after differentiation for 7 days in both CNF hydrogel and MG, expression of genes was tested for DM and EM conditions. In Figure S3 it is shown that gene expression is not statistically different between the great majority of the CNF concentrations, therefore the data was averaged over all cell donors and CNF conditions. For comparison, primary hepatocytes and a liver sample were analyzed simultaneously. Overall, expression levels of genes are always higher in DM compared to EM conditions, while in some cases the CNF hydrogel even outperforms Matrigel^{TM}. For example, expression levels of adult phase I specific enzymes, which belong to the cytochrome P450 family (CYP3A4, CYP1A2, CYP2D6, CYP2C19), demonstrate organoid functionality (Figure 4,). From these genes, CYP3A4 is expressed at 59 % (p = 0.0373) higher levels in CNF DM compared to MG DM. For the phase II enzymes, UDP glucuronosyltransferase (UGT) (Figure 4K) and sulfotransferase (SULT) (Figure 4J), SULT presents a 32 % (p = 0.0205) higher level of expression in the case of CNF DM over MG DM. Finally, phase III enzymes mitochondrial ribosomal protein S2 (MRP2) (Figure 4I) and ATP binding cassette subfamily B member 11 (BSEP)

(Figure 4E) both show no significant difference between organoids in CNF hydrogel or Matrigel™ in DM. Only the stem cell marker leucine rich repeat containing G protein-coupled receptor 5 (LGR5), is expressed at significantly lower levels in both DM conditions (MG or CNF) compared to EM. Interestingly, some expression of this stem cell marker remained in CNF hydrogels (55 %, p = 0.0117), while no expression was observed in Matrigel™ with DM (Figure 4H).
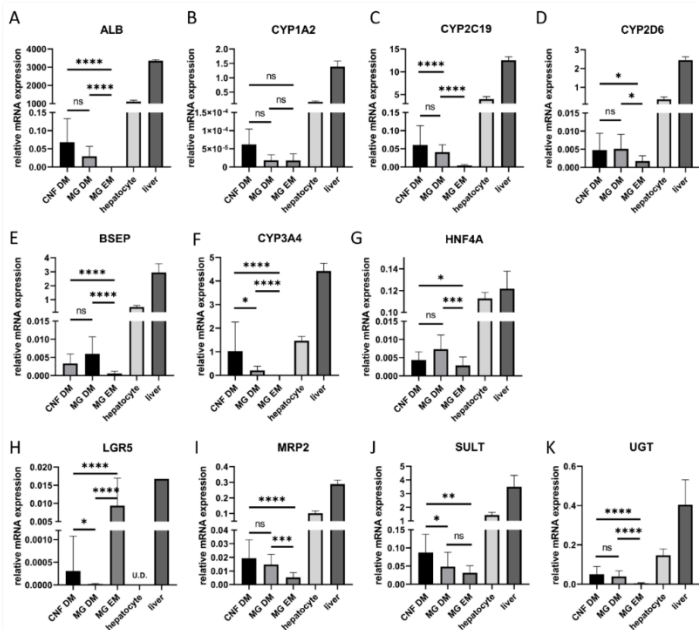
Figure 4: Relative gene expression to GAPDH and RPL19 of liver organoids differentiated in Matrigel™ and CNF hydrogels (MG DM, CNF DM) for 7 days or cultured for 7 days in Matrigel™ with EM (MG EM), with levels of native liver and hepatocytes as controls. Data is averaged over all CNF hydrogel concentrations (0.2 – 0.6 % w/v) and donors. A) Albumin expression (n=15 for MG EM, n=15 for MG DM, n=39 for CNF), B) CYP1A2 expression (n=4 for MG EM, n=8 for MG DM, n=21 for CNF), C) CYP2C19 expression (n=15 for MG EM, n=15 for MG DM, n=39 for CNF), D) CYP 2D6 expression (n=15 for MG EM, n=15 for MG DM, n=42 for CNF), E) BSEP expression (n=15 for MG EM, n=15 for MG DM, n=40 for CNF), F) CYP3A4 expression (n=15 for MG EM, n=15 for MG DM, n=40 for CNF), G) HNF4a expression (n=15 for MG EM, n=15 for MG DM, n=41 for CNF), H) LGR5 expression (n=12 for MG EM, n=12 for MG DM, n=33 for CNF), I) MRP2 expression (n=15 for MG EM, n=15 for MG DM, n=42 for CNF), J) SULT expression (n=12 for MG EM, n=13 for MG DM, n=29 for CNF), K) UGT expression (n=15 for MG EM, n=14 for MG DM, n=35 for CNF). All data depicted as mean ± SD (*p < 0.05, **p < 0.01 ***p < 0.001, ****p < 0.0001, ns: not significant), ANOVA with Tukey's post-hoc test.

4.4.3 Transaminase activity

In order to further evaluate the performance of CNF hydrogels for differentiation of human liver organoid cultures in comparison to MG, the functionality of the hepatocyte-like cells was investigated by measuring the transaminase activity. For this purpose, cells were collected after 7 days of culture, where organoids in CNF hydrogels were differentiated with DM, whereas organoids in MG were cultured in both EM and DM respectively. No significant differences between any CNF hydrogel concentrations (Figure S4) results were seen and therefore data was averaged over donors and gel concentrations. Multiple hepatic markers were significantly higher in organoids under CNF DM conditions compared to MG DM conditions, such as alanine aminotransferase (ALAT) (28%, $p < 0.0001$) (Figure 5), aspartate transaminase (ASAT) (22 %, $p = 0.009$), albumin production (85 %, $p < 0.0001$), and glutamate dehydrogenase (GLDH) production (14%, $p = 0.0459$). Interestingly, ALAT enzyme, albumin, and GLDH production is not significantly different in Matrigel™ when DM or EM is used. In contrast, organoids cultured in CNF hydrogel demonstrated higher levels of these differentiation signals compared to Matrigel™.
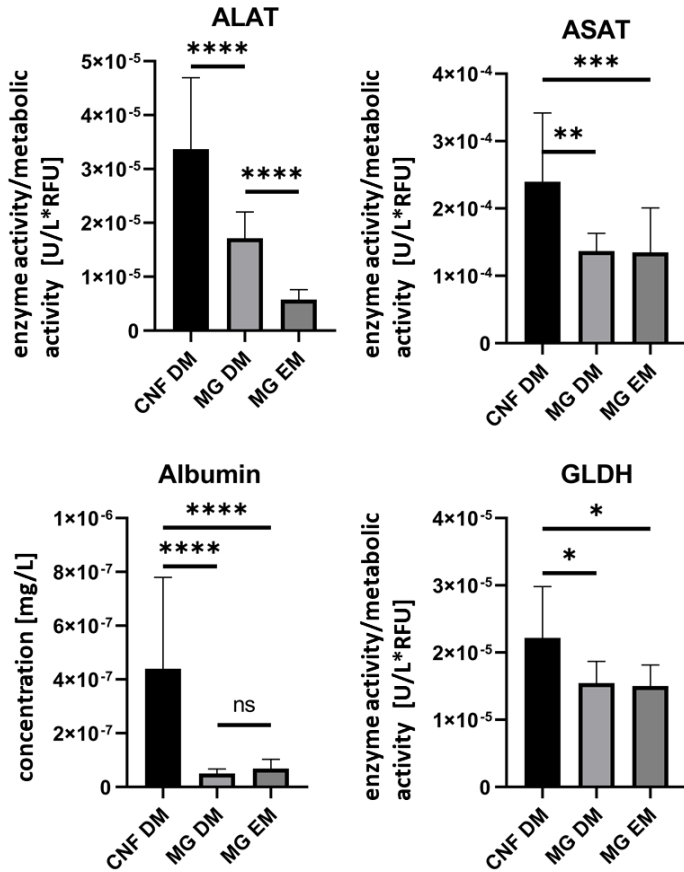
Figure 5: Functional read-out in relative enzyme activity and albumin concentration corrected to the metabolic activity of hepatocyte-like cells lysed after 7 days of differentiation in CNF hydrogel (data averaged over all concentrations) and Matrigel^{TM} in DM (CNF DM (n=16 for Albumin and GLDH, n=24 for ALAT and ASAT), MG DM (n=6 for Albumin and GLDH, n=9 for ALAT and ASAT)) as well as in Matrigel^{TM} in EM (MG EM (n=6 for Albumin and GLDH, n=9 for ALAT and ASAT)) as comparison. Data is averaged over all donors, all data depicted as mean ± SD (*p < 0.05, **p < 0.01 ***p < 0.001, ****p < 0.0001, ns: not significant), ANOVA with Tukey's post-hoc test.

115

4.4.4 (Immuno-)cytology

For visualization and determination of specific expression sites, sections of the human liver organoids from all donors cultured in CNF hydrogel in DM or MG in DM or EM for 7 days, were stained immunocytochemically. Antibodies against the differentiation markers albumin, HNF4a, MRP2, tight junction protein and polarization marker ZO1, as well as for glycogen accumulation with the Periodic acid-Schiff stain (PAS) were applied (Figure 6). The increase in albumin RNA levels in CNF hydrogels was confirmed by immunocytochemistry (Figure 6C), especially when compared to MG EM conditions (Figure 6A). The localization of albumin in MG is on the luminal side (Figure 6B), whereas it is on the apical side of the organoid in CNF. The early hepatocyte specification marker HNF4a is a transcription factor in the nuclei of organoids, therefore every staining outside the nuclei is unspecific. The specific nuclear staining can only be seen in CNF DM (Figure 6F) conditions, in MG EM and DM it is unspecific (Figure 6D, E). Another marker is MRP2, a protein expressed in the canalicular apical part of a hepatocyte that functions in biliary transport and therefore equally serves as a differentiation and polarization marker.[25] It is clearly visible that MRP2 stains more positive in the apical membrane of the organoids in CNF

hydrogel and accumulates more towards the luminal side of the organoid (Figure 6I), whereas the staining is more positive towards the basal part of the organoid for MG (Figure 6H). The staining in EM condition is negative. Similarly, the tight junction protein ZO1 should be located towards the end of the lateral membrane in proximity to the bile cuniculi, indicating the polarity of hepatocytes.[25] It is observed in Figure 6L that the staining for ZO1 in CNF hydrogel is clearly located along the plasma membrane with a preference for the basal side of the organoid, while the staining is less specific for both Matrigel™ conditions (Figure 6J and K). Accumulation of glycogen in the differentiated organoids is observed in both CNF hydrogel and MG (Figure 6N, O) at higher levels compared to EM conditions (Figure 6M).
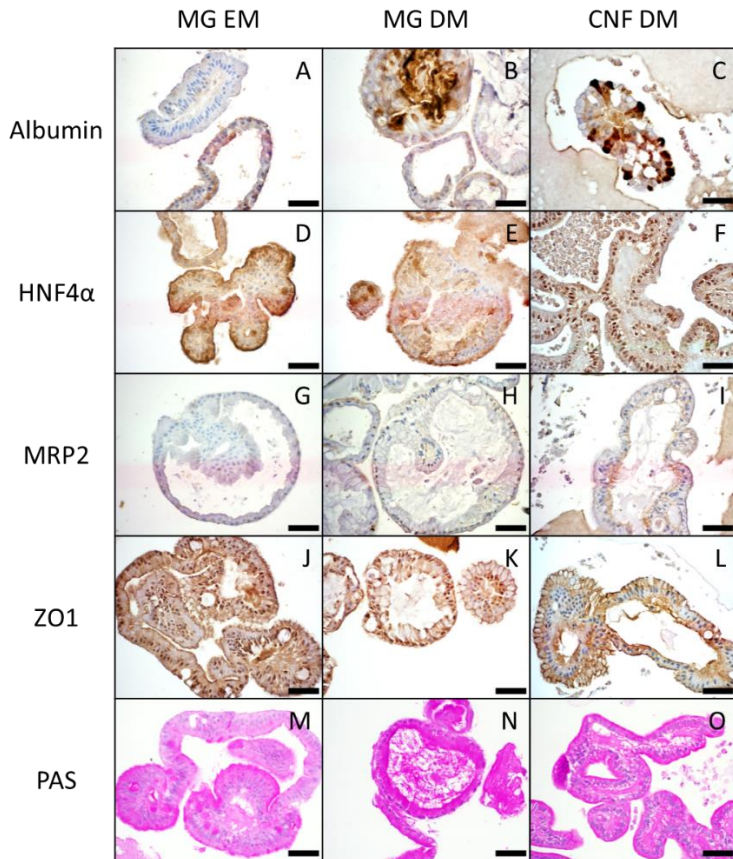
Figure 6: Representative immunohistochemical and PAS stainings of human liver organoids cultured in MG or CNF respectively. A) Albumin staining, MG EM, donor h2; B) Albumin staining, MG DM, donor h5; C) Albumin staining, CNF 0.2, donor h5; D) HNF4a staining, MG EM, donor h2; E) HNF4a staining, MG DM, donor h2; F) HNF4a staining, CNF 0.2, donor h2; G) MRP2 staining, MG EM, donor h2; H) MRP2 staining, MG DM, donor h2, I) MRP2 staining, CNF 0.6, donor h2; J) ZO1 staining, MG EM, donor h5; K) ZO1 staining, MG DM, donor h5; L) ZO1 staining, CNF 0.6, donor h5; M) PAS staining, MG EM, donor h5; N) PAS staining, MG DM, donor h2; O) PAS staining, MG EM, donor h2. Scale bar: 50 µm.

4.5 Discussion

In this study, we have shown that CNF hydrogels are a viable alternative for Matrigel™ and improve the hepatic differentiation of organoids. In the current configuration, the CNF hydrogel does not sustain organoid proliferation (data not shown) but does induce hepatic maturation. The positive attributes of CNF hydrogel and its potential for organoid differentiation are discussed below.

4.5.1 Cellulose nanofibril hydrogel characterization

The relatively high resistance of CNF hydrogel to strain is an indicator for constant remodeling of the nanofibril network[26], even in an atomic force microscopy image of a very low CNF concentration (0.005 % w/v) it has been shown that the nanofibrils are very densely packed and prevent the cells from working around the fibers.[18] The self-healing character of the gel was demonstrated by the alternating strain experiment. The reversible switch of dominance between *G'* and *G''* at high strains show that the CNF hydrogel network broke down and flowed like a viscous solution but recovered completely without any loss of its properties, which shows that there was no destruction on the molecular level.[26] The low gradient of *G'* and *G''* in the frequency sweep demonstrated that the gel had a strong internal network and is quite structured.[26]

Compared to CNF hydrogel, Matrigel™ exhibits similar behavior at lower frequencies but the crossover point of G' and G'' is already below 100 rad/s. [27] For CNF, the storage modulus G' decreased linearly up to 13 % strain, which is similar compared to Matrigel™, but in contrast to the CNF hydrogel, Matrigel™ has a very low viscous response, which is demonstrated by the unmeasurable loss modulus G".[27] In addition, Matrigel™ does not possess the capability to restore its structure after release like CNF hydrogel. The lack of self-healing properties are a major reason for the absence of successful permanently cross-linked hydrogels in clinical settings.[28] Therefore, the CNF hydrogel has an advantage in tissue engineering and regenerative medicine due to its unique properties, as it is injectable due to its shear-thinning character and self-healing after breaking.

The observed swelling of CNF hydrogel in demineralized water is caused by the Higgs-Donnan effect,[29] where the deprotonation of the C6 carboxyl group of the hydrogel results in water entering into the gel in order to equalize the difference in osmotic pressure. Therefore, the gel will not stop swelling until it is completely dissolved in water. Deprotonation is not possible in PBS; therefore, no negative charges lead to swelling of the gel. This means that CNF hydrogel is stable in salt containing solutions as

medium used for organoid cultures but can be swollen and disintegrated into demineralized water.

4.5.2 Human liver organoid performance

Expansion of human liver organoids in CNF hydrogel is not successful, as metabolic activity in the CNF hydrogel does not significantly increase over time as opposed to Matrigel™. This might be caused by the characteristics of the hydrogel, which through its mechanical properties, and potentially mismatch in degradation rate, may limit the organoids in proliferation. It has been shown that organoid formation and expansion occurs in a narrow mechanical window; stiffer gels support expansion (1.3 kPa for intestinal organoids), whereas differentiation requires softer gels (0.2 kPa).[30] However, little is known about how the mesh size and degradation rate of the hydrogel affects these processes, even though they are highly coupled to the mechanical properties. Generally, cells sense the bulk scaffold elasticity, while in viscoelastic materials they can further mechanically remodel their surrounding depending on the relaxation rate and cell type.[31] In future investigations, the mechanical properties of the CNF hydrogel could be adapted in order to suit the application of organoid expansion, and softened over time through controlled enzymatic degradation. Additionally, ECM

components proven to be advantageous for organoid growth, such as laminin-111, collagen IV, and fibronectin, could be incorporated.[32]

Morphological appearance and metabolic activity results of the human liver organoids in Matrigel[TM] in EM and DM conditions are consistent with previously shown results.[9] The morphology of the organoids in CNF hydrogel appear darker, not as round and with a less even surface as compared Matrigel[TM] cultures. This is due to an inversed polarity of the cells where the apical side of the organoid is oriented outwards and presents this more irregular appearance, as has been previously shown for intestinal organoids.[33] This change in polarity was corroborated with immunocytology showing polarity specific proteins and is due to the lack of ECM proteins regulating the polarity in the CNF hydrogel that are present in Matrigel[TM].[33] Where the ECM components are in direct contact with the cells, it creates the basolateral membrane. Especially laminins are believed to cause this effect which lead to a cascade of integrin signaling and establishes polarity.[34]

As opposed to Matrigel[TM], organoids in CNF hydrogel presented a decrease in metabolic activity within the first 4 days, which was most likely caused by cell death due to the different exposure of organoids during initial handling.

Because the CNF hydrogel coagulates and loses its self-healing characteristic when mixed with salt-containing solutions, the organoids extracted from the Matrigel™, where they were expanded in, were mixed with the CNF hydrogel in the presence of demineralized water, while media was directly added after plating of the hydrogel. The loss of its self-healing characteristics is hypothesized to be caused by protonation of the CNF hydrogel's carboxyl groups by sodium cations. Because of the positively charged sodium cations, the previously negatively charged carboxyl groups lose their repulsive forces, which are required for the materials self-healing character through ionic interactions[17] and therefore CNFs agglomerates. Thus, the organoids placed in the CNF hydrogel needed to adjust to the new environmental conditions, which resulted in a reduced viability at the beginning of differentiation. On the other hand, metabolic activity levels prove that the cells stabilized and stayed viable over the remaining culture period. After an initial acceptable reduction of 23 % in metabolic activity, cells regained their stability once culture medium was added and diffused into the gel, delivering the necessary nutrients for cell survival and function. In a previous report, a similar effect was observed, where fibroblasts spheroids inside CNF hydrogel first demonstrated a dead

outer cell layer upon inclusion into the hydrogel to then recover viability in this area after a culture period of two weeks.[24] This effect could in the future be alleviated by introducing other groups, which cannot be protonated, onto the surface of the cellulose nanofibrils instead of the carboxyl groups. In addition, incorporation of moieties that stimulate cell activity and proliferation, as shown in other hydrogels,[35] could improve the overall functionality of the hepatocyte-like organoids.

Apart from the surrounding medium conditions that influence the liver organoid cells, another factor is the stiffness of the gel. As Matrigel^{TM} and 0.6 % (w/v) CNF hydrogel are soft hydrogels according to their Young's moduli (~255 Pa for CNF hydrogel and +440 Pa for Matrigel^{TM} [36]), there is no great difference on the macroscale. It is known that the ECM close to hepatocytes is soft (E ~ 1.5 kPa)[37] and that soft surfaces promote hepatic stem cells to differentiate into hepatocytes.[38] On the other hand, soft matrices have also proven to be beneficial for intestinal organoid differentiation.[30] Importantly, despite the low Young's modulus, CNF hydrogel is composed of very stiff nanofibrils (E = 138 GPa),[18,19] providing mechanical cues on the nanoscale that can influence cell differentiation and performance.[37] The hepatic organoids in CNF hydrogel

124

appeared much darker and differently shaped compared to Matrigel[TM], which could be due to collapse and folding caused by mechanical forces and/or the lack of growth factors, laminin, and adhesion sites in the CNF hydrogel. However, this difference in appearance did not have a negative effect on the performance of the differentiated organoids. Remarkably, liver organoids were still able to form in the CNF hydrogel and fuse together into larger constructs, although the gel is not degradable without the addition of the enzyme cellulase.[14,22,23] This indicates that the environment can adapt to the organoid structures and is beneficial for the cells.

The functionality of the hepatocyte-like cells in CNF hydrogel was on average higher when the different read-outs were compared. The organoids in the CNF hydrogel were metabolically active and produced higher levels of enzymes (ALAT, ASAT, GLDH, albumin) compared to Matrigel[TM]. Overall, differentiation in CNF hydrogels seemed to have occurred at a higher level compared to Matrigel[TM], which is also indicated by the significantly higher levels of albumin production compared to both MG DM and MG EM. However, this observation is not confirmed by the gene expression analysis, which shows that albumin was expressed at similar levels in either hydrogel in DM condition, but significantly higher than in

the EM condition. In addition, immunostaining presented a similar expression of albumin, albeit oppositely located in the organoid. Even though some conflicting results may be caused by the large variability in data in the case of albumin enzyme activity amongst all functional read-outs, it can still be concluded that all analysis methods reveal that albumin production is at least as high in the CNF hydrogel as in Matrigel™. In contrast, the differentiation marker LGR5 did show higher expression levels in CNF hydrogel compared to Matrigel™, which indicates that more stem cells were still present in CNF after differentiation. On the other hand, even though the marker for hepatocyte fate, HNF4a, did not show a significant difference in gene expression, the immunostaining demonstrated more specific nuclear staining in the case of CNF hydrogel as opposed to Matrigel™, indicating that indeed the cells developed into functional hepatocytes. This finding is emphasized by the expression levels of the enzymes that are involved in the metabolism of xenobiotics (phase I to III), which show that the CNF hydrogel performed at least equally as well as the gold standard of Matrigel™ and was even superior in two cases (CYP3A4 and SULT). In all tested genes except for CYP1A2, which did not display any differences, expression levels showed successful differentiation, as

they were consistently higher than levels in organoids remaining in EM. Results are comparable to other organoid studies in Matrigel[TM] and poly(ethylene glycol) hydrogels[9,35,39], as well as with cell lines (HepaRG progenitor cells) in nanofibrillar cellulose and hyaluronan-gelatin (HG) hydrogels.[8]

Although the expression of the hepatic markers was higher in the CNF conditions compared to Matrigel[TM], the overall expression of these genes in native hepatocytes and liver samples were still higher. This shows that the liver organoids still did not fully reach the same maturity. It is known that several other factors in the microenvironment are needed to improve this hepatic maturation, including co-culture, smaller microgels produced with microfluidics, amongst others.[40] Interestingly, both the polarization markers MRP2 and ZO1, which are located at the apical membrane of a native hepatocyte and at the apical membrane or in close proximity thereof, respectively,[25,41] showed a different localization in organoids cultured in CNF hydrogel compared to Matrigel[TM]. Polarization of cells is induced by the ECM in livers or by ECM mimicking materials *in vitro* and is very important for the function of the cells.[3] The needed apicobasal polarity can be found in both CNF hydrogel and Matrigel[TM], however, it was more

pronounced in CNF but polarity was inversed. In the CNF hydrogel, the basal membrane of the hepatocytes was facing away from the lumen, which presents advantages for toxicity and drug uptake testing, because the compounds would not have to be included inside the organoids but can be administered with the medium from the outside. The MRP2 and ZO1 staining further indicate the formation of bile canaliculi-like structures, another hallmark for the structure of liver tissue.

An extensive review on hydrogels for liver tissue engineering has been published recently, naming many advantages and disadvantages of multiple natural and synthetic hydrogels with respect to the specific demands for liver tissue engineering.[3] Biocompatible CNF hydrogel specifically fulfils some of these requirements as it has the ability to culture autologous cell sources, as also proven in this study.[6,8,12,21] Furthermore, previous studies have shown that there is a potential for vascular tissue engineering in CNF material[14,20,42] and the chemistry allows for the addition of bioactive functional groups on to the fiber surface. As previously mentioned, the CNF hydrogel has a defined chemistry from only plant origin, which in principle would enable FDA approval[3] and compliance with GMP conditions, opening up the possibility for clinical translation.[43] Due to its mechanical

properties in the required range of $0.2 - 1$ kPa[3] and its shear-thinning characteristic, CNF hydrogel is suitable for bioprinting and through the addition of cellulase enzymes, it is also degradable.[12,22,24]

4.6 Conclusion

In conclusion, this study shows that the differentiation of liver organoids into functional hepatocyte-like cells is at least as successful in CNF hydrogel compared to Matrigel[TM] and sometimes superior The TEMPO-oxidized CNF hydrogel showed advantages with regard to the expression of hepatic genes, overall hepatocyte function, and organoid polarization. In combination with the natural biocompatibility, the mechanical properties of CNF hydrogels, such as the rapid self-healing and shear-thinning behavior, prove to provide a supportive environment for the differentiation of liver organoids and offer to be a good alternative to Matrigel[TM] in tissue engineering and regenerative medicine. Further improvements might be possible through the addition of the degrading cellulase enzyme,[24] adding other bioactive moieties to the nanofibrils, producing smaller CNF microgels, or by further tuning of the elastic modulus of the hydrogel.[17]

4.7 Acknowledgments

4.8 References

1. Murphy SL, Xu J, Kochanek KD, Curtin SC, Arias E. National Vital Statistics Reports Deaths : Final Data for 2013. Natl Vital Stat Reports. 2017;66(6):1-75. http://www.cdc.gov/nchs/data/nvsr/nvsr58/nvsr58_19.pdf.

2. Rudge C, Matesanz R, Delmonico FL, Chapman J. International practices of organ donation. Br J Anaesth. 2012;108(SUPPL. 1):48-55. doi:10.1093/bja/aer399

3. Ye S, Boeter JWB, Penning LC, Spee B, Schneeberger K. Hydrogels for Liver Tissue Engineering. 2019.

4. Ananthanarayanan A, Narmada BC, Mo X, McMillian M, Yu H. Purpose-driven biomaterials research in liver-tissue engineering. Trends Biotechnol. 2011;29(3):110-118. doi:10.1016/j.tibtech.2010.10.006

5. Leise MD, Poterucha JJ, Talwalkar JA. Drug-Induced Liver Injury. Mayo Clin Proc. 2014;89(1):95-106. doi:http://dx.doi.org/10.1016/j.mayocp.2013.09.016

6. Bhattacharya M, Malinen MM, Lauren P, et al. Nanofibrillar cellulose hydrogel promotes three-dimensional liver cell culture. J Control Release. 2012;164(3):291-298. doi:10.1016/j.jconrel.2012.06.039

7. Janorkar A V., Harris LM, Murphey BS, Sowell BL. Use of three-dimensional spheroids of hepatocyte-derived reporter cells to study the effects of intracellular fat accumulation and subsequent cytokine exposure. Biotechnol Bioeng.

2011;108(5):1171-1180. doi:10.1002/bit.23025

8. Malinen MM, Kanninen LK, Corlu A, et al. Differentiation of liver progenitor cell line to functional organotypic cultures in 3D nanofibrillar cellulose and hyaluronan-gelatin hydrogels. Biomaterials. 2014;35(19):5110-5121. doi:10.1016/j.biomaterials.2014.03.020

9. Huch M, Gehart H, Van Boxtel R, et al. Long-term culture of genome-stable bipotent stem cells from adult human liver. Cell. 2015;160(1-2):299-312. doi:10.1016/j.cell.2014.11.050

10. Booij TH, Price LS, Danen EHJ. 3D Cell-Based Assays for Drug Screens: Challenges in Imaging, Image Analysis, and High-Content Analysis. SLAS Discov. 2019;24(6):615-627. doi:10.1177/2472555219830087

11. K. S, B. S, P. C, N. S, H. C, J. M. Converging biofabrication and organoid technologies: the next frontier in hepatic and intestinal tissue engineering? Biofabrication. 2017;9(1):013001. doi:https://doi.org/10.1088/1758-5090/aa6121

12. Lou Y-R, Kanninen L, Kuisma T, et al. The Use of Nanofibrillar Cellulose Hydrogel As a Flexible Three-Dimensional Model to Culture Human Pluripotent Stem Cells. Stem Cells Dev. 2014;23(4):380-392. doi:10.1089/scd.2013.0314

13. Hughes CS, Postovit LM, Lajoie GA. Matrigel: a complex protein mixture required for optimal growth of cell culture. Proteomics. 2010;10(9):1886-1890. doi:10.1002/pmic.200900758

14. Bačáková L, Novotná K, Pařzek M. Polysaccharides as cell carriers for tissue engineering: The use of cellulose in vascular wall

reconstruction. Physiol Res. 2014;63(SUPPL.).

15. Saito T, Uematsu T, Kimura S, Enomae T, Isogai A. Self-aligned integration of native cellulose nanofibrils towards producing diverse bulk materials. Soft Matter. 2011;7(19):8804-8809. doi:10.1039/c1sm06050c

16. Saito T, Nishiyama Y, Putaux J-L, Vignon M, Isogai A. Homogeneous Suspensions of Individualized Microfibrils from TEMPO-Catalyzed Oxidation of Native Cellulose. Biomacromolecules. 2006;7(6):1687-1691. doi:10.1021/bm060154s

17. Syverud K, Pettersen SR, Draget K, Chinga-Carrasco G. Controlling the elastic modulus of cellulose nanofibril hydrogels—scaffolds with potential in tissue engineering. Cellulose. 2015;22(1):473-481. doi:10.1007/s10570-014-0470-5

18. Torres-Rendon JG, Femmer T, De Laporte L, et al. Bioactive gyroid scaffolds formed by sacrificial templating of nanocellulose and nanochitin hydrogels as instructive platforms for biomimetic tissue engineering. Adv Mater. 2015;27(19):2989-2995. doi:10.1002/adma.201405873

19. Torres-Rendon JG, Köpf M, Gehlen D, et al. Cellulose Nanofibril Hydrogel Tubes as Sacrificial Templates for Freestanding Tubular Cell Constructs. Biomacromolecules. 2016;17(3):905-913. doi:10.1021/acs.biomac.5b01593

20. Pooyan P, Tannenbaum R, Garmestani H. Mechanical behavior of a cellulose-reinforced scaffold in vascular tissue engineering. J Mech Behav Biomed Mater. 2012;7:50-59. doi:10.1016/j.jmbbm.2011.09.009

21. Pooyan P, Kim IT, Jacob KI, Tannenbaum R,

Garmestani H. Design of a cellulose-based nanocomposite as a potential polymeric scaffold in tissue engineering. Polymer (Guildf). 2013;54(8):2105-2114. doi:10.1016/j.polymer.2013.01.030

22. Hu Y, Catchmark JM. Integration of cellulases into bacterial cellulose: Toward bioabsorbable cellulose composites. J Biomed Mater Res - Part B Appl Biomater. 2011;97 B(1):114-123. doi:10.1002/jbm.b.31792

23. Sannino A, Demitri C, Madaghiele M. Biodegradable cellulose-based hydrogels: Design and applications. Materials (Basel). 2009;2(2):353-373. doi:10.3390/ma2020353

24. Krueger M, Spee B, Walther A, De Laporte L, Kock LM. Nanofibrillar Cellulose as an Enzymatically and Flow Driven Degradable Scaffold for Three-Dimensional Tissue Engineering. ASME J Eng Sci Med Diagnostics Ther. 2019.

25. Mitaka T, Ooe H. Characterization of hepatic-organoid cultures. Drug Metab Rev. 2010;42(3):472-481. doi:10.3109/03602530903492020

26. Rowland MJ, Atgie M, Hoogland D, Scherman OA. Preparation and Supramolecular Recognition of Multivalent Peptide-Polysaccharide Conjugates by Cucurbit[8]uril in Hydrogel Formation. Biomacromolecules. 2015;16(8):2436-2443. doi:10.1021/acs.biomac.5b00680

27. Zuidema JM, Rivet CJ, Gilbert RJ, Morrison FA. A protocol for rheological characterization of hydrogels for tissue engineering strategies. 2013:1063-1073. doi:10.1002/jbm.b.33088

28. Saunders L, Ma PX. Self-Healing Supramolecular

Hydrogels for Tissue Engineering Applications. Macromol Biosci. 2019;19(1):1-11. doi:10.1002/mabi.201800313

29. Grignon J, Scallan AM. Effect of pH and neutral salts upon the swelling of cellulose gels. J Appl Polym Sci. 1980;25(12):2829-2843. doi:10.1002/app.1980.070251215

30. Gjorevski N, Sachs N, Manfrin A, et al. Designer matrices for intestinal stem cell and organoid culture. Nature. 2016;539(7630):560-564. doi:10.1038/nature20168

31. Bahlmann LC, Fokina A, Shoichet MS. Dynamic bioengineered hydrogels as scaffolds for advanced stem cell and organoid culture. MRS Commun. 2017;7(3):472-486. doi:10.1557/mrc.2017.72

32. Sorrentino G, Rezakhani S, Yildiz E, et al. Mechano-modulatory synthetic niches for liver organoid derivation. bioRxiv. 2019:810275. doi:10.1101/810275

33. Co JY, Margalef-Català M, Li X, et al. Controlling Epithelial Polarity: A Human Enteroid Model for Host-Pathogen Interactions. Cell Rep. 2019;26(9):2509-2520.e4. doi:10.1016/j.celrep.2019.01.108

34. Lee JL, Streuli CH. Integrins and epithelial cell polarity. J Cell Sci. 2014;127(15):3217-3225. doi:10.1242/jcs.146142

35. Klotz BJ, Oosterhoff LA, Utomo L, et al. A Versatile Biosynthetic Hydrogel Platform for Engineering of Tissue Analogues. Adv Healthc Mater. 2019;1900979:1-13. doi:10.1002/adhm.201900979

36. Shauheen S. Soofia, Julie A. Lasta, Sara J.

Liliensieka, Paul F. Nealeyb and CJ, Murphy. Elastic modulus of Matrigel as determined by AFM. J Struct Biol. 2009;167(3):216-219. doi:10.1016/j.jsb.2009.05.005.The

37. Reilly GC, Engler AJ. Intrinsic extracellular matrix properties regulate stem cell differentiation. J Biomech. 2010;43(1):55-62. doi:10.1016/j.jbiomech.2009.09.009

38. Jain E, Damania A, Kumar A. Biomaterials for liver tissue engineering. Hepatol Int. 2014;8(2):185-197. doi:10.1007/s12072-013-9503-7

39. Kruitwagen HS, Oosterhoff LA, Vernooij IGWH, et al. Long-Term Adult Feline Liver Organoid Cultures for Disease Modeling of Hepatic Steatosis. Stem Cell Reports. 2017;8(4):822-830. doi:10.1016/j.stemcr.2017.02.015

40. Chen C, Soto-Gutierrez A, Baptista PM, Spee B. Biotechnology Challenges to In Vitro Maturation of Hepatic Stem Cells Chen. Gastroenterology. 2018;154(5):1258-1272. doi:10.1053/j.gastro.2018.01.066

41. Treyer A, Müsch A. Hepatocyte Polarity. Compr Physiol. 2013;3:243-287. doi:10.1002/cphy.c120009

42. Bäckdahl H, Helenius G, Bodin A, et al. Mechanical properties of bacterial cellulose and interactions with smooth muscle cells. Biomaterials. 2006;27(9):2141-2149. doi:10.1016/j.biomaterials.2005.10.026

43. Bhatia SN, Underhill GH, Zaret KS, Fox IJ. Cell and tissue engineering for liver disease. Sci Transl Med. 2014;6(245). doi:10.1126/scitranslmed.3005975

44. Benítez AJ, Torres-Rendon J, Poutanen M, Walther A. Humidity and multiscale structure govern mechanical properties and deformation modes in films of native cellulose nanofibrils. Biomacromolecules. 2013;14(12):4497-4506. doi:10.1021/bm401451m

45. Benítez AJ, Walther A. Cellulose nanofibril nanopapers and bioinspired nanocomposites: A review to understand the mechanical property space. J Mater Chem A. 2017;5(31):16003-16024. doi:10.1039/c7ta02006f

4.9 Supplementary Material
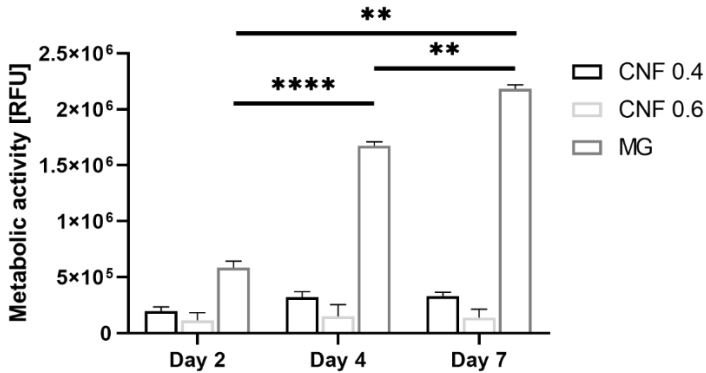
Figure S1: Metabolic activity of organoids cultured under EM conditions for 7 days in MG, CNF 0.4 and CNF 0.6, n=3 for each condition, data depicted as mean ± SD (**p < 0.01 ***p < 0.001, no indication: not significant), ANOVA with Tukey's post-hoc test.
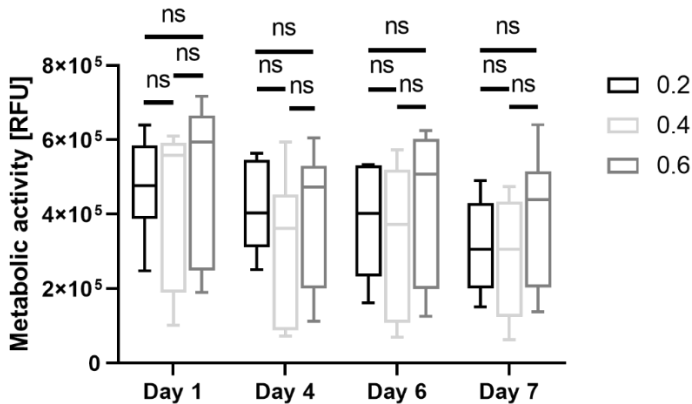
Figure S2: Metabolic activity at day 1, 4, 6 and 7 for different CNF hydrogel concentrations (0.2% w/v, 0.4% w/v, 0.6% w/v) cultured in DM, data averaged over donors, data depicted as mean ± SD (n= 6 for CNF 0.2, n=9 for CNF 0.4 and 0.6), (ns: not significant), multiple t-test with Holm-Sidak method.
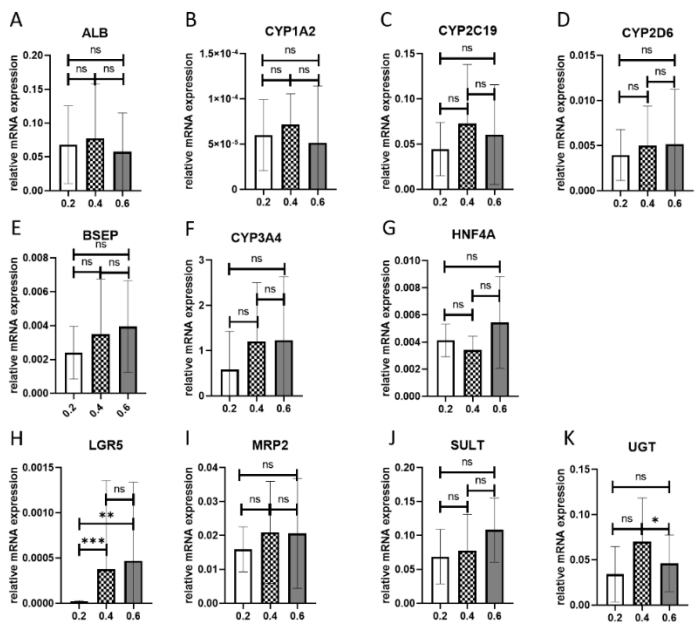
Figure S3: Relative gene expression to GAPDH and RPL19 of liver organoids differentiated in CNF hydrogels in DM of different concentrations (0.2% w/v, 0.4% w/v, 0.6% w/v) for 7 days. Data is averaged over all donors. A) Albumin expression (n=12 for CNF 0.2, n=14 for CNF 0.4, n=13 for CNF 0.6), B) CYP1A2 expression (n=9 for CNF 0.2, n=7 for CNF 0.4, n=5 for CNF 0.6), C) CYP2C19 expression (n=11 for CNF 0.2, n=14 for CNF 0.4, n=14 for CNF 0.6), D) CYP 2D6 expression (n=12 for CNF 0.2, n=15 for CNF 0.4, n=15 for CNF 0.6), E) BSEP expression (n=12 for CNF 0.2, n=14 for CNF 0.4, n=14 for CNF 0.6), F) CYP3A4 expression (n=12 for CNF 0.2, n=15 for CNF 0.4, n=15 for CNF 0.6), G) HNF4a expression (n=12 for CNF 0.2, n=14 for CNF 0.4, n=14 for CNF 0.6), H) LGR5 expression (n=10 for CNF 0.2, n=13 for CNF 0.4, n=13 for CNF 0.6), I) MRP2 expression (n=12 for CNF 0.2, n=15 for CNF 0.4, n=15 for CNF 0.6), J) SULT expression (n=6 for CNF 0.2, n=12 for CNF 0.4, n=11 for CNF 0.6), K) UGT expression (n=11 for CNF 0.2, n=12 for CNF 0.4, n=12 for CNF 0.6). Data depicted as mean ± SD (*p < 0.05, **p < 0.01 ***p < 0.001, ns: not significant), mixed-effects analysis with Tukey's post-hoc test.
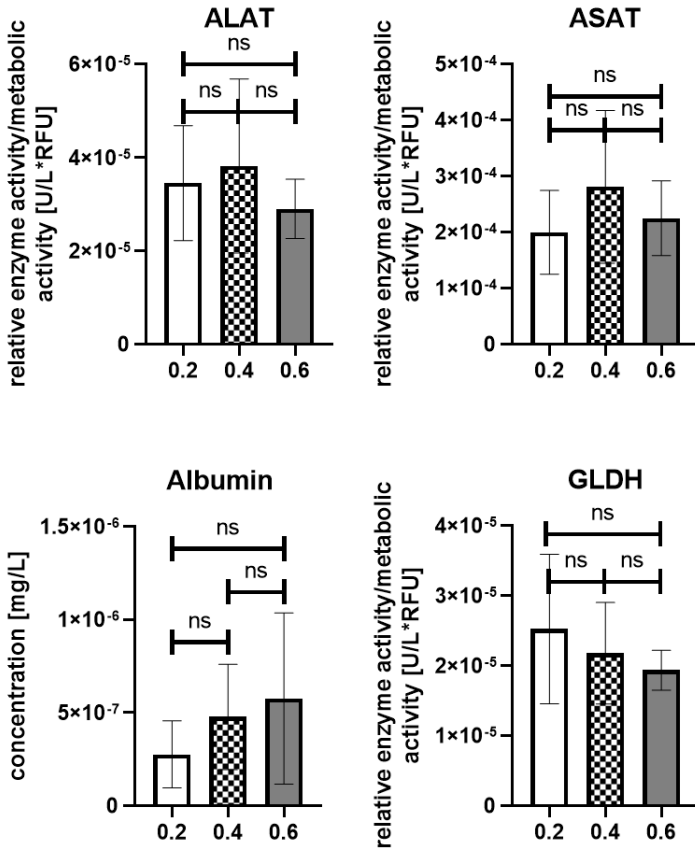
Figure S4: Functional read-out in relative enzyme activity and albumin concentration corrected to the metabolic activity of hepatocyte-like cells lysed after 7 days of differentiation in CNF hydrogel of different concentrations (0.2% w/v, 0.4% w/v, 0.6% w/v) in DM (CNF 0.2 (n= 6 for Albumin, GLDH, ALAT and ASAT), CNF 0.4 (n= 4 for Albumin, GLDH, n=8 for ALAT and n = 9 for ASAT), CNF 0.6 (n= 6 for Albumin, GLDH, n=9 for ALAT and ASAT)). Data is averaged over donors and depicted as mean ± SD (ns: not significant) mixed-effects analysis with Tukey's post-hoc test.

Part II. *Ex Vivo* Models

5 High level of polarized engraftment of porcine intrahepatic cholangiocyte organoids in decellularized liver scaffolds

Melanie Krüger[1]*, Roos-Anne Samsom[1], Loes A. Oosterhoff[1], Monique E. van Wolferen[1], Hans S. Kooistra[2], Niels Geijsen[3], Louis C. Penning[2], Linda M. Kock[4,5], Pilar Sainz-Arnal[6], Pedro M. Baptista[6#], Bart Spee[1#]

[1]Department of Clinical Sciences, Faculty of Veterinary Medicine, Utrecht University, Uppsalalaan 8, 3584 CT Utrecht, The Netherlands

[2]Department of Clinical Sciences, Faculty of Veterinary Medicine, Utrecht University, Yalelaan 108, 3584 CM Utrecht, The Netherlands

[3]Department of Anatomy and Embryology, Leiden University Medical Center, Leiden 2300 RC, The Netherlands

[4]LifeTec Group BV, Kennedyplein 10-11, 5611 ZS Eindhoven, The Netherlands;

[5]Department of Biomedical Engineering, Eindhoven University of Technology, De Rondom 70, 5612 AP Eindhoven, The Netherlands

[6]Laboratory of Organ Bioengineering and Regenerative Medicine, Health Research Institute of Aragon (IIS Aragon), Zaragoza, Spain

*Corresponding Author, #Authors contributed equally

5.1 Abstract

In Europe alone, each year 5500 people require a life-saving liver transplantation, but 18% die before receiving one due to the shortage of donor organs. Whole organ engineering, utilizing decellularized liver scaffolds repopulated with autologous cells, is an attractive alternative to increase the pool of available organs for transplantation. The development of this technology is hampered by a lack of a suitable large animal model representative of the human physiology and a reliable and continuous cell source. We have generated porcine intrahepatic cholangiocyte organoids from adult stem cells and demonstrate that these cultures remained stable over multiple passages whilst retaining the ability to differentiate into hepatocyte- and cholangiocyte-like cells. Recellularization onto porcine scaffolds was efficient and the organoids homogeneously differentiated, even showing polarization. Our porcine intrahepatic cholangiocyte system, combined with porcine liver scaffold paves the way for developing whole liver engineering in a relevant large animal model.

5.2 Introduction

Liver diseases impose a great burden on our society, in terms of suffering and death as well as economically, and in most countries it is predicted to increase even further[1–3]. These diseases such as drug induced liver injury[4], alcoholic liver disease[5], liver cancer[6], non-alcoholic fatty liver disease[7] and others together account for 2 million deaths per year worldwide. In Europe alone more than 5,500 liver transplants are performed each year, which is the only available treatment for end stage liver disease at this moment[8,9]. However, due to insufficient amounts of donor organs, 18% of people listed for a liver transplantation in Europe died before receiving a transplant[10]. Therefore, an alternative to liver transplantation is urgently needed.

One such alternative is to decellularize livers that are discarded for transplantation, but provide a biological optimal scaffold for transplanted cells, such as intrahepatic cholangiocyte (ICOs)[11–17]. This native extracellular matrix (ECM) promotes cell differentiation, proliferation, attachment, and cell migration[15,18,19]. Moreover liver-ECM maintains hepatocyte function, possibly due to the intact three-dimensional structure[13,20]. Thus far recellularization of decellularized liver ECM with

reimplantation has been performed in rodents[21,22], providing proof-of-principle, but a larger animal model is needed in preclinical-studies[23–26].

Pigs present a very suitable model in this respect due to a physiology that is very close to human[27], and decellularized porcine scaffolds can be repopulated at a low degree with rat/human liver organoids[15,28,29]. This low engraftment was possibly caused by the species differences between donor cells in the decellularized ECM-scaffold, as ideally autologous cells should be used[22]. Even more importantly, porcine progenitor cells can help advance this preclinical research towards human patients as they represent a more human-relevant animal model. The lack of established porcine ICOs impeded this research so far.

Therefore, the aim of this study was to establish ICO culture from porcine adult stem cells and repopulate porcine decellularized liver scaffolds with these organoids. This would pave the way for whole organ bioengineering that can be used as an alternative for organ donation in the future.

5.3 Materials and Methods

5.3.1 Isolation porcine liver cells and culture hepatic organoids

Livers from four individual pigs were derived from fresh slaughterhouse material, placed in cooled DMEM/F12 media (Gibco™, Thermo Fisher Scientific, Waltham, MA, USA) and transported to the lab on ice. Porcine liver tissue was cut down into small tissue fragments of 2-3 mm^3 using sterile blades and petri dishes and frozen down in dimethyl sulfoxide (DMSO)-based freezing medium (Thermo Fisher Scientific, Waltham, MA, USA) until further processing. Before cell isolation, the tissue was thawed rapidly to 37 ˚C in a water bath. After further mechanical dissection into fragments of 1-2 mm^3, liver tissue was enzymatically digested in DMEM (Life Technologies, Carlsbad, CA, USA) containing 0.3 mg/mL type II collagenase (Life Technologies) and 0.3 mg/mL dispase (Life Technologies) at 37 ˚C until biliary duct fragments appeared in the suspension observed through the microscope (2-4 hours). The isolated cells and biliary duct fragments were mixed with Matrigel™ (Corning, Glendale, AZ, USA) and plated in a 24-wells plate in drops of 50 µL. Porcine ICOs were grown in expansion medium (EM) based on advanced DMEM/F12 (Life Technologies)

containing 1% (v/v) Glutamax (Life Technologies), 1% (v/v) Penicillin-Streptomycin (Life Technologies), 1% (v/v) HEPES (Life Technologies), 30% (v/v) Wnt3a-conditioned medium (prepared as in [30]), 1% (v/v) N2 (Invitrogen, Waltham, MA, USA), 10 mM nicotinamide (Sigma-Aldrich, Saint Louis, MO, USA), 2% (v/v) B27 without vitamin A (Invitrogen), 10% (v/v) R-spondin conditioned medium (Rspo1-Fc expressing cell line kindly gifted by Calvin J. Kuo, Stanford University, CA, USA), 1.25 mM N-acetylcysteine (Sigma-Aldrich), 10 µM Y-27632 (Selleckchem, Munich, Germany), 5 µM A83-01 (Tocris Bioscience, Bristol, UK), 50 ng/mL human epidermal growth factor (EGF, Invitrogen), 0.1 µg/mL human noggin (Peprotech, London, UK), 0.1 µg/mL fibroblast growth factor 10 (FGF10, Peprotech), 10 nM gastrin (Sigma-Aldrich), 25 ng/mL hepatocyte growth factor (HGF, Peprotech), 10 µM forskolin (Sigma-Aldrich), and 1% (v/v) primocin (Invitrogen). For an overview of the medium composition please see Supplementary Table 2.

5.3.2 Porcine intrahepatic cholangiocyte organoid differentiation

Prior to differentiation, porcine ICOs from 4 donors (n = 3 per donor) in the same passage number (p4) were cultured in EM with 25 ng/mL BMP7 (Peprotech) for five days. Differentiation medium (DM) was based on advanced DMEM/F12 (Life Technologies) containing 1% (v/v) Glutamax (Life Technologies), 1% (v/v) Penicillin-Streptomycin (Life Technologies), 1% (v/v) HEPES (Life Technologies), 1% (v/v) N2 (Invitrogen), 2% (v/v) B27 without vitamin A (Invitrogen), 1.25 mM N-acetylcysteine (Sigma-Aldrich), 5 µM A83-01 (Tocris Bioscience), 50 ng/mL human epidermal growth factor (EGF, Invitrogen), 0.1 µg/mL human noggin (Peprotech), 0.1 µg/mL FGF19 (R&D Systems, Minneapolis, MN, USA), 10 nM gastrin (Sigma-Aldrich), 25 ng/mL hepatocyte growth factor (HGF, Peprotech), 30 µM dexamethasone (Sigma-Aldrich), 10 µM DAPT (y-secretase inhibitor, Selleckchem), and 25 ng/mL BMP7 (Peprotech), and 1% (v/v) primocin (Gentaur, Kampenhout, Belgium). Differentiation medium was refreshed every three days until the end of differentiation culture (day 5 and 9).

5.3.3   De- and recellularization

The process of porcine liver decelluarization and recellularization is schematically depicted in Figure 3A.

Decellularization of porcine livers

Decellularization of porcine livers was performed according to the previously published protocol by Pla-Palacin et al.[31]. In short, whole livers are dissected from pig cadavers and portal vein and hepatic artery are cannulated and subsequently perfused with alternating charges of distilled water and decellularization solution containing Triton X-100. The decellularized livers were then cut into circular discs of 5 mm diameter and 200 μm height.

Recellularization of liver scaffolds

Before reseeding, the scaffolds were incubated for 1 hour at 37 ˚C with 200 μL EM with 25 ng/mL BMP7 in a humidified incubator at 37 ˚C, 5% CO_2 and 21% oxygen. After the incubation the medium was removed, and the scaffolds were placed in an incubator at 37 ˚C for 1 hour to dry. Each scaffold was seeded with 200,000 cells as organoid fragments in 10 μL EM with the addition of 25 ng/mL BMP7 in a 96-wells plate. After 1 hour incubation

in an incubator at 37 ˚C, 250 µL EM with 25 ng/mL BMP7 was added to each well. The EM was refreshed twice a day. After two days, the scaffolds were transferred to a 24 well plate and the medium was changed to DM. The DM was refreshed every 2-3 days until the end of differentiation at day 5, which has proven to be the best timepoint based on preliminary experiments (data not shown).

5.3.4 Functional analyses

Metabolic activity

To test the metabolic activity of the organoids grown in expansion medium, Alamar Blue (Invitrogen) was diluted in DMEM/F12 without phenol red (1:20, Life Technologies) and incubated with the samples (n = 3 per donor) for 2 hours at 37 ˚C. The fluorescence was measured with a spectrophotometer (Fluoroskan Ascent FL, Thermo Fisher Scientific, Waltham, MA, USA) at 544/570 nm. The Alamar Blue assay was performed on all four donors in passage (p2) and the intensity was measured at day 0, 2, 6, and 8 after plating.

Gene expression

To get an overview of the gene expression profile of porcine ICOs in EM (in Matrigel^{TM}) and DM conditions (in

Matrigel™ and discs) RNA was isolated from organoids (n = 3 per donor, condition and time point) using the RNAeasy Micro/Mini Kit (Qiagen, Hilden, Germany) following manufacturer's instructions. Subsequently, quality and quantity were defined with Nanodrop equipment (DS-11 Spectrophotometer, DeNovix). cDNA was prepared using the iScript cDNA Synthesis Kit (Bio-Rad, Hercules, CA). Quantitative PCR was performed on Bio-Rad MyiQ Cycler using SYBRgreen 10 supermix (Bio-Rad). Quantification of target gene expression was normalized to the geometric mean of the reference genes glyceraldehyde-3-phosphate dehydrogenase (GAPDH), ribosomal protein S19 (RPS19), hydroxymethylbilane synthase (HMBS), and tyrosine-3-monooxygenase/tryptophan 5-monooxygenase activation protein zeta (YWHAZ), as required under MIQE-precise[32]. The delta-Cq method was used for analysis. Selected target genes were HNF1B (Hepatocyte nuclear factor 1 homeobox B), G-protein coupled receptor 5 (LGR5), albumin (ALB), cytochrome P450, family 3, subfamily alpha, polypeptide 22 (CYP3A22), hepatocyte nuclear factor 4 alpha (HNF4A), transferrin (TF), fumarylacetoacetate hydrolase (FAH), and transthyretin (TTR). The primer details are shown in Table 1.

Table 1: Primer information for porcine specific qRT-PCR. Glyceraldehyde-3-phosphate dehydrogenase (GAPDH); Ribosomal

protein S19 (RPS 19); Hydroxymethylbilane synthase (HMBS); Tyrosine-3-monooxygenase/tryptophan 5-monooxygenase activation protein zeta (YWHAZ); G-protein coupled receptor 5 (LGR5); Albumin (ALB); Cytochrome P450 family 3, subfamily alpha, polypeptide 22 (CYP3A22); Hepatocyte nuclear factor 4 alpha (HNF4A); Transferrin (TF); Fumarylacetoacetate hydrolase (FAH); Transthyretin (TTR).

Gene	Forward Primer 5'à 3'	Reverse Primer 5'à 3'	NCBI reference sequence
GAPDH	CTGCCCAGAACATCATCCC	CAGTGAGCTTCCCGTTGAG	NM_001206359.1
RPS19	AAAGAAACGGTGTCATGCCC	AGGCCTTTCCCATCTTGGT	XM_005655906.3
HMBS	GATGGGCAACTCTACCTGAC	CAAGCTGTGGGTCATCCTC	NM_001097412.1
YWHAZ	CAAAGACAGCATTTGATGAAGCC	ATCTCCTTGGGTATCCGATGTC	NM_001315726.1
HNF1B	CCACCAACAAGAAGATGCGT	CAAACACTCTGCTCTGTTGC	NM_213956.1
LGR5	CAACTTGCAGAAGATTTACCCAG	GCTAAATTCAGAGATCGGAGG	NM_001315762.1
ALB	CGCTCATAGTTCGTTACACC	CTTACAACACCTAGAGCCCA	NM_001005208.1
CYP3A22	CATCAACACGAAAGAAATCTTTGGG	GTCTCGTGGGTTGTTGAGG	NM_001195509.1
HNF4A	CTTCTTTGACCCAGATGCC	GTCGTTAGATGTAACTCTCCAG	NM_001044571.1
TF	GCCATCAGGGATAAAGAAGCA	GCCCATAGAACTCTGCCAC	NM_001244653.1
FAH	CCAAGATGTCTTTGATCAGCCA	CCGAAGTTCTGTGTCATCTCTG	XM_003356648.4
TTR	AATATGCAGAGGTTGTGTTCACAG	CTGTGGTGGAGTAAGAGTAGGG	NM_214212.1

Immunofluorescence

Liver tissue biopsies and organoids harvested from Matrigel™ (n = 3 per donor and condition) on day 5 were fixed in 4% (w/v) phosphate buffered formaldehyde (PFA) with 0.1% (w/v) eosin for 1 hour and embedded in 2.5% (w/v) agar (BD). The embedded organoids were dehydrated with gradient ethanol and xylene (Klinipath, Duiven, The Netherlands), embedded in paraffin (Leica, Wetzlar, Germany), and sectioned into 4 µm thin sections.

First the slides were incubated at 60 ˚C for 10 minutes.
Sections were stained for keratin 19 (K19), albumin (ALB),
multidrug resistance protein 1 (MDR1) and proliferation
marker Ki-67 for all conditions (EM, DM, discs); for tight
junction protein 1 (ZO1) in DM and discs; and hepatocyte
nuclear factor 4 alpha (HNF4A), keratin 18 (K18). For
each antibody, the antigen retrieval method, antibody
dilution and incubation times are summarised in Table 2.
Slides were analysed using a Leica SPEII fluorescent
microscope.

Table 2: Antibody information for immunofluorescent staining. Keratin 19 (K19); Albumin (ALB); Hepatocyte nuclear factor 4 alpha (HNF4A); Proliferation marker (Ki 67); Tight junction protein 1 (ZO1); Keratin 18 (K18); Multidrug resistance protein 1 (MDR1).

Antibody	Dilution	Incubation Time	Antigen Retrieval	Washing Buffer	Secondary Antibody	Supplier
K19	1:50	Overnight	Citrate 98 ˚C for 30 min	PBS/ Tween 0.1%	AF488 goat-anti-rabbit 1:200	Abcam (ab76539)
ALB	1:1,500	Overnight	Citrate 98 ˚C for 30 min	PBS/ Tween 0.1%	AF488 goat-anti-mouse 1:200	Sigma (A6684)
HNF4A	1:500	Overnight	Tris/EDTA 98 ˚C for 30 min	TBS/ Triton 0.2%	AF488 goat-anti-rabbit 1:200	Santa Cruz (sc-8987)
Ki-67	1:50	Overnight	Citrate	PBS/ Tween 0.1%	AF488 goat-anti-rabbit 1:200	Dako (M7240)
ZO-1	1:250	Overnight	Pepsin 0.4% in 0.2N HCl 20 min at 37 ˚C	PBS/ Tween 0.1%	AF488 goat-anti-rabbit 1:200	Invitrogen (40-2300)
K18	1:100	Overnight	Citrate 98 ˚C 3 for 0 min	PBS/ Tween 0.1%	AF488 goat-anti-mouse 1:200	Santa Cruz (sc-51582)
MDR1	1:200	Overnight	Tris/EDTA 98 ˚C for 30 min	PBS/ Tween 0.1%	AF488 goat-anti-rabbit 1:200	Novus bio (NBP1-90291)

Clinical chemistry

For measurement of the expression of liver transaminases and albumin production in differentiated organoids, cells were lysed in MilliQ (MilliPore, Burlington, MA, USA) at day 5 (and stored at -20 ˚C (n = 3 for each donor and timepoint). Albumin (ALB), Aspartate Transaminase (ASAT), Lactate dehydrogenase (LDH), and Glutamate Dehydrogenase (GLDH) were measured using the DxC-600 Beckman (Backman Coulter, Brea, CA, USA) standard protocols, and the values were corrected for the total protein counts.

Engraftment efficiency

Engraftment percentage was determined by analyzing representative 4x images of decellularized discs for each donor that were stained with Hematoxylin and Eosin with ImageJ software. The total scaffold area was determined after which the areas without cells were subtracted.

Statistics

All statistics have been performed with Graphpad Prism 8.0 and all data is normally distributed. Data is shown as mean ± SD. Viability data was analyzed using a mixed-model with Tukey's multiple comparison test, with

examination of residual plot for fit and Q-Q plot for normality. Enzyme data was analyzed using 2-way repeated measures ANOVA with Sidak's multiple comparisons test. A p-value of $p<0.05$ was considered statically significant.

5.4 Results

5.4.1 Organoid Expansion

The cells derived from porcine liver tissue samples were cultured in Matrigel^{TM} and biliary duct fragments could be observed in the hydrogel scaffold (see Figure 1B). Over the next days of culture in EM media the formation of cyst-like spherical structures and their growth could be observed and their morphology stayed stable until at least passage 6 (see Figure 1B). Organoid growth was also shown by metabolic activity measurement (see Figure 1A), where activity significantly increased from day to day up to 451 % compared to the start of culture ($p < 0.0001$). In Figure 1C gene expression (values in Supplementary Table 1) shows that with increasing passage the expression level of stem cell marker Leucine Rich Repeat Containing G Protein-Coupled Receptor 5 (LGR5) and Hepatocyte nuclear factor 1 homeobox B (HNF1B) slightly increased, whereas expression of all other hepatocyte specific markers such as Hepatocyte nuclear factor 4

alpha (HNF4A), Albumin (ALB), Transferrin (TF), Transthyretin (TTR), Fumarylacetoacetate hydrolase (FAH), Cytochrome P450 3A22 (CYP3A22, porcine analogue to human CYP3A4) remained stable over time.

Staining for hepatocyte marker albumin as well as polarization marker Multidrug resistance 1 (MDR1) shows that there was already slight presence of the protein in the expanding organoids, although less compared to native liver tissue (Figure 1D and Supplementary Figure 1). In contrast, the organoids stained strongly for the ductular marker K19 and the proliferation marker Ki67 stained roughly 30 percent of the cells within the organoid showing continued expansion (Figure 1D).
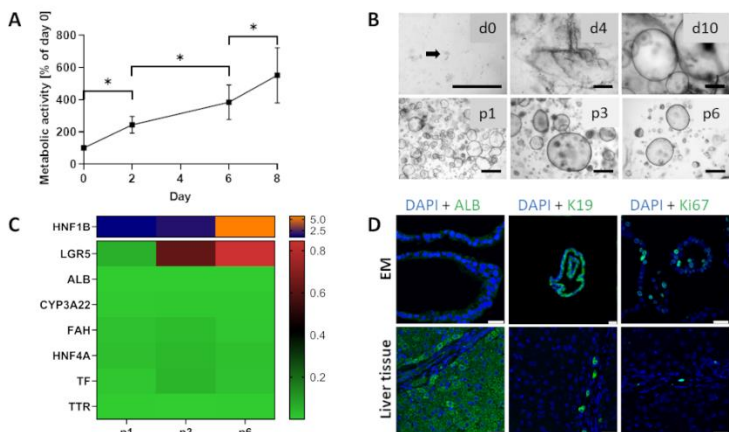
Figure 1: A) Metabolic activity according to Alamar Blue assay of porcine ICOs over 8 days of culture in EM media as percentage of day 0. Data depicted as mean ± SD (n = 4), *p< 0.0001. B) Establishment of organoid culture from porcine liver tissue samples in representative phase-contrast images of duct isolation and organoid culture. After digestion, biliary ducts fragments were observed in culture (d0, arrow). Ducts were cultured in Matrigel^{TM} and defined medium. After 4 days in culture (d4) spherical structures appeared that grew out to organoids within 10 days (d10). Representative phase-contrast images of porcine ICOs in different passages (p1, p3, and p6). Scale bars represent 500 µm. C) Heatmap showing gene expression relative to liver over 6 passages of organoid culture (median of donors, n = 3 per donor) with increased HNF1B (Hepatocyte nuclear factor 1 homeobox B) and LGR5 (G-protein coupled receptor 5) expression and stable ALB (Albumin), CYP3A22 (Cytochrome P450, family 3, subfamily alpha, polypeptide 22), FAH (Fumarylacetoacetate hydrolase), HNF4A (Hepatocyte nuclear factor 4 alpha), TF (Transferrin), TTR (Transthyretin) expression. D) Representative immunofluorescent staining for ALB, K19 (Keratin 19), Ki67 (Proliferation marker) expression (in green) and nuclei (DAPI in blue) for organoids in EM (Expansion medium) conditions after day 5-7 and native liver tissue. Scale bars represent 25 µm.

5.4.2 Organoid Differentiation

After differentiation of the porcine ICOs for 5 days, the grand mean of the albumin level had significantly increased by 71 mg/L ($p < 0.0001$) in DM compared to EM. Multiple comparisons show that for donor 3 the albumin level has even increased by 89 mg/L ($p = 0.0002$) and by 78 mg/L ($p = 0.0005$) for donor 2. Equally, mean ASAT activity was significantly higher (278 U/L; $p < 0.0001$) in DM compared to EM despite some variation between donors that ranged from no significant changes amongst the medium conditions for donors 3 and 4 to an increase of 847 U/L ($p < 0.0001$) for donor 1. LDH activity levels were significantly lower after 5 days in differentiation medium (788 U/L; $p = 0.013$), which was mainly due to the large decrease of activity of donor 3 (1654 U/L; $p = 0.041$), as all other donors showed no significant difference between EM and DM levels. Mean GLDH activity after 5 days of culture in DM conditions compared to EM increased by 111 U/L ($p < 0.0001$) with as much as 270 U/L ($p < 0.0001$) and 198 U/L ($p < 0.0001$) for donors 1 and 2, respectively.

As opposed to EM conditions, albumin was much more strongly expressed after differentiation of the organoids as demonstrated by the immunofluorescent staining in

Figure 2B. Similarly, keratin 19 was more widespread around the nuclei compared to organoids under expansion conditions. The proliferation marker Ki67 is visible in fewer cells of the differentiated organoids than in expanding specimen. Polarization marker MDR1 accumulated on the luminal side of the ICOs compared to EM conditions, where it was not present at all (Supplementary Figure 1). The tight junction protein ZO1 accumulated similarly on the luminal side of the organoids in both EM and DM conditions.

In Figure 2C, the heatmap clearly illustrates differentiation by 46.4-fold reduction of LGR5 expression in the differentiated organoids, as well as an increase in HNF1B (1.1-fold), CYP3A22 (15.5-fold), FAH (1.4-fold) and HNF4A (2.6-fold) expression. Both ALB and TTR expression showed no difference between these two conditions and TF was expressed slightly less in DM compared to EM.
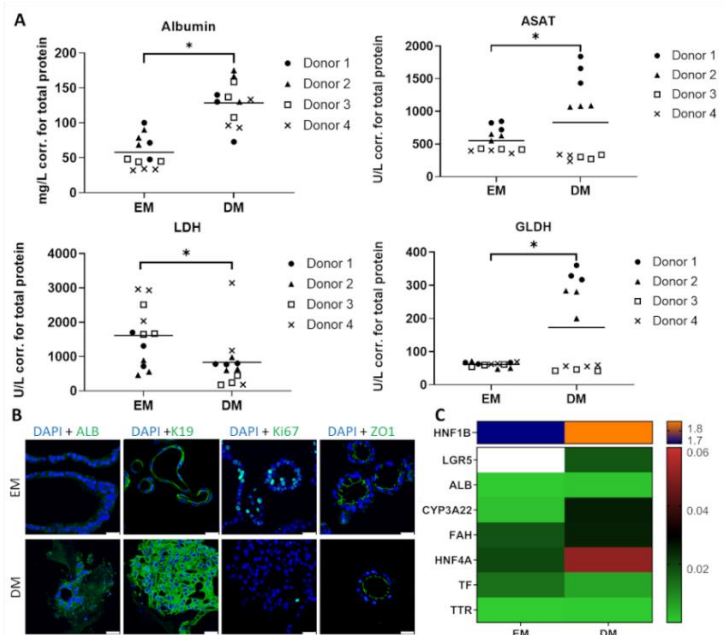
*Figure 2: A) Functional read-out in albumin secretion and enzyme activity (ASAT (Aspartate transaminase), LDH (Lactate dehydrogenase), GLDH (Glutamate dehydrogenase)) corrected for total protein after 5 days in DM (Differention medium) compared to EM (Expansion medium). Data depicted as grand mean (n = 4), * p < 0.05, B) Representative immunofluorescent staining for hepatocyte marker ALB (Albumin), ductular marker K19 (Keratin 19), proliferation marker (Ki67), polarization marker ZO1 (Tight junction protein 1) expression (all in green) and nuclei (DAPI in blue) for organoids in DM conditions after day 5 compared to EM conditions. Albumin and K19 are increased in DM, whereas Ki67 is decreased and ZO1 stable. Scale bars represent 25 µm. C) Heatmap showing gene expression relative to liver after 5 days of culture for DM conditions compared to EM conditions (median of donors, n = 3 per donor) with decreased expression of LGR5 (G-protein coupled receptor 5) (EM value above the top end of the scale) and TF (Transferrin), stable ALB and TTR (Transthyretin) expression, and increased expression of HNF1B (Hepatocyte nuclear factor 1 homeobox B), CYP3A22 (Cytochrome P450, family 3, subfamily alpha, polypeptide 22), FAH (Fumarylacetoacetate hydrolase), and HNF4A (Hepatocyte nuclear factor 4 alpha).*

5.4.3   Decellularized discs

Successful decellularization of livers was confirmed by the lack of nuclei and DNA present (see Figure 3C), and exemplary images of native versus decellularized liver scaffolds can be seen in Figure 3C as well. The organoids seeded onto these scaffolds showed lower expression of stemness markers LGR5 compared to EM control as well as lower expression of HNF1B (see Figure 3B). All hepatic markers were expressed by organoids seeded onto scaffolds. As seen by similar expression levels of HNF4A, ALB, TF, TTR, FAH and CYP3A22 between ICO's on scaffolds and in DM, maturation of the hepatocyte-like cells was at a comparable level.

The immunofluorescent stainings showed that the organoids efficiently infiltrated the scaffold and proceeded to express several distinct markers (Figure 3D). Albumin showed a positive staining in the vast majority of the cells seeded onto scaffolds. The hepatic markers HNF4A and K18 stained positive in several areas of the scaffolds indicating a hepatic differentiation in specific zones within the scaffold. The location of MDR1 also showed that the cells polarised on the scaffolds and formed canaliculi between cells. Some proliferative cells were observed in the scaffold as determined by a positive nuclear staining

for Ki67. Notably, organoids remained positive for ductular marker K19 on the scaffolds. Tight junction protein ZO1 was also positive throughout the scaffold indicating the creation of tight junctions between cells. The high engraftment efficiency, very similar to native tissue for most donors, can be seen in Figure 3E.
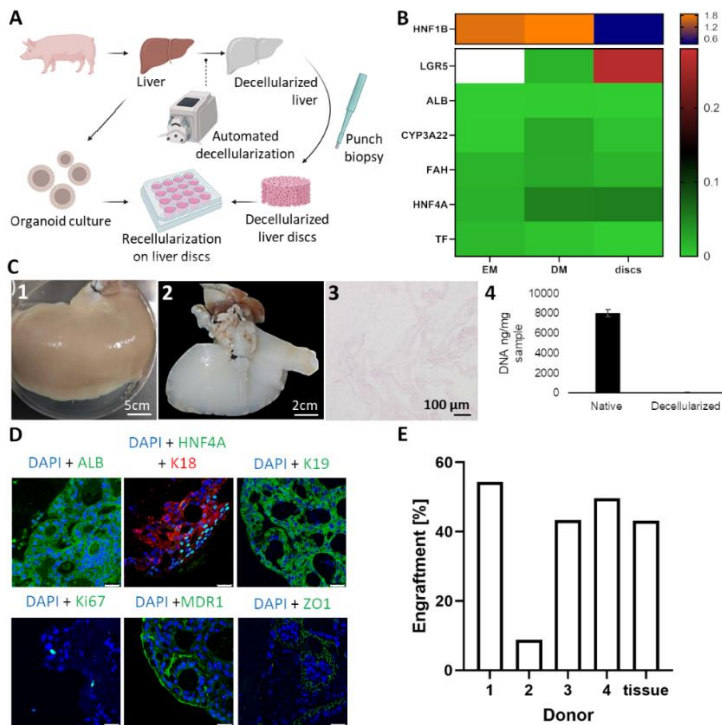
Figure 3: A) Scheme demonstrating how porcine materials are used to tissue engineer livers from decellularized tissue and hepatic organoids. B) Heatmap showing gene expression relative to liver after 5 days of culture for recellularized discs compared to EM (Expansion medium) and DM (differentiation medium) conditions (median of donors, n = 3 per donor) with increased expression of LGR5 (G-protein coupled

receptor 5) and HNF4A (Hepatocyte nuclear factor 4 alpha) in discs (EM value LGR5 off the top end of the scale) and decreased HNF1B (Hepatocyte nuclear factor 1 homeobox B), TF (Transferrin), stable ALB (Albumin) expression, and less CYP3A22 (Cytochrome P450, family 3, subfamily alpha, polypeptide 22), FAH (Fumarylacetoacetate hydrolase) expression compared to DM. C) Porcine liver decellularization and characterization – 1) Native porcine liver 2) Decellularized porcine right liver lobe 3) Hematoxylin & Eosin staining showing full cellular ablation 4) DNA extraction from the decellularized liver tissue shows a clear reduction of the amount of DNA present when compared with native hepatic tissue. D) Representative immunofluorescent staining for nuclei (DAPI in blue) and hepatocyte marker ALB, ductular marker K19 (Keratin 19), proliferation marker (Ki67), polarization markers MDR1 (Multidrug resistance protein 1), ZO1(Tight junction protein 1) (all in green) and hepatocyte marker K18 (Keratin 18) (in red) expression for organoids in recellularized discs after day 5. ALB, MDR1 and Ki67 show positive staining, K18 and K19 are highly expressed, and HNF4A only evident in part of the discs. Scale bars represent 25 µm. E) Engraftment percentage of 4 donors and native tissue based on image analysis of representative H&E stainings.

5.5 Discussion

In this study we show that ICOs can be successfully grown and differentiated from porcine liver tissue. Both the morphology as well as gene expression are stable over time and are both comparable to human ICOs grown in Matrigel[TM33,34] and to the limited data on porcine ICOs[27]. The ability of the porcine ICOs to differentiate was proven by the loss of stem cell and progenitor cell characteristics, increase in hepatocyte and cholangiocyte markers and functional assays that demonstrated increased liver enzyme activity, and epithelial polarity of the cells as

shown by ZO1 localization[35]. Notably, expression of HNF1B was very variable between donors, which might be due to different extraction locations of liver tissue and should therefore be taken into consideration in future experiments[36]. Although most donors behaved similarly in the clinical chemistry assays performed, two donors showed less hepatic differentiation for ASAT and GLDH. At this stage it remains unclear what the discrepancy for these two measurements is, although one indication is given by the low engraftment efficiency for donor 2. The positive staining of K19 validated the presence of ductal cells[37], as did the increase of the transcription factor HNF1B only expressed by biliary epithelial cells[38]. The discrepancy between the increased albumin protein levels and the constant albumin gene expression levels in differentiated compared to expanding cells could potentially be explained by the fact that albumin gene expression is known to be feedback regulated by the presence of albumin in serum[39].

Notably, immunofluorescent staining for K18 was very high and was observed in proximity of HNF4A positive cells, which further confirms the transformation towards hepatocyte-like cells[40]. The high expression of K18 could be explained by the hypothesis that as these keratins protect hepatocytes against apoptosis, the cells on the

discs are experiencing stress but are functional enough to activate counteractions and differentiate towards hepatocyte cell fate[37]. The organoids had been fragmented before seeding onto the scaffold, but nevertheless proceeded to self-organize as is evident by the polarization seen in MDR1 and ZO1 stainings[35]. The formation of canaliculi as shown here by K19 and MDR1 positive staining has previously been unsuccessful when human fetal hepatocytes have been used to repopulate decellularized porcine scaffolds even after 13 days of perfusion time[15]. It is possible that this is caused by cross-species differences between scaffold and cell source.

Although differentiation was largely successful, the resulting cells do not exhibit the same characteristics as native hepatocytes or cholangiocytes as seen for example in the localized expression of HNF4A or the lack of liver transaminase production of some donors and further optimization/maturation is necessary. Additionally, animal derived components such as Matrigel[TM] and Wnt cannot be used in a clinical setting and must be replaced by alternatives such as other ECM-mimicking hydrogels (cellulose nanofibril[34], gelPEG[41], Gelatin-methacrylol or other hydrogels[42]) and Wnt-surrogates[43].

Additionally, medium compositions could be further optimized in future studies. In the present study proliferation of organoids in expansion medium is mediated by R-spondin that activates Wnt signaling and is therefore present in EM medium but absent in DM medium[44]. Here, the combination of hepatocyte growth factor and dexamethasone drives maturation towards hepatocyte-like cells[45], as do FGF19 and BMP7[46]. Maturation could be enhanced by adding other compounds or ECM components during the differentiation such as Oncostatin M or fibronectin[47,48].To increase both cholangiocyte and hepatocyte differentiation, addition of collagen type I to the culture system have been proven to be of advantage[44,48]. Maturation of bile duct structures is achieved in the current study by utilizing the Notch inhibitor DAPT in DM medium, but biliary differentiation could be increased by addition of laminin and collagen IV[48].

In this study only small scaffold pieces were utilized to allow the cells to repopulate the ECM by diffusion which was very successful as seen by the engraftment percentage. However, in order to achieve complete population, it would be beneficial to use perfused liver scaffolds that make use of the native vascular network in the decellularized organ[18,28,31]. Thereby it is of advantage

to use fragmented organoids that are capable of self-organization as the whole organoids would be too large to pass through the smaller microvasculature of the liver and would also fail to repopulate the scaffold. Organoids, in particular porcine ones, possess the added advantage of being a representative model for disease modelling and drug research[27]. In addition to the administration of cells to the scaffold, co-culture of several cell-types is needed for differentiation[49], but also to gain full functionality of a native liver including bile secretion. As seen by the decrease of HNF1B expression, also differentiation into cholangiocytes and therefore bile duct formation is not at the level as seen in the DM Matrigel condition, whereas differentiation into hepatocyte-like cells was preferred as seen by the increase of HNF4A. Other required co-culture cells include parenchymal and non-parenchymal cells[50] as well as vascular endothelial cells[51]. Recently a novel method to scale up ICO production based on human stem cells was presented[40], which if applied successfully to the porcine model could lead to the cell amounts necessary to engineer whole livers. This method allows 40-fold expansion of organoids in spinner flasks in only 2 weeks as opposed to the regular 6-fold expansion in static cultures and further aids in differentiation towards hepatocytes. Therefore, further research will focus on co-

culturing of several cell-types, which ideally are grown in animal-free media at large scale to enable clinical application. Furthermore, engraftment efficiency in larger scaffolds could be achieved by perfusion of the scaffolds with cell-containing medium.

5.6 Conclusion

The aim of this work was to establish ICOs from porcine adult stem cells, which has been successful as they did not only show stable liver stem cell characteristics over multiple passages, but also differentiated into hepatocyte- and cholangiocytes-like cells. This differentiation was also possible on decellularized porcine liver scaffolds and the cells repopulated the liver discs, which has been very effective, and polarization even showed formation of canaliculi. This is an important step towards bioengineering whole liver tissue in a relevant large-animal model. With further improvements of organoids and repopulation of scaffolds with multiple cell types, the presented model can aid in understanding and treating liver diseases but also make whole organ engineering possible for transplantation and alleviate the organ donor shortage.

5.7 Acknowledgments

5.8 References

1. Asrani SK, Devarbhavi H, Eaton J, Kamath PS. Burden of liver diseases in the world. J Hepatol. 2019;70(1):151-171. doi:10.1016/j.jhep.2018.09.014

2. Pimpin L, Cortez-Pinto H, Negro F, et al. Burden of liver disease in Europe: Epidemiology and analysis of risk factors to identify prevention policies. J Hepatol. 2018;69(3):718-735. doi:10.1016/j.jhep.2018.05.011

3. Gola A, Davis S, Greenslade L, et al. Economic Analysis of Costs for Patients With End Stage Liver Disease Over the Last Year of Life. BMJ Support Palliat Care. 2015;5(1):110.2-110. doi:10.1136/bmjspcare-2014-000838.23

4. Bale SS, Vernetti L, Senutovitch N, et al. In Vitro Platforms for Evaluating Liver Toxicity. 2014;239(9):1180-1191. doi:10.1177/1535370214531872.In

5. Kaplan W. Priority Medicines for Europe and the World 2013 Update. Published 2013. http://apps.who.int/medicinedocs/documents/s20245en/s20245en.pdf

6. Bruix J, Han K, Gores G, Llovet JM, Mazzaferro V. Liver cancer : Approaching a personalized care. J Hepatol. 2015;62(1):S144-S156. doi:10.1016/j.jhep.2015.02.007

7. Scherer A, Dufour JF. Treatment of Non-Alcoholic Fatty Liver Disease. Dig Dis. 2016;34(1):27-31. doi:10.1159/000447278

8. Åberg F, Mäklin S, Räsänen P, et al. Cost of a quality-adjusted life year in liver transplantation: The influence of the indication and the model for

end-stage liver disease score. Liver Transplant. 2011;17(11):1333-1343. doi:10.1002/lt.22388

9. Blachier M, Leleu H, Peck-Radosavljevic M, Valla D-C, Roudot-Thoraval F. The burden of liver disease in Europe: A review of available epidemiological data. J Hepatol. 2013;58(3):593-608. doi:10.1016/j.jhep.2012.12.005

10. Jochmans I, Van Rosmalen M, Pirenne J, Samuel U. Adult Liver Allocation in Eurotransplant. Transplantation. 2017;101(7):1542-1550. doi:10.1097/TP.0000000000001631

11. Kulig KM, Vacanti JP. Hepatic tissue engineering. Transpl Immunol. 2004;12(3-4):303-310. doi:10.1016/j.trim.2003.12.005

12. Baptista PM, Siddiqui MM, Lozier G, Rodriguez SR, Atala A, Soker S. The use of whole organ decellularization for the generation of a vascularized liver organoid. Hepatology. 2011;53(2):604-617. doi:10.1002/hep.24067

13. Soto-Gutierrez A, Zhang L, Medberry C, et al. A Whole-Organ Regenerative Medicine Approach for Liver Replacement. Tissue Eng Part C Methods. 2011;17(6):677-686. doi:10.1089/ten.tec.2010.0698

14. Zhou P, Lessa N, Estrada DC, et al. Decellularized Liver Matrix as a Carrier for the Transplantation of Human Fetal and Primary Hepatocytes in Mice. Published online 2011:418-427. doi:10.1002/lt.

15. Barakat O, Abbasi S, Rodriguez G, et al. Use of Decellularized Porcine Liver for Engineering Humanized Liver Organ. J Surg Res. 2012;173(1):e11-e25. doi:10.1016/j.jss.2011.09.033

16. Furuta T, Furuya K, Zheng Y, Oda T. Novel alternative transplantation therapy for orthotopic liver. World J Transplant. 2020;10(3):64-78. doi:10.5500/wjt.v10.i3.64

17. Rossi EA, Quintanilha LF, Nonaka CKV, Souza BS de F. Advances in Hepatic Tissue Bioengineering with Decellularized Liver Bioscaffold. Stem Cells Int. 2019;2019(Article ID 2693189):1-13. doi:10.1155/2019/2693189

18. Yagi H, Fukumitsu K, Fukuda K, et al. Human-scale whole-organ bioengineering for liver transplantation: A regenerative medicine approach. Cell Transplant. 2013;22(2):231-242. doi:10.3727/096368912X654939

19. Ko IK, Peng L, Peloso A, et al. Bioengineered transplantable porcine livers with re-endothelialized vasculature. Biomaterials. 2015;40:72-79. doi:10.1016/j.biomaterials.2014.11.027

20. Ren H, Shi X, Tao L, et al. Evaluation of two decellularization methods in the development of a whole-organ decellularized rat liver scaffold. Liver Int. 2013;33(3):448-458. doi:10.1111/liv.12088

21. Zhang H, Siegel CT, Li J, et al. Functional liver tissue engineering by an adult mouse liver-derived neuro-glia antigen 2-expressing stem/progenitor population. J Tissue Eng Regen Med. 2018;12(1):e190-e202. doi:10.1002/term.2311

22. Takeishi K, Collin de l'Hortet A, Wang Y, et al. Assembly and Function of a Bioengineered Human Liver for Transplantation Generated Solely from Induced Pluripotent Stem Cells. Cell Rep. 2020;31(9):107711. doi:10.1016/j.celrep.2020.107711

23. Kirk AD. Crossing the bridge: Large animal models in translational transplantation research. Immunol Rev. 2003;196:176-196. doi:10.1046/j.1600-065X.2003.00081.x

24. Merrifield CA, Lewis M, Claus SP, et al. A metabolic system-wide characterisation of the pig: A model for human physiology. Mol Biosyst. 2011;7(9):2577-2588. doi:10.1039/c1mb05023k

25. Bassols A, Costa C, Eckersall PD, Osada J, Sabrià J, Tibau J. The pig as an animal model for human pathologies: A proteomics perspective. Proteomics - Clin Appl. 2014;8(10):715-731. doi:10.1002/prca.201300099

26. Ribitsch I, Baptista PM, Lange-Consiglio A, et al. Large Animal Models in Regenerative Medicine and Tissue Engineering: To Do or Not to Do. Front Bioeng Biotechnol. 2020;8:972:1-28. doi:10.3389/fbioe.2020.00972

27. Olayanju A, Jones L, Greco K, Goldring CE, Ansari T. Application of porcine gastrointestinal organoid units as a potential in vitro tool for drug discovery and development. J Appl Toxicol. 2019;39(1):4-15. doi:10.1002/jat.3641

28. Ansari T, Southgate A, Obiri-Yeboa I, et al. Development and characterization of a porcine liver scaffold. Stem Cells Dev. 2020;29(5):314-326. doi:10.1089/scd.2019.0069

29. Lin P, Chan CWW, Badylak SF, Bhatia SN. Assessing Porcine Liver-Derived Biomatrix for Hepatic Tissue Engineering. Tissue Eng - Part A. 2004;10(7/8):1046-1053. doi:http://doi.org/10.1089/ten.2004.10.1046

30. Willert K, Brown JD, Danenberg E, et al. Wnt proteins are lipid-modified and can act as stem cell

growth factors. Nature. 2003;423(6938):448-452. doi:10.1038/nature01611

31. Iris Pla-Palacın, Sainz-Arnal P, Morini S, Almeida M, Baptista PM. Liver Bioengineering Using Decellularized Whole-Liver Scaffolds. Methods Mol Biol. 2017;1577:293-305. doi:10.1007/7651_2017_98

32. Bustin SA, Beaulieu J-F, Huggett J, et al. MIQE précis: Practical implementation of minimum standard guidelines for fluorescence-based quantitative real-time PCR experiments. BMC Mol Biol. 2010;11(1):74. doi:10.1186/1471-2199-11-74

33. Huch M, Gehart H, Van Boxtel R, et al. Long-term culture of genome-stable bipotent stem cells from adult human liver. Cell. 2015;160(1-2):299-312. doi:10.1016/j.cell.2014.11.050

34. Krüger M, Oosterhoff LA, van Wolferen ME, et al. Cellulose Nanofibril Hydrogel Promotes Hepatic Differentiation of Human Liver Organoids. Adv Healthc Mater. 2020;9(6):1901658. doi:10.1002/adhm.201901658

35. Treyer A, Müsch A. Hepatocyte Polarity. Compr Physiol. 2013;3:243-287. doi:10.1002/cphy.c120009

36. Rimland CA, Tilson SG, Morell CM, et al. Regional Differences in Human Biliary Tissues and Corresponding In Vitro–Derived Organoids. Hepatology. 2021;73(1):247-267. doi:10.1002/hep.31252

37. Ku NO, Strnad P, Zhong BH, Tao GZ, Omary MB. Keratins let liver live: Mutations predispose to liver disease and crosslinking generates Mallory-Denk bodies. Hepatology. 2007;46(5):1639-1649. doi:10.1002/hep.21976

38. Limaye PB, Alarcón G, Walls AL, et al. Expression of specific hepatocyte and cholangiocyte transcription factors in human liver disease and embryonic development. Lab Investig. 2008;88(8):865-872. doi:10.1038/labinvest.2008.56

39. Pietrangelo A, Panduro A, Chowdhury JR, Shafritz DA. Albumin gene expression is down-regulated by albumin or macromolecule infusion in the rat. J Clin Invest. 1992;89(6):1755-1760. doi:10.1172/JCI115778

40. Schneeberger K, Sánchez-Romero N, Ye S, et al. Large-Scale Production of LGR5-Positive Bipotential Human Liver Stem Cells. Hepatology. 2020;72(1):257-270. doi:10.1002/hep.31037

41. Klotz BJ, Oosterhoff LA, Utomo L, et al. A Versatile Biosynthetic Hydrogel Platform for Engineering of Tissue Analogues. Adv Healthc Mater. 2019;1900979:1-13. doi:10.1002/adhm.201900979

42. Schneeberger K, Spee B, Costa P, Sachs N, Malda J. Converging biofabrication and organoid technologies: the next frontier in hepatic and intestinal tissue engineering? Biofabrication. 2017;9(1):013001. doi:10.1088/1758-5090/aa6121

43. Janda CY, Dang LT, You C, et al. Surrogate Wnt agonists that phenocopy canonical Wnt and β-catenin signalling. Nature. 2017;545(7653):234-237. doi:10.1038/nature22306

44. Chen C, Jochems PGM, Salz L, et al. Bioengineered bile ducts recapitulate key cholangiocyte functions. Biofabrication. 2018;10(3). doi:10.1088/1758-5090/aac8fd

45. Kamiya A, Kinoshita T, Miyajima A. Oncostatin M

and hepatocyte growth factor induce hepatic maturation via distinct signaling pathways. FEBS Lett. 2001;492(1-2):90-94. doi:10.1016/S0014-5793(01)02140-8

46. Fatehullah A, Tan SH, Barker N. Organoids as an in vitro model of human development and disease. Nat Cell Biol. 2016;18(3):246-254. doi:10.1038/ncb3312

47. Zhang W, Li W, Liu B, Wang P, Li W, Zhang H. Efficient generation of functional hepatocyte-like cells from human fetal hepatic progenitor cells in vitro. J Cell Physiol. 2012;227(5):2051-2058. doi:10.1002/jcp.22934

48. Vyas D, Baptista PM, Brovold M, et al. Self-assembled liver organoids recapitulate hepato-biliary organogenesis in vitro. Hepatology. 2018;67(2):750-761. doi:https://doi.org/10.1002/hep.29483

49. Bhandari RNB, Riccalton LA, Lewis AL, et al. Liver tissue engineering: A role for co-culture systems in modifying hepatocyte function and viability. Tissue Eng. 2001;7(3):345-357. doi:10.1089/10763270152044206

50. Otsuka H, Sasaki K, Okimura S, Nagamura M, Nakasone Y. Micropatterned co-culture of hepatocyte spheroids layered on non-parenchymal cells to understand heterotypic cellular interactions. Sci Technol Adv Mater. 2013;14(6). doi:10.1088/1468-6996/14/6/065003

51. Meng F, Assiri A, Dhar D, Broering D. Whole liver engineering: A promising approach to develop functional liver surrogates. Liver Int. 2017;37(12):1759-1772. doi:10.1111/liv.13444

5.9 Supplementary Material

Supplementary Table 1: Relative gene expression to liver per condition (EM (expansion medium), DM (differentiation medium), p1,3,6 (passage), discs (recellularized scaffolds). LGR5 (G-protein coupled receptor 5), HNF1B (hepatocyte nuclear factor 1 homeobox B), ALB (Albumin), CYP3A22 (Cytochrome P450, family 3, subfamily alpha, polypeptide 22), HNF4A (Hepatocyte nuclear factor 4 alpha), TF (Transferrin), FAH (Fumarylacetoacetate hydrolase), TTR (Transthyretin).

Marker	Condition	Relative gene expression to liver [Median (interquartile range)]
LGR5	EM, p1	5.84×10^{-02} (1.87×10^{-01}, 1.75×10^{-02})
	EM, p3	6.24×10^{-01} (6.97×10^{-01}, 3.56×10^{-01})
	EM, p6	8.45×10^{-01} ($1.87 \times 10^{+00}$, 7.64×10^{-01})
	EM	7.90×10^{-01} ($1.47 \times 10^{+00}$, 3.76×10^{-01})
	DM	1.70×10^{-02} (5.01×10^{-02}, 3.40×10^{-03})
	Discs	2.64×10^{-01} ($1.60 \times 10^{+00}$, 4.26×10^{-02})
HNF1B	EM, p1	$1.03 \times 10^{+00}$ ($7.49 \times 10^{+01}$, 6.71×10^{-01})
	EM, p3	$1.69 \times 10^{+00}$ ($5.24 \times 10^{+01}$, $1.24 \times 10^{+00}$)
	EM, p6	$5.72 \times 10^{+00}$ ($1.32 \times 10^{+01}$, $3.51 \times 10^{+00}$)
	EM	$1.69 \times 10^{+00}$ ($2.20 \times 10^{+00}$, 8.14×10^{-01})
	DM	$1.88 \times 10^{+00}$ ($2.24 \times 10^{+00}$, $1.33 \times 10^{+00}$)
	Discs	3.25×10^{-01} (3.38×10^{-01}, 2.83×10^{-01})
ALB	EM, p1	1.42×10^{-03} (3.62×10^{-03}, 6.86×10^{-04})
	EM, p3	8.12×10^{-04} (1.76×10^{-03}, 4.62×10^{-04})
	EM, p6	2.55×10^{-04} (9.32×10^{-04}, 1.01×10^{-04})
	EM	1.87×10^{-04} (1.16×10^{-03}, 2.37×10^{-06})
	DM	1.19×10^{-03} (4.32×10^{-03}, 7.03×10^{-05})
	Discs	1.26×10^{-04} (1.70×10^{-04}, 3.34×10^{-05})
CYP3A22	EM, p1	7.97×10^{-03} (2.34×10^{-02}, 1.71×10^{-03})
	EM, p3	9.94×10^{-03} (8.17×10^{-02}, 3.00×10^{-03})
	EM, p6	1.02×10^{-02} (4.05×10^{-02}, 4.44×10^{-03})
	EM	1.65×10^{-03} (1.52×10^{-02}, 2.76×10^{-05})
	DM	2.56×10^{-02} (6.35×10^{-02}, 7.02×10^{-03})
	Discs	8.85×10^{-03} (1.57×10^{-02}, 8.06×10^{-04})
HNF4a	EM, p1	3.07×10^{-02} (9.79×10^{-02}, 1.48×10^{-02})
	EM, p3	4.26×10^{-02} (1.10×10^{-01}, 2.22×10^{-02})
	EM, p6	2.63×10^{-02} (6.18×10^{-02}, 8.73×10^{-03})
	EM	1.94×10^{-02} (4.06×10^{-02}, 1.10×10^{-02})
	DM	5.10×10^{-02} (1.22×10^{-01}, 3.82×10^{-02})
	Discs	5.31×10^{-02} (1.99×10^{-01}, 1.48×10^{-02})
TF	EM, p1	1.29×10^{-02} (2.76×10^{-01}, 5.12×10^{-03})
	EM, p3	4.88×10^{-02} (2.46×10^{-01}, 3.06×10^{-02})
	EM, p6	2.27×10^{-02} (6.22×10^{-02}, 9.58×10^{-03})
	EM	1.34×10^{-02} (6.59×10^{-02}, 6.50×10^{-05})
	DM	5.85×10^{-03} (1.53×10^{-02}, 1.68×10^{-03})
	Discs	5.82×10^{-04} (1.45×10^{-03}, 9.38×10^{-05})

FAH	EM, p1	2.29×10^{-02} (3.94×10^{-02}, 1.24×10^{-02})
	EM, p3	3.42×10^{-02} (9.93×10^{-02}, 2.42×10^{-02})
	EM, p6	1.38×10^{-02} (4.61×10^{-02}, $0.00 \times 10^{+00}$)
	EM	1.77×10^{-02} (2.76×10^{-02}, $1,25 \times 10^{-02}$)
	DM	2.51×10^{-02} (3.70×10^{-02}, 1.09×10^{-02})
	Discs	1.65×10^{-02} (6.95×10^{-01}, 9.44×10^{-03})
TTR	EM, p1	6.12×10^{-05} (1.07×10^{-04}, 1.85×10^{-05})
	EM, p3	3.75×10^{-05} (1.33×10^{-04}, 2.09×10^{-05})
	EM, p6	3.80×10^{-05} (2.98×10^{-04}, 2.82×10^{-05})
	EM	7.56×10^{-06} (6.52×10^{-05}, 8.73×10^{-07})
	DM	2.00×10^{-04} (9.31×10^{-04}, 5.32×10^{-05})
	Discs	n/a

Supplementary Table 2: Medium composition Expansion and Differentiation Medium

Component	Concentration in Expansion Medium (EM)	Concentration in Differentiation Medium (DM)
Advanced DMEM/F12		
Glutamax	1% (v/v)	1% (v/v)
Penicillin-Streptomycin	1% (v/v)	1% (v/v)
HEPES	1% (v/v)	1% (v/v)
Wnt3a-conditioned medium	30% (v/v)	-
N2	1% (v/v)	1% (v/v)
Nicotinamide	10 mM	-
B27 without vitamin A	2% (v/v)	2% (v/v)
R-spondin conditioned medium	10% (v/v)	-
N-acetylcysteine	1.25 mM	1.25 mM
Y-27632	10 µM	-
A83-01	5 µM	5 µM
Human epidermal growth factor (EGF)	50 ng/mL	50 ng/mL
Human noggin	0.1 µg/mL	0.1 µg/mL
Fibroblast growth factor 10 (FGF10)	0.1 µg/mL	-
Gastrin	10 nM	10 nM
Hepatocyte growth factor (HGF)	25 ng/mL	25 ng/mL
Forskolin	10 µM	-
Primocin	1% (v/v)	1% (v/v)
FGF19	-	0.1 µg/mL
Dexamethasone	-	30 µM
DAPT (y-secretase inhibitor)	-	10 µM
BMP7	-	25 ng/mL
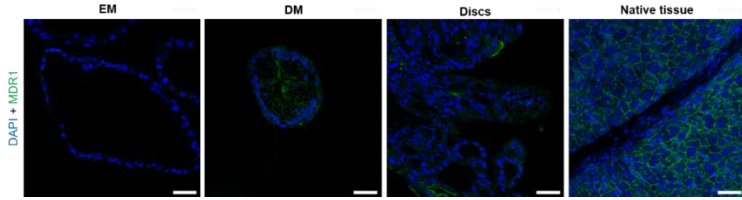
Supplementary Figure 1: Representative immunofluorescent staining for nuclei (DAPI in blue) and polarization marker MDR1 (Multidrug resistance protein 1) (all in green) for organoids in EM (Expansion Medium) and DM (Differentiation Medium) conditions, recellularized discs after day 5 and native liver tissue. MDR1 shows polarization of organoids in DM conditions and on discs. Scale bars represent 25 μm.

6 Normothermic *ex vivo* liver platform using porcine slaughterhouse organs for disease modeling

Melanie Krüger[1,2#], Alicia Ruppelt[1,3#*], Benjamin Kappler[1], Elke van Soest[1], Roos Anne Samsom[2], Guy C.M. Grinwis[4], Niels Geijsen[2], J. Bernd Helms[5], Marco Stijnen[1], Linda M. Kock[1,6], Marco Rasponi[3], Hans S. Kooistra[2], Bart Spee[2]

[1]LifeTec Group BV, Eindhoven, The Netherlands

[2]Department of Clinical Sciences, Faculty of Veterinary Medicine, Utrecht University, Utrecht, The Netherlands

[3]Dipartimento di Elettronica, Informazione e Bioingegneria, Politecnico di Milano, Milan, Italy

[4]Veterinary Pathology Diagnostic Centre, Department of Biomedical Health Sciences, Faculty of Veterinary Medicine, Utrecht University, Utrecht, The Netherlands

[5]Department of Biomolecular Health Sciences, Faculty of Veterinary Medicine, Utrecht University, Utrecht, Netherlands

[6]Department of Biomedical Engineering, Eindhoven University of Technology, Eindhoven, The Netherlands

[#]These authors have contributed equally to this work.
[*]Corresponding author

6.1 Abstract

Metabolic and toxic liver disorders, such as fatty liver disease (steatosis) and drug-induced liver injury, are highly prevalent and potentially life-threatening. To allow for the study of these disorders from the early stages onward, without using experimental animals, we collected porcine livers in a slaughterhouse and perfused these livers normothermically. With our simplified protocol, the perfused slaughterhouse livers remained viable and functional over five hours of perfusion, as shown by hemodynamics, bile production, indocyanine green clearance, ammonia metabolism, gene expression and histology. As a proof-of-concept to study liver disorders, we show that an infusion of free fatty acids and acetaminophen results in early biochemical signs of liver damage, including reduced functionality. In conclusion, the present platform offers an accessible system to perform research in a functional, relevant large animal model while avoiding using experimental animals. With further improvements to the model, prolonged exposure could make this model a versatile tool for studying liver diseases and potential treatments.

6.2 Introduction

Liver diseases in humans impose a great burden on society, in terms of suffering and death as well as economically, and account for two million deaths per year worldwide [1–3]. More than 5500 liver transplants are performed in Europe each year, which currently is the only available treatment for end-stage liver diseases [4]. Moreover, there is a lack of understanding of the aetiology and/or pathogenesis for many of the most prevalent non-viral liver diseases, such as drug-induced liver injury (DILI)[5], alcoholic liver disease [6], liver cancer [7] and Metabolic Associated Fatty Liver Disease (MAFLD) [8].

Despite many efforts, neither the currently available *in vivo* nor *in vitro* systems represent satisfactory DILI models, in part due to the complexity of the diseases, and need to be improved significantly[9]. The latter also applies to the diagnosis and understanding of the hepatic diseases [10]. Therefore, there is a clear need for a reliable model to study liver diseases starting from very early stages to understand the underlying pathophysiology, design preventive strategies, improve diagnosis and find cures and treatments.

One option to study the effect of drugs, liver diseases and their treatments are *ex vivo* liver models. For many

decades, organs have been kept viable outside the body through ex vivo machine perfusion. Recently, research evolved to preserve them for transplantation using ex vivo machine perfusion [11]. It keeps the organs in a physiological state without energy depletion and accumulation of waste products and, therefore, can also maintain organs with previous damage and extends utilization [11,12].

In transplantation research, different normothermic perfusion devices and protocols have been developed and applied to keep donor livers or donor liver grafts viable until transplantation [11–22]. Although these devices are mostly used for transplantation purposes, they can also be very valuable in a research setting [22], using for example, (slaughterhouse) animal livers. Most devices and methods are, however, very complex, which has led to reduced feasibility due to practical reasons, costs, and ease of use [22,23]. The design of the perfusion circuits varies widely in literature with regard to the number of pumps used, whether the system is draining openly or closed, and which oxygenators and heat exchangers are used [22]. Although all systems have a dual inflow into the hepatic artery (HA) and portal vein (PV), pressures and flows, the composition of the perfusion fluid as well as temperature, oxygen levels and perfusion duration differ among studies

[22]. Generally, every pump introduces mechanical stress that can damage the red blood cells, although centrifugal pumps are overall less damaging than other pumps [24]. Therefore, it is more beneficial to use only one centrifugal pump if possible. In addition to a pump supplying the PV, a second pump is often used to enable a pulsatile inflow into the HA, although there is no clear significant advantage to pulsatility [22]. Many different additives are given to the perfusion fluids, such as anticoagulants, vasodilators, insulin, varying nutrients, antibiotics, or bile salts [22]. However, the need for many of these additives, except for anticoagulants, especially in short-term perfusion, is unclear. Some of them might even have adverse effects, such as insulin and glucose, that can cause glycogen depletion in hepatocytes [22]. Furthermore, the need for dialysis during short-term perfusion is unclear, as it is found to be not strictly necessary in the presence of sufficient nutrients [25].

Porcine organs are considered potential relevant models as they are of appropriate size for transplantation, have comparable anatomy, immunology [18] and bile composition [22] compared to humans. In a review by Maione et al. [22], porcine isolated liver perfusion models were assessed in terms of their usefulness for ischemic reperfusion injury research [22]. Unfortunately, most models had limitations,

especially regarding reproducibility of results and standardization of models. Therefore, a model focused on the basic elementary components would assist in reaching this aim. All of the 16 reviewed models utilized pig livers harvested in animal experiments, to this date very few groups worked with slaughterhouse livers. The group of Grosse-Siestrup developed a perfused porcine model using livers obtained from a slaughterhouse [26], which was successfully utilized for demonstrating diclofenac toxicity [27] and fungal infections [28]. However, the maximum perfusion time was 220 min, which is probably due to increasing liver failure even in control livers as indicated by high levels of hepatic damage markers [26]. The circuit design contained three pumps, two of them roller pumps, and a dialysis unit [27,28], making the set-up not only complex but also increases the risk of hemolysis especially over extended perfusion periods. In another study by Izamis et al. [29], slaughterhouse porcine livers were perfused and examined with dynamic contrast-enhanced ultrasound, but could only be sustained on asanguineous perfusate for 3 h [29]. The group aimed to create a cost- effective and simple design, but mostly focused on the quality of perfusion and monitoring thereof—not the vitality and functionality of the livers. The use of another perfusion fluid than whole blood limits the

usefulness in terms of hemodynamic parameters [22], viability and even cost-effectiveness of the model. Consequently, a simple and cost-effective design that is shown to preserve viability and functionality in a relevant ex vivo perfused liver model is lacking.

Although hepatotoxicity has been tested previously on *ex vivo* slaughterhouse livers using diclofenac [27], currently no such model for acetaminophen toxicity exists. The only *ex vivo* liver models used for acetaminophen toxicity are based on human liver pieces [30], or animal experiments using pigs [31]. For steatosis only models introducing the disease in experimental animals exist [32], or alternatively, the much less representative precision-cut liver slices [33] or *in vitro* cell cultures [34].

We developed a minimal design and approach in order to be able to keep porcine livers obtained from a slaughterhouse viable outside of the body in a reproducible, stable manner. In this way, we intended to create a model that can be used for disease and treatment research instead of animal models, which is in compliance with the 3R principle without necessitating very complex and, therefore, costly and difficult aspects that could prevent such an application. To further assess the potential of the model for research purposes, we aimed to develop an *ex*

vivo model representing the basic mechanisms that can lead to steatosis. Additionally, we aimed to verify whether hepatotoxicity can be studied in our model and, therefore, exposed the *ex vivo* liver to acetaminophen.

6.3 Materials and Methods

6.3.1 Liver and Blood Procurement

Livers were harvested from clinically healthy Dutch Landrace Hybrid pigs at four- to-six months of age and an average body weight of 110 kg. The pigs, raised for human consumption, were sedated with CO_2 and subsequently exsanguinated at the slaughterhouse. The livers were collected after a warm ischemic time of 25 min after the death of the animal. Compliance of the slaughter process with the protocols of EC regulations 1069/2009 was supervised by the Dutch Ministry of Agriculture, Food and Food Quality and approved by the Food and Consumer Product Safety Authority. No ethical approval was required due to the fact that liver tissue was removed from already terminated animals. Animals were terminated for food production, but liver tissue is not used for human consumption. The complete gastrointestinal tract was excised from the pigs, and the liver was isolated from the tract subsequently. The bile duct was ligated immediately, and the portal vein was cannulated and

subsequently flushed with 2 L of cold Custodiol® solution (Dr. Franz Köhler Chemie GmbH, Bensheim, Germany) containing a total of 25,000 U heparin (5000 U/L, LEO Pharma, Amsterdam, The Netherlands). The perfusate was collected, stored and transported together with the liver at 4 °C.

Blood was pooled from two electro-stunned pigs per experiment in the slaughterhouse. After stunning, the pigs were hung from their hind legs and exsanguinated by opening the carotid arteries and jugular veins. On average, 7–8 L of blood was mixed with 550 mL of modified Tyrode's solution to buffer the blood and maintain osmotic pressure, containing a total of 60,000 U heparin and stored and transported in a jerry can. The total time between the death of the pig, cold storage, and reperfusion was maximally 3.5 h. To minimize contamination during harvesting and blood collection, all instruments and transport components were packed and handled sterile.

6.3.2 Circuit Design

The liver was perfused through both the HA and PV with a pressure-driven continuous flow (Figure 1A and Figure S1). The perfusion fluid was circulated from the reservoir through an arterial filter (38 µm, Medtronic, Dublin,

Ireland) and an oxygenator with an integrated heat exchanger (EOS ECMO, LivaNova, London, UK) into the liver and through the open vena cava back into the reservoir. The oxygenation level of the blood was maintained above 95%. The pressure in the HA was set by a centrifugal pump (Biomedicus 550, Dublin, Ireland), whereas the static pressure in the PV was achieved by controlling the height of a second reservoir. Pressures and flow rates were measured at the inlets of the HA and PV. The circuit was primed and deaired with 4.5 L of a modified Tyrode's solution (priming solution), which was then supplemented with porcine blood to achieve a total perfusion volume of 7–8 L. The total perfusion volume was reduced to 5 L during the experiments with administration of continuous free fatty acid (FFA) and 300 mg/L acetaminophen (APAP).

6.3.3   Reperfusion

Prior to perfusion, the blood was filtered through a 200 μm filter (Sentinel filter, EATON, Dublin, Ireland) in order to remove any possible blood clots or contaminations. The blood was then oxygenated, and blood gas values were measured with a VetScan i-Stat 1 (Abaxis, Union City, CA, USA). Based on these values, the initial pH was set to a physiological level (7.35–7.45) using 1 mmol/L

190

sodium bicarbonate, and the target of 1 mmol/L ionized calcium was balanced by using calcium chloride (both from VWR, Amsterdam, The Netherlands).

In the meantime, the liver was weighed and prepared on melting ice. The HA, bile duct and caudal vena cava were cannulated while ensuring that the liver vessels were free of air. Vena cava remained open to drain freely into a custom-built receptacle, and HA and PV were connected to the circuit while avoiding air from entering the vessels. To reduce reperfusion injury, reperfusion was started with a pressure of 22–35 mmHg in the HA and 3–5 mmHg in the PV. Blood rewarming was started upon reperfusion and set to 38 ℃. As the resistance of the liver reduced over time, pressures were slowly increased for about an hour until they reached physiological levels of 90 (±9.5) mmHg in the HA and 7 (±2.3) mmHg in the PV [13].

After these hemodynamic values were reached, the livers were either perfused without further treatment or perfused with APAP or FFA. For livers without treatment (n = 3), bile production and blood gas parameters were measured every 60 min, pressures and flows were recorded, and pH, as well as the level of ionized calcium, were balanced. Blood samples were drawn at timepoints 0, 30, 60, 180, and 300 min and an indocyanine green (ICG) functionality

assay was performed at timepoints 0, 60, 180 and 300 min. Tissue samples for histology were taken before and after 5 h of perfusion, and analysis was executed as described below.

6.3.4   Free fatty acid treatment

To induce an early-stage steatotic liver, four perfused livers were treated with free fatty acids. Two perfused livers (FFA_bol) were treated with only one bolus mixture (t = 0) of 1.2 mM oleate (C18:1) (90% purity, Thermo Fisher GmbH, Kandel, Germany) and

0.6 mM palmitate (C16:0) (95% purity, Thermo Fisher GmbH) with 16% (*w/v*) fatty acid-free BSA (Fraction V, Gold Biotechnology, Inc., St. Louis, MO, USA) and two perfused livers (FFA_cts) were treated with the same initial bolus mixture (t = 0), but additionally, 25% of the initial dose was administered every 30 min to keep the concentration of free fatty acids in the liver at a constant level. The FFA bolus mixtures were administered with the start of reperfusion in order to allow the maximally available time for FFA metabolism. These concentrations were based on pilot experiments (data not shown) and literature [34,35]. During the experiment, bile production and blood gas parameters were measured every 60 min, pressures and flow rates were recorded, and pH, as well

as ionized calcium, were balanced. Blood samples for hematology were taken and analyzed as described below.

Additionally, tissue samples were flash frozen by first submerging them in isopropanol (2-propanol, Merck KGaA, Darmstadt, Germany) at −80 °C, then embedding them in Tissue-Tek optimal cutting temperature (O.C.T.) Compound (Sakura Finetek USA Inc., Torrance, CA, USA) and snap frozen in isopentane solution (VWR), samples were stored at −80 °C until further processing. Liver functionality was measured with an ICG assay, and the livers were weighed before and after perfusion.

6.3.5   Acetaminophen treatment

To test acetaminophen toxicity on the *ex vivo* livers, 500 mg of the active component N-acetyl-para-aminophenol (APAP; Centrafarm Services B.V., Breda, The Netherlands) was dissolved in distilled water at a concentration of 4 mg/mL, and after dissolution, the NaCl level was adapted to the physiological level of 9 g/L. The APAP solution was administered with two different plasma concentrations. The first group received a bolus directly into the blood circulation (APAP_155, $n = 3$) to amount to 155 mg/L of APAP in plasma as it is between the toxic dose of 150 mg/L but below the lethal dose of 160 mg/L

193

[36]. In the second group, a higher concentrated bolus was administered to amount to 300 mg/L plasma concentration (APAP_300, $n = 3$). Prior to APAP administration, the livers were perfused for 60–90 min to reach desired pressures and flows in order to avoid additional adverse effects on the liver during the initial reperfusion; the timepoint of APAP administration was defined as t = 0. Blood samples were taken 40 min before APAP administration and at the timepoints 10, 20, 30, 40, 60, 100, 140, 180, 220, and 300 min and treated and analyzed as described below. Blood gas measurements, pH, and ionized calcium level balance were executed at -40, 0, 60, 180, 220, and 300 min. Liver functionality was determined by an ICG assay, as described below. Tissue samples for histology were taken in the slaughterhouse, before the start of perfusion and after perfusion and were fixed in formalin as described below. The livers were also weighed before and after perfusion.

6.3.6 Analysis

Blood gas parameters were measured during the experiments, and pH and levels of ionized calcium were maintained manually. Bile production was equally measured by weighing the produced bile. Pressures and flow rates in HA and PV were monitored and recorded

continuously. Blood samples were drawn from the oxygenator, centrifuged at $2300 \times g$ for 15 min and stored at $-80\ °C$ or $4\ °C$ overnight, depending on the anal- ysis. The next day, samples were transported to a clinical laboratory (Máxima Medisch Centrum, Veldhoven, The Netherlands) for analysis of concentrations of free fatty acid, urea, aspartate transaminase (AST), lactate dehydrogenase (LDH), ammonia, and lactate in a C8000 analyser (Roche Diagnostics International AG, Rotkreuz, Switzerland). After 5 h of perfusion, tissue samples were taken from an incision in the left lateral lobe with a biopsy punch (8 mm Ø, Megro GmbH & Co. KG, Wesel, Germany) for histology and RNA analysis. Tissue samples for histology were fixed in 10% *v/v* neutral-buffered formalin solution (4% *v/v* formaldehyde, Sigma-Aldrich, Zwijndrecht, The Netherlands) for one hour and then stored in 70% *v/v* ethanol (VWR) until further processing. Samples for RNA analysis were stored in RNAlater® solution (Thermo Fisher Scientific, Eindhoven, The Netherlands) at $-20\ °C$ until further analysis. As a control, tissue samples from livers were taken directly after slaughtering in the slaughterhouse. After perfusion, the liver was weighed again.

Gene expression

Biopsies stored in RNAlater® (Thermo Fisher Scientific, Eindhoven, The Netherlands) were lysed with 350 µL RLT buffer (Qiagen, Hilden, Germany) containing 1% (v/v) 2-Mercaptoethanol (Sigma-Aldrich). Isolation of mRNA was done according to the manufacturer's instructions with a RNeasy micro-kit (Qiagen), and the total mRNA was measured with a NanoDrop ND-1000 spectrophotometer (Thermo Fisher Scientific) at 260/280 nm. For the synthesis of complementary DNA (cDNA) from 500 ng mRNA, the manufacturer's protocol for the used iScript cDNA Synthesis Kit (Bio-Rad, Hercules, CA, USA) was applied. Quantitative PCR (qPCR) was performed using a Bio-Rad CFX384 Real-Time PCR Detection System (Bio-Rad) with 10 ng cDNA per reaction and iQ™ SYBR® Green Supermix (Bio-Rad). Primers are listed in Table S1. Data were analyzed with BioRad CFX manager software, and relative gene expression was calculated according to the $2^{-\Delta CT}$ formula (E/100 × $2^{-\Delta CT}$, with E = efficiency and ΔCT = mean threshold cycle gene of interest—mean reference gene threshold cycle) and normalized to the reference genes YWHAZ and RSP19. The normalized data was log-transformed for representation in the heatmap.

Histology

The formalin-fixed biopsies were routinely embedded in paraffin and cut into 5 µm sections before they were deparaffinized and rehydrated.

For immunohistochemistry, the slides were blocked in 10% (*v/v*) of normal goat serum (Sigma-Aldrich) in PBS after antigen retrieval. Antigen retrieval for albumin (ALB) and multi-drug resistance protein 2 (MRP2/ABCC2) staining was achieved in a citrate buffer (pH 6.0) for 30 min at 98 °C. For hepatocyte nuclear factor 4 alpha (HNF4a), antigen retrieval was performed in a Tris EDTA buffer (pH 9.0) for 30 min at 98 °C, and zonula occludens-1 (ZO1) antigen retrieval was performed with proteinase K (Dako, Santa Clara, CA, USA) for 10 min at room temperature (RT). The primary antibody for albumin (Sigma-Aldrich) was incubated at a 1:1000 dilution; HNF4a (LSbiosciences, Washington, DC, USA) in a 1:500 dilution; MRP2 (Monosan, Uden, The Netherlands) in a 1:1000 dilution; and ZO1 (Invitrogen, Carlsbad, CA, USA) in a 1:250 dilution, all incubations were performed overnight at 4 °C. The wash buffer for albumin, HNF4a, MRP2 and ZO1 was PBS with 0.1% (*v/v*) Tween 20. Envisioning of the antibodies was achieved with a Bright DAB substrate kit (VWR, PA, USA). As a counterstain hematoxylin (Dako,

Glostrup, Denmark) was applied and slides were mounted with Vectamount (Vector Laboratories, Peterborough, United Kingdom) after dehydration. Images were taken on the Olympus BX60 microscope (Olympus, Leiderdorp, the Netherlands) and processed with Image-J software (NIH, Madison, WI, USA).

The H&E staining was performed according to a standard protocol. Incubation with hematoxylin was performed for 4 min at RT and eosin (Merck) was incubated for 1 min at RT. For the Oil Red O staining, cryostat slides of 10 µm thickness were cut from fresh frozen liver tissues. The slides were fixed for 4 min with 4% (*w/v*) phosphate buffered formaldehyde (VWR) prior to incubation for 10 min with freshly prepared Oil Red O solution (VWR). Counterstaining was performed for 4 min with hematoxylin, and slides were mounted with Aqua-Mount medium (Thermo Fisher Scientific).

Indocyanine green functionality assay

To perform a dynamic liver function test, indocyanine green (ICG, Carl Roth, 7695–2) was added at timepoints 0, 60, 180 and 300 min to the perfusate at 5 mg/L from a stock solution of 5 mg/mL. A blank sample was taken before ICG injection. After 2 min of circulation, the first sample was taken and set as timepoint zero (t = 0).

Plasma samples (1 mL) were taken at 4, 6, 8, 10, 15, 20, 25 and 30 min after injection. Absorbance was measured at 805 nm with a CLARIOstar (BMG Labtech; Ortenberg, Germany) in triplicates. The ICG half-life was calculated as ln2/k from the fitted curve $C_{ICG}(t) = C_0 \times e^{-kt}$. The ICG functionality test was only established as a standard analysis method for the untreated livers and the repetition of the experiments, which are livers treated with continuously administered free fatty acids and livers treated with 300 mg/L APAP.

Data analysis

All data was processed, and statistical analysis where the sample size is n ≥ 3 was performed with GraphPad Prism 8 (San Diego, CA, USA). For the enzyme activity of un-treated livers, an ordinary one-way ANOVA analysis was performed followed by a Tukey's post-hoc test. Transaminase values for APAP-treated livers were compared using a one- tailed paired *t*-test. A comparison of liver functionality was performed using a two-way ANOVA followed by a Turkeys post-hoc test. All analyzed data was normally distributed with equal variances as tested by examining the Q-Q plot of residuals and scatter plots of residuals over predicted values. Differences were considered statistically significant for $p < 0.05$ and are

represented by an asterisk, n refers to the sample size for each statistical analysis. Data are presented as mean values with standard deviation for all data sets.

6.4 Results

6.4.1 Untreated livers

To determine the success of perfusion, hemodynamic parameters were assessed throughout the perfusion time. Reperfusion of the livers started with low pressures, which resulted in low flow rates through both the HA and PV (Figure 1B and Supplementary Table S2). At a starting pressure of 4.2 ± 1.3 mmHg in the PV, the initial flow was 211 ± 159 mL/min; whereas the pressure in the HA was 29 ± 6 mmHg, which resulted in a flow of 14 ± 11 mL/min. Upon rewarming and the reduction of the liver resistance, applied pressures were increased over time until 120 min when the physio- logical pressures were reached. The pressure of the PV of 7.2 ± 1 mmHg resulted in a flow of 864 ± 133 mL/min, and the HA pressure of 85 ± 5 mmHg led to perfusion of 380 ± 93 mL/min. Both flow rates remained constant during the perfusion time when pressures stayed on set values until termination of the experiment after 300 min.

To determine the viability of the perfused livers, the tissue injury markers LDH and AST were measured, and bile production was monitored as a sign of functionality. In Figure 1C, an initial increase of both enzymes is visible until 60 min of perfusion. LDH increased from 797 ± 15 U/L at the start of perfusion to 1967 ± 493 U/L at the end of perfusion, and AST increased from 89 ± 69 U/L to 2302 ± 1063 U/L. Over the subsequent 240 min, the LDH and AST levels did not increase significantly anymore. Figure 1D shows the bile production over time with a maximum total bile production of 25 ± 5 g with the first measurable production after 60 min of perfusion. H&E staining showed that the liver morphology after 5 h of perfusion was well maintained when compared to the control sample directly from the slaughterhouse (Figure 1G). The architecture of the liver was visible in both samples and the portal triads with PV. In addition, the HA and bile ducts were intact. After perfusion, the red blood cells were visible inside the tissue and mild sinusoidal dilatation was evident.

Liver function was further determined by ICG clearance from the perfusate, and an average half-life of 15.8 ± 8.4 min was determined for untreated livers during all measured timepoints without a significant increase in half-life over 5 h of perfusion (Figure 1E).

Another indication of the functionality and metabolic activity of the liver is the con- version of ammonia to urea (Figure 1F). The initially high ammonia content in the blood of 745 ± 374 µmol/L reduced to 231 ± 71 µmol/L in the first 60 min, after which it remained at the same level. Urea production was first detected after 30 min, and it accumulated over time. Another liver function marker is glucose metabolism. Glucose levels showed an in- crease within the first 60 min of perfusion from 5.87 ± 0.83 mmol/L to 9.97 ± 3.41 mmol/L and decreased again to 5.53 ± 1.38 mmol/L after 5 h of perfusion (Table S2). To further evaluate the performance of the liver, gene expression levels of indicative liver proteins were measured (Figure 2A). Gene expression of the livers after perfusion was very similar compared to the control sample from the slaughterhouse for all tested samples. There was a high expression for the ALB gene encoding serum albumin as well as the cytochrome P450 isoform CYP3A22, the porcine analogue of human CYP3A4, a phase I specific enzyme. Hepatocyte nuclear factor 4 alpha (HNF4A), the genes encoding fumarylacetoacetate hydrolase (FAH), and transthyretin (TTR) were expressed at lower but equally constant levels.
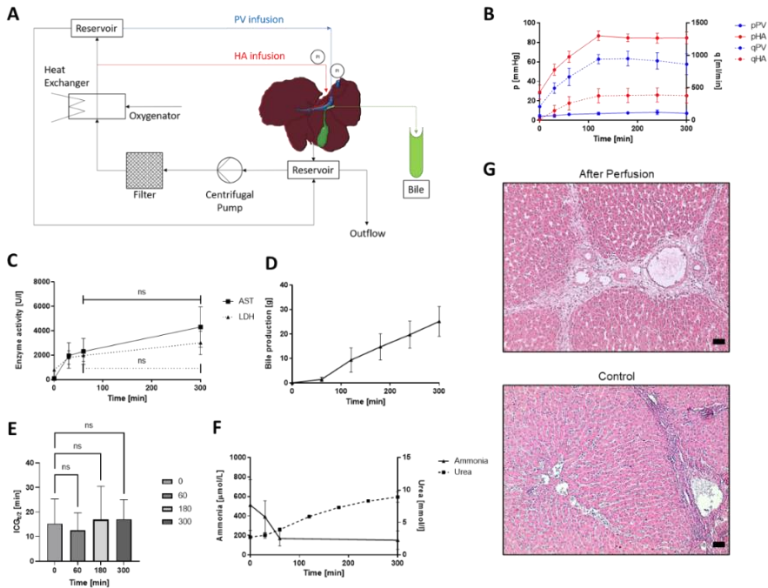
Figure 1: (A) Scheme of perfusion circuit design. (B) Portal vein and hepatic artery pressures (pPV and pHA) and flows (qPV and qHA) over 300 min of ex vivo liver perfusion with initially low starting pressures that reach physiological levels after 120 min. (C) Enzyme activity (LDH and AST) in blood over the perfusion duration with no statistically significant increase after the first 60 min. (D) Bile production over time, n = 3. (E) Indocyanine green (ICG) half-life of untreated livers measured at timepoints 0, 60, 180 and 300 without statistically significant differences. (F) Conversion of ammonia to urea over the perfusion period, scale bars represent 50 µm. (G) Representative H&E staining of control samples fresh from the slaughterhouse and after 5 h of perfusion with intact morphology; ns—not significant.

For visualization of expression levels and localization within the liver acinus of albumin, HNF4A, MRP2, and ZO1, immunohistological stainings were performed (Figure 2B) in the perfused livers and compared to fresh livers directly from the slaughterhouse. Equal to the gene expression data, the overall expression levels were very

similar between the control and perfused livers. Albumin staining was mainly found in the cytoplasm, some cells in the perfused liver did not show albumin expression, whereas all cells in the control were positive. HNF4A is a transcription factor in the nucleus of cells that should not stain outside the nuclei. In both perfused liver and the control HNF4A staining was specific in the nucleus and at the same level. Another marker, MRP2, is present in biliary transport and is expressed in hepatocytes at the canalicular/apical side. Especially in the perfused liver, MRP2 immunopositive staining was mainly seen in the area towards the bile canaliculi. Similarly, the tight junction protein ZO1 was located towards the bile canaliculi, and the expression levels were very similar for both the control and perfused samples.
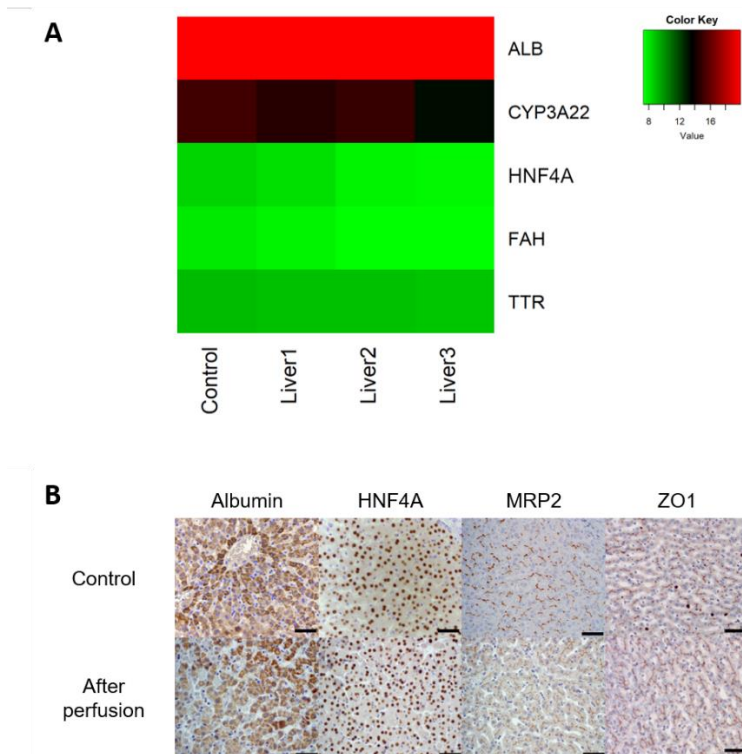
Figure 2: A: Heatmap of DNA expression of ALB, CYP3A22, HNF4A, FAH, TTR from liver samples taken directly in the slaughterhouse (control) and after 5 h of perfusion (Liver 1,2, and 3), DNA data is normalized to YWHAZ and RSP19 using the 2−ΔCT formula and log-transformed, n = 3; B: Representative immunohistology for control samples from the slaughterhouse and after 5 h of perfusion stained for albumin, HNF4A, MRP2, ZO1, scale bars represent 50 μm, n = 3.

205

6.4.2   Free fatty acid treatment

As proof of principle, two livers were treated with a high bolus concentration of free fatty acids (FFA_bol) and two livers with a continued high concentration (FFA_cts) over 5 h of perfusion. The concentration of free fatty acids in the perfusate of FFA_bol was reduced by 93% at the end of perfusion, in the largest reduction took place within the first 60 min of perfusion (Figure 3A). The final FFA_bol concentration at the end of perfusion (0.215 ± 0.02 mmol/L) was comparable with the concentration found in the blood of untreated livers (0.154 ± 0.03 mmol/L). The free fatty acid concentration in the blood strongly increased in the first 60 min for FFA_cts by 180% and only slowly decreased insignificantly over the remaining 4 h of perfusion. In Figure 3E, Oil Red O staining visualizes the FFA in the tissue of FFA_bol and FFA_cts. The Oil Red O staining of FFA_bol at T300 showed the presence of numerous small and larger red globules in the tissue after treatment. The distribution appeared to be somewhat zonal, with a more prominent number of globules in the periportal area than in the centrilobular region. These globules seemed to follow the liver cell cords but often appeared to be located in the space of Disse or within the sinusoids and only infrequently within the hepatocytes.

FFA_bol shows FFA droplets aligned in the trabecula at the beginning and end of perfusion, as well as FFA_cts at T0. However, this was not visible for FFA_cts at T300, where the FFA droplets did not align along clearly defined hepatic cords, indicating a disruption of the parenchymal architecture with dissociation of the hepatocytes. Additionally, only a limited presence of lipid droplets within the cytoplasm of hepatocytes was visible for both treatments. Notably, bile production was significantly reduced in the FFA-treated livers compared to untreated ones (2.8 ± 0.6 g/h and 4.6 ± 0.2 g/h for FFA_bol and FFA_cts, respectively, compared to 25 ± 5 g/h in untreated livers) (Figure 3D). The liver damage marker AST was not significantly increased during the 5 h of perfusion, but the livers with continuously administered FFA had higher AST levels compared to the untreated group, and those livers received only the bolus FFA. However, the AST levels in the FFA_cts perfusate were already increased prior to treatment (Figure 3C). Continuously administered FFA resulted in a clear increase of ICG half-life of 106 min ± 62 min after 3 h of perfusion compared to 12 min ± 4.3 min of untreated livers (Figure 3B). Also, the weight of the liver increased by 376 g compared to 164 g for untreated livers (Supplementary Table S3).
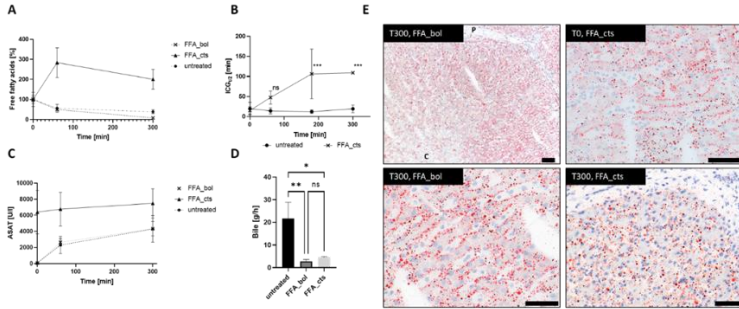
*Figure 3: (**A**) Free fatty acid (FFA) concentration of untreated livers (n = 3), FFA_bol (n = 2) and FFA_cts (n = 2) over 5 h perfusion period. (**B**) ICG half-life of FFA_cts and untreated livers measure at timepoints 0, 60, 180 (*** p = 0.001) and 300 (*** p = 0.002). (**C**) Transaminase concentrations (AST) of FFA_bol, FFA_cts and untreated livers. (**D**) Total bile production after 5 h of perfusion, FFA_bol ** p = 0.0064, FFA_cts * p = 0.011. (**E**) Representative Oil Red O stainings of FFA_cts before treatment (T0) and of FFA_bol and FFA_ctst after 5 h of perfusion (T300). P—portal, C—centrilobular; scale bars represent 50 µm.*

6.4.3 Acetaminophen treatment

To assess the effect of APAP, transaminase released by the liver cells was measured in the blood. Average concentrations of AST did not increase significantly over 5 h of perfusion, but slightly higher AST plasma concentrations for 155 mg/mL (APAP_155) and 300 mg/mL (APAP_300) were measured compared to untreated livers (Figure 4A). H&E staining of APAP_300 samples showed a slight leukocyte infiltration before reperfusion, and prominent congestions were visible after

5 h of perfusion (Figure 4D). Some apoptosis or single cell necrosis were visible as well, but no zonal changes were seen in the hepatocytes. Furthermore, liver weight during the APAP perfusion, on average, increased by 421 g (see Supplementary Table S4), and glucose levels in blood decreased from 16.23 ± 13 mmol/L before APAP injection to 8.35 ± 5.8 mmol/L after 5 h of perfusion for APAP_155 and to 5.37 ± 0.61 mmol/L for APAP_300 (see Supplementary Table S4). Bile production was significantly reduced over 5 h of perfusion to 4.8 ± 0.9 g/h for APAP_155 and to 1.6 ± 1.1 g/h for APAP 300 compared to untreated livers (25 ± 5 g/h) (Figure 4C). Albumin production, on the other hand, was constant over time as measured for APAP_155 (see Supplementary Table S4). The ICG functionality test showed no significant increase in ICG half-life over 5 h of perfusion for APAP_300 (Figure 4B).
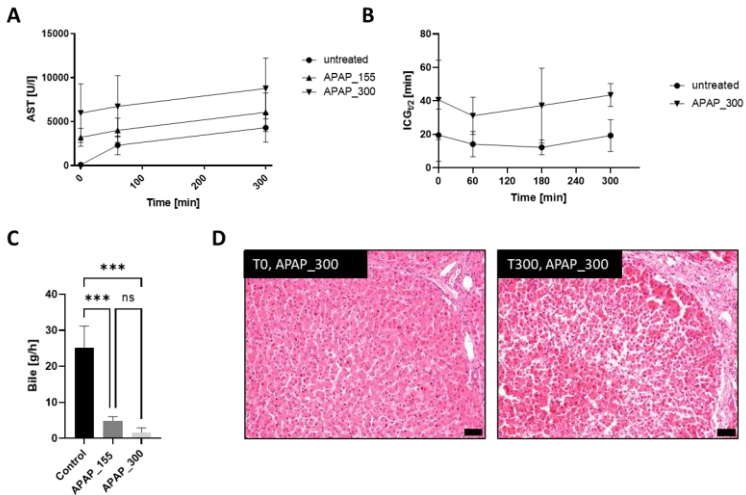
*Figure 4: (**A**) Transaminase concentrations (AST) of acetaminophen (APAP)-treated livers (n = 3), APAP added at 0 min. (**B**) ICG half-life of APAP_300 and untreated livers measure at timepoints 0, 60, 180 and 300. (**C**) Bile production of APAP_155 (*** p = 0.0004), APAP_300 (*** p = 0.0001) and untreated livers. (**D**) Representative H&E staining of APAP_300 before the start of perfusion and after 300 min of APAP toxicity; scale bars represent 50 µm.*

6.5 Discussion

We aimed to develop a straightforward design and protocol to perfuse slaughterhouse porcine livers in order to keep them viable and functional outside of the body in a stable and repeatable manner while complying with the 3R principle. This was successful, and perfusion periods were extended compared to previous studies using slaughterhouse organs [26,29]. Additionally, we were able to demonstrate the model's potential to study the basic

underlying mechanisms for liver diseases, such as a very novel *ex vivo* lipid uptake and to study the effects of compounds causing liver damage, such as acetaminophen.

Ex vivo porcine livers obtained from a slaughterhouse were perfused successfully in the laboratory. In vivo measurements of livers of pigs with slightly lower weight (90 kg) showed average PV flows of 1000 ± 200 mL/min and HA flows of 250 ± 70 mL/min [20], which shows that the final flows reached in our perfused slaughterhouse livers were at physiological levels without the need of added vasodilators as is common in *ex vivo* perfusion [20,22]. A limitation of using livers from a slaughterhouse where animals are used for human consumption is that the animal cannot be anticoagulated prior to harvesting or exsanguination. Hence, intrahepatic thrombosis is a major risk using slaughterhouse organs. Therefore, the livers were flushed directly after procurement with a heparinized flushing solution and transported submerged in a heparinized flushing solution to avoid intrahepatic thrombosis. Brüggenwirth et al. [37] described successful *ex vivo* perfusion for 24 h after a warm ischemic time of 30 min, also using slaughterhouse animals without injected anticoagulant prior to harvesting.

Our results showed restored flow to the desired values, and the histology of our control group showed well-preserved vessels. Therefore, we concluded that there is no severe intrahepatic thrombosis. In addition, using allogenic blood did not result in hemolytic reactions. This was also shown by Pool et al. [38], who compared the feasibility of porcine allogeneic blood in *ex vivo* normothermic perfusion with autologous blood. However, using autologous blood or cross-matching blood types might be necessary for long-term perfusion. Additionally, blood pooling can be avoided by reducing the perfusate volume needed in the circuit. This would also reduce the risk of contamination during blood collection. To minimize the number of additives during perfusion and during FFA and APAP administration, no antibiotic was used, which increased the risk of infections. However, during short-term (5 h) perfusion, the effect of infections is expected to be limited, and no pockets of infections were shown by histology. Nevertheless, to reach long-term perfusion, the addition of antibiotics is necessary [39], and future research should focus on the risk of bacterial infections due to slaughterhouse harvesting.

As a measure against reperfusion injury, which is a major issue in *ex vivo* but also clinical environments [22,40,41], we developed a protocol where starting pressures were low

at first in order to allow adaptation of the livers and rewarm them slowly; the latter has been previously shown to have beneficial effects [18,42]. The former is hypothesized to be the reason why no vasodilators were needed in this set-up, as sinusoids are able to adapt to the conditions slowly with increasing pressures, which was seen when this protocol was not applied, as in these cases, physiological flows could not be reached (data not shown). This effect has also been reported in the literature, e.g., in coronary artery perfusion [43]. We also found that using our protocol, reperfusion injury indicated by an increase in AST as well as LDH in the first 60 min of perfusion and by histology was considerably less than when higher pressures were used at the start of reperfusion (data not shown). Levels are difficult to compare with literature data, as often liver weights are not reported, harvesting conditions or treatments are different, set-ups are different, and in all cases, more supplements were given to the blood [11–14,16,19–22,27–29].

In another study performed on slaughterhouse livers, AST levels reached on average 1695 ± 519 U/L after 90 min of perfusion [44] and LDH 1339 ± 249 U/L after 220 min [26], which is lower than that found after 60 min in the present study without significant changes over the remaining

perfusion time (4304 ± 1347 U/L for AST and 3000 ± 778 U/L for LDH). One reason for the high AST levels could be a higher starting value due to a longer warm ischemic time, which is due to the particular slaughtering process. This time window was about 25 min in the present study; other procedures achieved 14 min [44] or less. It is well known that the duration of warm ischemic time corresponds to hepatic damage, specifically to hepatocytes, as expressed by increased AST levels [45]. This hypothesis is further supported by much lower damage marker values in experiments performed with lab animals [46]. The increase in both AST and LDH in combination with the observed dilated sinusoids during perfusion are a sign that liver cells are damaged during the change of physiological conditions of the *ex vivo* perfusion. Nevertheless, it can also be seen AST levels do not increase significantly after the initial rise; the remaining increase could limit function. Therefore, further improvements to the model should be aimed at stopping the damage marker increase while achieving longer perfusion times.

Longer-term studies have shown that recovery can occur in a previously damaged liver after only a few days [20]. Further experimentation with, for example, a slow increase in oxygen supply [18], or a short period of hypothermic oxygenated machine perfusion before normothermic

perfusion [47], could aid in reducing initial damage in the future. Additionally, the effect of CO_2 sedation as applied in the slaughterhouse used in this study on liver functionality needs to be further investigated to ensure no increase in initial damage in comparison to livers harvested from euthanized lab animals and ensure a consistent disease model using slaughterhouse livers.

As an indicator of the liver's functionality [18], total bile production of around 25 g after 5 h with onset after 1 h of perfusion was measured, and when bile production is calculated over the last 4 h of perfusion with an average bile density of 928 kg/m3 [48], bile production averaged 6.7 mL/h. This bile production is comparable to data found in literature, 10 mL/h [13] after 5 h in non-slaughterhouse porcine livers, and 5.4 mL/h [45] after 90 min in slaughterhouse porcine livers. It has previously been shown that no significant depletion of bile salts occurs within the first 10 h of normothermic machine perfusion (NMP) [49], therefore its addition is unnecessary as proven by no reduction in bile production.

Another indicator of functionality is the synthesis of urea from ammonia [20]. Due to the closed circuit without a dialysis system, urea accumulation is expected and indicates metabolic activity in the hepatocytes [50]. This

was 8.9 ± 0.67 mmol/L after 300 min in our study, comparable with literature data in slaughterhouse porcine livers of 10.3 ± 0.8 mmol/L of urea production after 220 min of perfusion [26]. The high urea production compared to ammonia elimination is a sign of the breakdown of proteins over the perfusion time, which indicates that the liver is in a catabolic state [51].

In addition, glucose metabolism in our group of untreated livers stabilized to blood glucose levels within the desired range (3.5–6.5 mmol/L), indicating liver functionality 20, [52] without any addition of glucose or insulin within the 5 h of perfusion. However, a significant blood glucose increase was visible after 60 min of perfusion, which has been previously reported in the literature [37,52–55]. Becker et al. [55] described the release of glucose resulting in high blood glucose within the first phase after reperfusion as a consequence of ischemia-reperfusion injury and subsequent decrease of glucose levels, indicating the recovery of the liver. This was also shown by Izamis et al. [56], who described glucose release due to glycogenolysis within the first 2 h of perfusion after ischemic times.

Additionally, all gene expressions were stable over the time of perfusion, and especially the expression of albumin was constant at a high level, whereas albumin production

216

usually decreases in the initial phase of NMP in most studies [20,32,44]. These findings were confirmed by the immunohistological stainings, which throughout demonstrated stable expression as well as localization of all markers. Furthermore, liver functionality was shown by ICG clearance from the perfusate. ICG is almost exclusively cleared by hepatocytes and excreted into bile without metabolism and enterohepatic recirculation. However, clearance also depends on liver blood flow and blood protein concentration [57,58].

Because stable blood flow and constant albumin expression were measured in the present study, the results of ICG clearance are clearly correlating to hepatocyte functionality and are not influenced by variations in blood protein concentrations or liver blood flow. The measured ICG half-life (15.8 ± 8.4 min) presents a comparable result to ICG half-life (approximately 14 min) in pigs with 30 min warm ischemia time, confirming the functionality of our *ex vivo* perfused livers [59]. The small increase in weight of the livers over the perfusion time in our study could be explained by the slight sinusoidal dilatation that was visible histologically but also indicated that no significant edema developed [60]. The exact nature of these lesions needed to be addressed in future studies. Therefore, we have shown that we can keep *ex vivo* porcine slaughterhouse livers in a

viable and functional state. This was achieved with a less complex set-up compared to previous studies, which makes the application of the model for many research topics such as DILI, MAFLD, or other diseases more feasible due to the increased reproducibility and lower costs.

To demonstrate that the model has the potential to study the effects of diseases with respect to fat metabolism, such as steatosis, proof of principle experiments creating a damage model by supplying the livers with high FFA concentration were conducted. In the FFA bolus experiments, reduction of the FFA concentration within the first 60 min of perfusion showed that the liver takes up the fat and the Oil Red O staining confirmed this finding, although most of the lipids appeared to be located extracellularly. Extracellular localization of the droplets might be a temporal phenomenon, and hepatocytes eventually might take up the FFAs but require a longer perfusion than 300 min. Steatosis is known to start along the blood vessels [61], which was also observed in our study of the bolus FFA treatment. Early steatosis is characterized by lipid accumulation in macro- or microvesicular vacuoles in more than 5% of hepatocytes [62], which appeared to be in an early stage in this experiment as well. Observing that the majority of FFAs were taken up from perfusate by the

liver in the first 60 min, FFA was administered continuously in a second experiment to keep the blood concentration high and to achieve an increase in severity. The continued supplementation of FFAs showed a rising concentration in the first 60 min of perfusion and only a slight decrease at a high level for the remaining 4 h of perfusion.

In addition, the ICG clearance showed a significant decrease in liver functionality com- pared to the untreated livers. ICG clearance has been reported previously as a successful measurement to identify already moderate steatotic livers [63], and therefore confirms early steatosis in our continuously treated model. Liver histology of the continuously supplied FFA after perfusion displayed a higher FFA concentration in the tissue compared to bolus and showed FFA present in the sinusoids as well as in the hepatocytes after perfusion, confirming the assumption of the liver taking up FFA. However, Oil Red O-stained liver sections visualized lipid accumulation already in tissue before reperfusion, indicating the presence of lipids without additional FFA administration in the harvested tissue. Further research needs to show if this could be a limitation of the model using slaughterhouse pigs due to the fact that pigs are fed to attain maximum growth, which might result in a higher blood FFA concentration. Nevertheless, continuous FFA administration resulted in

increasing liver damage, as shown by the decreasing ICG clearance and reduced bile production. In the NMP perfusion of the already steatotic pig livers, the initial bile production was reduced before it recovered [32], showing that steatosis leads to decreased bile production, which is what is reflected in the much lower overall bile production in the FFA-treated livers compared to the untreated controls.

A further indication of liver damage is the increase in the weight of the liver during perfusion, which is commonly associated with hepatic steatosis [64]. Although both FFA administration protocols resulted in only limited lipid uptake into the hepatocytes without any visible necrosis or significantly increased damage markers, the results of our experiments suggest that the model is useful for studying early metabolic mechanisms and potential solutions to prevent the onset of a disease. With the prolongation of the exposure to FFA, the progression of the disease could potentially be studied, leading to insights into both the pathogenesis but also the potential of NMP for reducing steatosis [11,32]. Additionally, the timing for FFA administration could be improved with prolonged perfusion times.

In the present study, FFAs were administered from the start of reperfusion to exploit their possible uptake potential. The effect of FFA administration on reperfusion injury is unclear and starting the treatment after hemodynamic parameters have reached the target values might be beneficial to study the effects of FFAs on the liver. We have shown for the first time that it is possible in an *ex vivo* setting, utilizing slaughterhouse organs, to create a relevant metabolic model to study lipid uptake in livers which represents the first phase of the mechanism and, with further progression, could lead to a steatotic disease model. A larger sample size may lead to even more significantly relevant results. By learning about the kinetics and mechanism and attaining longer perfusion times, further disease stages might be achieved to create even more potential to study pathology.

In a further demonstration of an application of the perfused *ex vivo* porcine slaughterhouse liver model, a proof of principle study in the model was conducted with the well-known drug acetaminophen (APAP). Livers exposed to APAP do present only a few randomly distributed necrotic/apoptotic cells in the H&E stains, but the typical centrilobular lesions reported to be associated with APAP exposure [31,65] were not seen. However, a slightly higher concentration of the liver damage marker

AST was measured after ad- ministration, which is also reported in the literature [66]. Nevertheless, the marker does not show as high increases as those found in vivo studies on pigs that progressed towards ALF [31,65]. In addition, ICG analysis did not show a decrease in functionality of livers treated with plasma concentrations of either 155 mg/mL or 300 mg/L. This is most likely due to the fact that only one bolus of APAP was given to show toxicity, whereas in most studied cases, plasma concentrations were kept at a constant level as opposed to the present study. Additionally, even higher concentrations of APAP could be needed to reach ALF in pigs [67,68]. Similar to other hepatotoxicity studies using *ex vivo* perfused slaughterhouse pig livers [45], liver weight was increased in the current model over the time of perfusion, probably due to edema formation in livers.

A possible starting failure of the liver after APAP administration might be indicated by the observed reduction in blood glucose, as hypoglycemia is also associated with APAP intoxication [66,69]. The most striking difference could be found in bile production, which after APAP administration showed a significant decrease in total bile production after 5 h of perfusion compared to untreated livers. This might be a result of accumulating bile acids during APAP overdose, which also results in

decreasing bile production [70,71]. Hence, it might be beneficial for future research to analyze the bile composition, which has been a promising biomarker for monitoring liver function [72].

When progressing the model to a further disease stage, additional parameters such as methemoglobinemia are interesting to investigate. An increase in liver damage and induced ALF could be achieved in an *ex vivo* NMP model without ethical implications for animal experiments when administering high doses of the drug over extended periods of time would be possible. Hence, to improve the potential of the current model for toxicity studies, we would further develop the model with continuous administration and for longer periods of time. Further progression could be of interest and extended research on continuous exposure and increased perfusion times are necessary to prove that the model can represent all stages of the disease and that it functions similarly to the in vivo models in all aspects.

6.6 Conclusion

We developed a simple *ex vivo* perfused liver model for research based on slaughterhouse material that avoids animal experimentation, is relevant in terms of its viability and functionality parameters without the burden of

unnecessary complexity of the perfusion system. This has been successfully shown with parameters comparable to other experiments that even have more beneficial harvesting procedures like surgical environments or complex set-ups and protocols. Additionally, the model showed signs of liver damage due to acetaminophen and free fatty acid administration, which indicate a potential to use this setup to study basic metabolic mechanisms involved in the early stages of exposure to hepatotoxic substances and metabolic liver disease. With further improvements to the model, prolongation of exposure could lead to the progression of the disease, making this model a versatile tool for studying liver diseases and their potential treatments starting from the first phases.

6.7 Acknowledgments

6.8   References

1.	Gola A, Davis S, Greenslade L, et al. Economic Analysis of Costs for Patients With End Stage Liver Disease Over the Last Year of Life. BMJ Support Palliat Care. 2015;5(1):110.2-110. doi:10.1136/bmjspcare-2014-000838.23

2.	Pimpin L, Cortez-Pinto H, Negro F, et al. Burden of liver disease in Europe: Epidemiology and analysis of risk factors to identify prevention policies. J Hepatol. 2018;69(3):718-735. doi:10.1016/j.jhep.2018.05.011

3.	Asrani SK, Devarbhavi H, Eaton J, Kamath PS. Burden of liver diseases in the world. J Hepatol. 2019;70(1):151-171. doi:10.1016/j.jhep.2018.09.014

4.	Blachier M, Leleu H, Peck-Radosavljevic M, Valla DC, Roudot-Thoraval F. The burden of liver disease in Europe: A review of available epidemiological data. J Hepatol. 2013;58(3):593-608. doi:10.1016/j.jhep.2012.12.005

5.	Bale SS, Vernetti L, Senutovitch N, et al. In vitro platforms for evaluating liver toxicity. Exp Biol Med. 2014;239(9):1180-1191. doi:10.1177/1535370214531872

6.	Kaplan W. Who update essential medicines 2013 PPH. Published online 2013.

7.	Bruix J, Han K hyub, Gores G, Llovet JM, Mazzaferro V. Liver cancer : Approaching a personalized care. J Hepatol. 2015;62(1):S144-S156. doi:10.1016/j.jhep.2015.02.007

8.	Scherer A, Dufour JF. Treatment of Non-Alcoholic Fatty Liver Disease. Digestive Diseases. 2016;34(1):27-31. doi:10.1159/000447278

9.   Kuna L, Bozic I, Kizivat T, et al. Models of Drug Induced Liver Injury (DILI) – Current Issues and Future Perspectives. Curr Drug Metab. 2018;19(10):830-838. doi:10.2174/1389200219666180523095355

10. Kullak-Ublick GA, Andrade RJ, Merz M, et al. Drug-induced liver injury: Recent advances in diagnosis and risk assessment. Gut. 2017;66(6):1154-1164. doi:10.1136/gutjnl-2016-313369

11. Weissenbacher A, Vrakas G, Nasralla D, Ceresa CDL. The future of organ perfusion and re-conditioning. Transplant International. 2019;32(6):tri.13441. doi:10.1111/tri.13441

12. Ravikumar R, Leuvenink H, Friend PJ. Normothermic liver preservation: A new paradigm? Transplant International. 2015;28(6):690-699. doi:10.1111/TRI.12576

13. Butler AJ, Rees MA, Wight DGD, et al. Successful extracorporeal porcine liver perfusion for 72 HR. Transplantation. 2002;73(8):1212-1218. doi:10.1097/00007890-200204270-00005

14. Hessheimer AJ, Fondevila C, García-Valdecasas JC. Extracorporeal machine liver perfusion: Are we warming up? Curr Opin Organ Transplant. 2012;17(2):143-147. doi:10.1097/MOT.0b013e328351082a

15. Liu Q, Nassar A, Farias K, et al. Comparing Normothermic Machine Perfusion Preservation with Different Perfusates on Porcine Livers from Donors after Circulatory Death. American Journal of Transplantation. 2016;16(3):794-807. doi:10.1111/ajt.13546

16. Nassar A, Liu Q, Farias K, et al. Ex vivo normothermic machine perfusion is safe, simple,

and reliable: Results from a large animal model. Surg Innov. 2015;22(1):61-69. doi:10.1177/1553350614528383

17.   Jochmans I, Akhtar MZ, Nasralla D, et al. Past, Present, and Future of Dynamic Kidney and Liver Preservation and Resuscitation. American Journal of Transplantation. 2016;16(9):2545-2555. doi:10.1111/ajt.13778

18.   Marecki H, Bozorgzadeh A, Porte RJ, Leuvenink HG, Uygun K, Martins PN. Liver ex situ machine perfusion preservation: A review of the methodology and results of large animal studies and clinical trials. Liver Transplantation. 2017;23(5):679-695. doi:10.1002/lt.24751

19.   Ceresa CDL, Nasralla D, Jassem W. Normothermic Machine Preservation of the Liver: State of the Art. Curr Transplant Rep. 2018;5(1):104-110. doi:10.1007/s40472-018-0186-9

20.   Eshmuminov D, Becker D, Bautista Borrego L, et al. An integrated perfusion machine preserves injured human livers for 1 week. Nat Biotechnol. 2020;38(2):189-198. doi:10.1038/s41587-019-0374-x

21.   Jayant K, Reccia I, Shapiro AMJ. Normothermic ex-vivo liver perfusion: where do we stand and where to reach? Expert Rev Gastroenterol Hepatol. 2018;12(10):1045-1058. doi:10.1080/17474124.2018.1505499

22.   Maione F, Gilbo N, Lazzaro S, et al. Porcine Isolated Liver Perfusion for the Study of Ischemia Reperfusion Injury: A Systematic Review. Transplantation. 2018;102(7):1039. doi:10.1097/TP.0000000000002156

23. Vogel T, Brockmann JG, Friend PJ. Ex-vivo normothermic liver perfusion: An update. Curr Opin Organ Transplant. 2010;15(2):167-172. doi:10.1097/MOT.0b013e328337349d

24. Reddy SP, Bhattacharjya S, Maniakin N, et al. Preservation of porcine non-heart-beating donor livers by sequential cold storage and warm perfusion. Transplantation. 2004;77(9 SUPPL.):1328-1332. doi:10.1097/01.TP.0000119206.63326.56

25. Imber CJ, St. Peter SD, Inigo Lopez De CENARRUZABEITIA, et al. ADVANTAGES OF NORMOTHERMIC PERFUSION OVER COLD STORAGE IN LIVER PRESERVATION. Transplantation. 2002;73(5):701-709. doi:10.1097/00007890-200203150-00008

26. Grosse-Siestrup C, Nagel S, Unger V, et al. The isolated perfused liver: A new model using autologous blood and porcine slaughterhouse organs. J Pharmacol Toxicol Methods. 2001;46(3):163-168. doi:10.1016/S1056-8719(02)00184-3

27. Grosse-Siestrup C, Pfeffer J, Unger V, et al. Isolated Hemoperfused Slaughterhouse Livers as a Valid Model to Study Hepatotoxicity. Toxicol Pathol. 2002;30(6):749-754. doi:10.1080/0192623029016684

28. Thewes S, Reed HK, Grosse-Siestrup C, et al. Haemoperfused liver as an ex vivo model for organ invasion of Candida albicans. J Med Microbiol. 2007;56(PART 2):266-270. doi:10.1099/jmm.0.46760-0

29. Izamis ML, Efstathiades A, Keravnou C, Leen EL, Averkiou MA. Dynamic Contrast-Enhanced

Ultrasound of Slaughterhouse Porcine Livers in Machine Perfusion. Ultrasound Med Biol. 2014;40(9):2217-2230. doi:10.1016/j.ultrasmedbio.2014.03.031

30. Schreiter T, Sowa JP, Schlattjan M, et al. Human Ex-Vivo Liver Model for Acetaminophen-induced Liver Damage. Sci Rep. 2016;6. doi:10.1038/srep31916

31. Newsome PN, Henderson NC, Nelson LJ, et al. Development of an invasively monitored porcine model of acetaminophen-induced acute liver failure. BMC Gastroenterol. Published online 2010:10-34. doi:10.1186/1471-230x-10-34

32. Jamieson RW, Zilvetti M, Roy D, et al. Hepatic Steatosis and Normothermic Perfusion—Preliminary Experiments in a Porcine Model. Transplantation. 2011;92(3):289-295. doi:10.1097/TP.0b013e318223d817

33. Westra IM. Precision-Cut Liver Slices: An Ex vivo Model for the Early Onset and End-Stage of Liver Fibrosis. University of Groningen; 2014.

34. van der Laan LJW, Geijsen N, Spee B, et al. Long-Term Adult Feline Liver Organoid Cultures for Disease Modeling of Hepatic Steatosis. Stem Cell Reports. 2017;8(4):822-830. doi:10.1016/j.stemcr.2017.02.015

35. Gómez-Lechón MJ, Donato MT, Martínez-Romero A, Jiménez N, Castell JV, O'Connor JE. A human hepatocellular in vitro model to investigate steatosis. Chem Biol Interact. 2007;165(2):106-116. doi:10.1016/j.cbi.2006.11.004

36. Winek CL, Wahba WW, Winek CL, Balzer TW. Drug and chemical blood-level data 2001. Forensic Sci Int. 2001;122(2-3):107-123.

doi:10.1016/S0379-0738(01)00483-2

37. Brüggenwirth IMA, van Leeuwen OB, de Vries Y, et al. Extended hypothermic oxygenated machine perfusion enables ex situ preservation of porcine livers for up to 24 hours. JHEP Reports. 2020;2(2):100092. doi:10.1016/j.jhepr.2020.100092

38. Pool MBF, Hartveld L, Leuvenink HGD, Moers C. Normothermic machine perfusion of ischaemically damaged porcine kidneys with autologous, allogeneic porcine and human red blood cells. PLoS One. 2020;15(3). doi:10.1371/JOURNAL.PONE.0229566

39. Eshmuminov D, Mueller M, Brugger SD, et al. Sources and prevention of graft infection during long-term ex situ liver perfusion. Transplant Infectious Disease. 2021;23(4). doi:10.1111/TID.13623

40. Mendes-Braz M, Elias-Miró M, Jiménez-Castro MB, Casillas-Ramírez A, Ramalho FS, Peralta C. The current state of knowledge of hepatic ischemia-reperfusion injury based on its study in experimental models. J Biomed Biotechnol. 2012;2012. doi:10.1155/2012/298657

41. Siniscalchi A. Post reperfusion syndrome during liver transplantation: From pathophysiology to therapy and preventive strategies. World J Gastroenterol. 2016;22(4):1551. doi:10.3748/wjg.v22.i4.1551

42. Banan B, Xiao Z, Watson R, et al. Novel strategy to decrease reperfusion injuries and improve function of cold-preserved livers using normothermic ex vivo liver perfusion machine. Liver Transplantation. 2016;22(3):333-343. doi:10.1002/lt.24352

43. Fujita S, Roerig DL, Bosnjak ZJ, Stowe DF. Effects of vasodilators and perfusion pressure on coronary flow and simultaneous release of nitric oxide from guinea pig isolated hearts 1. Published online 1998:655-667. doi:10.1016/s0008-6363(98)00051-0

44. Grosse-Siestrup C, Unger V, Pfeffer J, et al. Hepatotoxic effects of polidocanol in a model of autologously perfused porcine livers. Arch Toxicol. 2004;78(12):697-705. doi:10.1007/S00204-004-0587-7

45. Schön MR, Kollmar O, Akkoc N, et al. Cold ischemia affects sinusoidal endothelial cells while warm ischemia affects hepatocytes in liver transplantation. Transplant Proc. 1998;30(5):2318-2320. doi:10.1016/S0041-1345(98)00638-1

46. Gilbo N, Wylin T, Heedfeld V, et al. Porcine Liver Normothermic Machine Perfusion: Methodological Framework and Potential Pitfalls. Transplant Direct. 2022;8(1):e1276. doi:10.1097/TXD.0000000000001276

47. Boteon YL, Laing RW, Schlegel A, et al. Combined Hypothermic and Normothermic Machine Perfusion Improves Functional Recovery of Extended Criteria Donor Livers. Liver Transplantation. 2018;24:1699-1715. doi:10.1002/lt.25315

48. McIntosh RL, Anderson V. A comprehensive tissue properties database provided for the thermal assessment of a human at rest. Biophys Rev Lett. 2010;05(03):129-151. doi:10.1142/S1793048010001184

49. Eshmuminov D, Leoni F, Schneider MA, et al. Perfusion settings and additives in liver

normothermic machine perfusion with red blood cells as oxygen carrier. A systematic review of human and porcine perfusion protocols. Transplant International. 2018;31(9):956-969. doi:10.1111/tri.13306

50. Reiling J, Lockwood DSR, Simpson AH, et al. Urea production during normothermic machine perfusion: Price of success? Liver Transplantation. 2015;21(5):700-703. doi:10.1002/LT.24094

51. Bruinsma BG, Sridharan G V., Weeder PD, et al. Metabolic profiling during ex vivo machine perfusion of the human liver. Sci Rep. 2016;6(March):1-13. doi:10.1038/srep22415

52. Sutton ME, Op Den Dries S, Karimian N, et al. Criteria for Viability Assessment of Discarded Human Donor Livers during Ex vivo Normothermic Machine Perfusion. PLoS One. 2014;9(11). doi:10.1371/journal.pone.0110642

53. Matton APM, De Vries Y, Burlage LC, et al. Biliary Bicarbonate, pH, and Glucose Are Suitable Biomarkers of Biliary Viability During Ex Situ Normothermic Machine Perfusion of Human Donor Livers. Transplantation. 2019;103(7):1405. doi:10.1097/TP.0000000000002500

54. Matton APM, Burlage LC, van Rijn R, et al. Normothermic machine perfusion of donor livers without the need for human blood products. Liver Transplantation. 2018;24(4):528-538. doi:10.1002/lt.25005

55. Becker D, Eshmuminov D, Keller R, et al. Automated Insulin Delivery - Continuous Blood Glucose Control during Ex Situ Liver Perfusion. IEEE Trans Biomed Eng. 2021;68(4):1399-1408. doi:10.1109/TBME.2020.3033663

56.   Izamis ML, Tolboom H, Uygun B, Berthiaume F, Yarmush ML, Uygun K. Resuscitation of Ischemic Donor Livers with Normothermic Machine Perfusion: A Metabolic Flux Analysis of Treatment in Rats. PLoS One. 2013;8(7). doi:10.1371/journal.pone.0069758

57.   Ott P, Keiding S, Bass L. Intrinsic hepatic clearance of indocyanine green in the pig: dependence on plasma protein concentration. Eur J Clin Invest. 1992;22(5):347-357. doi:10.1111/J.1365-2362.1992.TB01473.X

58.   De Gasperi A, Mazza E, Prosperi M. Indocyanine green kinetics to assess liver function: Ready for a clinical dynamic assessment in major liver surgery? World J Hepatol. 2016;8(7):355-367. doi:10.4254/wjh.v8.i7.355

59.   Lamesch P, Raygrotzki S, Evers B, Pichlmayr R. ICG Test als Verlaufsparameter nach unterschiedlichen Ischämiebelastungen der Leber — Eine tierexperimentelle Studie. In: Chirurgisches Forum '92 Für Experimentelle Und Klinische Forschung. Springer Berlin Heidelberg; 1992:171-176. doi:10.1007/978-3-642-77389-1_36

60.   Imber CJ, St. Peter SD, De Cenarruzabeitia IL, et al. Optimisation of bile production during normothermic preservation of porcine livers. American Journal of Transplantation. 2002;2(7):593-599. doi:10.1034/j.1600-6143.2002.20703.x

61.   Schleicher J, Dahmen U, Guthke R, Schuster S. Zonation of hepatic fat accumulation: Insights from mathematical modelling of nutrient gradients and fatty acid uptake. J R Soc Interface. 2017;14(133). doi:10.1098/rsif.2017.0443

62. Kanuri G, Bergheim I. In vitro and in vivo models of non-alcoholic fatty liver disease (NAFLD). Int J Mol Sci. 2013;14(6):11963-11980. doi:10.3390/ijms140611963

63. Seifalian AM, El-Desoky A, Davidson BR. Hepatic indocyanine green uptake and excretion in a rabbit model of steatosis. European Surgical Research. 2001;33(3):193-201. doi:10.1159/000049706

64. Nassir F, Rector RS, Hammoud GM, Ibdah JA. Pathogenesis and prevention of hepatic steatosis. Gastroenterol Hepatol (N Y). 2015;11(3):167-175.

65. Thiel C, Thiel K, Etspueler A, et al. A Reproducible Porcine Model of Acute Liver Failure Induced by Intrajejunal Acetaminophen Administration. European Surgical Research. 2011;46(3):118-126. doi:10.1159/000323411

66. Manibur Rahman T, Humphrey J.F. Hodgson. Animal models of acute hepatic failure. Int J Exp Pathol. 2000;81(2):145-157. doi:10.1046/j.1365-2613.2000.00144.x

67. He GL, Feng L, Cai L, et al. Artificial liver support in pigs with acetaminophen-induced acute liver failure. Worl Journal of Gastroenterology. 2017;23(18):3262-3268. doi:10.3748/wjg.v23.i18.3262

68. Dargue R, Zia R, Lau C, et al. Metabolism and Effects on Endogenous Metabolism of Paracetamol (Acetaminophen) in a Porcine Model of Liver Failure. Toxicological Sciences. 2020;175(1):87-97. doi:10.1093/toxsci/kfaa023

69. Beltrán-Olazábal A, Martínez-Galán P, Castejón-Moreno R, García-Moreno ME, García-Muro C, Esteban-Zubero E. Management of acetaminophen toxicity, a review.

IBEROAMERICAN JOURNAL OF MEDICINE. 2019;1:22-28. doi:/10.5281/zenodo.3470262

70.   Nasralla D, Coussios CC, Mergental H, et al. A randomized trial of normothermic preservation in liver transplantation. Nature. 2018;557(7703):50-56. doi:10.1038/s41586-018-0047-9

71.   Ghallab A, Hassan R, Hofmann U, et al. Interruption of Bile Acid Uptake by Hepatocytes after Acetaminophen Overdose Ameliorates Hepatotoxicity. European Association for the Study of the Liver (EASL); 2022. doi:10.1016/j.jhep.2022.01.020

72.   Brüggenwirth IMA, Porte RJ, Martins PN. Bile Composition as a Diagnostic and Prognostic Tool in Liver Transplantation. Liver Transplantation. 2020;26(9):1177-1187. doi:10.1002/lt.25771

6.9 Supplementary Material

Table S1: Primers used for DNA analysis

Gene	Forward	Reverse
YWHAZ	CAAAGACAGCATTTGATGAAGCC	ATCTCCTTGGGTATCCGATGTC
RSP19	AAAGAAACGGTGTCATGCCC	AGGCCTTTCCCATCTTGGT
ALB	CGCTCATAGTTCGTTACACC	CTTACAACACCTAGAGCCCA
CYP3A22	CATCAACACGAAAGAAATCTTTGGG	GTCTCGTGGGTTGTTGAGG
HNF4A	CTTCTTTGACCCAGATGCC	GTCGTTGATGTAATCCTCCAG
FAH	CCAAGATGTCTTTGATCAGCCA	CCGAAGTTCTGTGTCATCTCTG
TTR	AATATGCAGAGGTTGTGTTCACAG	CTGTGGTGGAGTAAGAGTAGGG
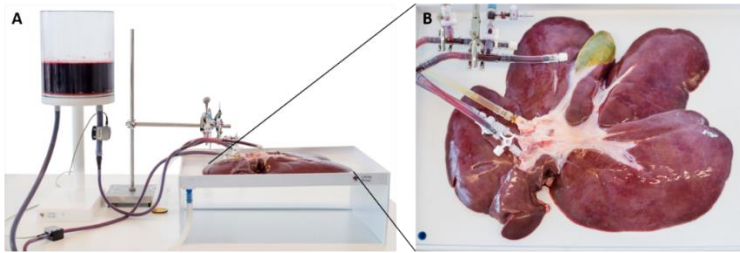
Figure S1: A: Image of custom-made liver receptacle with reservoir supplying the static PV pressure; B: Cannulated porcine liver with gall bladder.

Table S2: Blood gas analysis, hematology, pressures and flows, bile production and liver weight for untreated at timepoints 0, 30, 60, 300 min of ex vivo perfusion as mean and SD over n = 3 livers (untreated).

Timepoint [min]	Untreated					
	0		60		300	
Analyte	Mean	SD	Mean	SD	Mean	SD
Free fatty acids [mmol/L]	0.25	0.06	0.20	0.07	0.12	0.01
Urea [mmol/L]	2.73	0.12	3.90	0.22	8.90	0.67
AST [U/L]	89.33	56.45	2301.67	868.53	4304.00	1347.76
LDH [U/L]	796.67	12.47	1966.67	402.77	3000.00	778.89
Ammonia [µmol/L]	511.67	214.49	169.00	63.61	150.67	77.96
Lactate [mmol/L]	9.17	2.65	10.72	2.67	10.66	6.39
Portal vein pressure [mmHg]	4.19	1.32	5.50	0.16	8.49	1.28
Hepatic artery pressure [mmHg]	28.90	6.00	65.23	4.62	84.70	4.99
Portal vein Flow [mL/min]	211.33	158.77	668.67	108.30	864.33	133.18
Hepatic artery flow [mL/min]	13.67	10.66	263.67	85.17	379.67	92.78
pH	7.36	0.03	7.31	0.02	7.37	0.01
Glucose [mmol/L]	5.87	0.83	9.97	3.41	5.53	1.38
Hct [%]	27.00	2.16	25.33	1.70	25.67	2.62
Hb [g/dL]	9.20	0.73	8.60	0.59	8.73	0.88
Bile [g]			1.43	0.74	25.13	4.97
Weight	2566	245.14			2730.67	78.4

Table S3: Blood gas analysis, hematology, pressures and flows, bile production and liver weight for fatty livers livers at timepoints 0, 30, 60, 300 min of ex vivo perfusion as mean and SD over n = 2 livers (FFA_bol, FFA_cts).

Timepoint [min]	FFA_bol						FFA_cts					
	0		60		300		0		60		300	
Analyte	Mean	SD	Mean	SD	Mean	SD	Mean	SD	Mean	SD	Mean	SD
Free fatty acids [mmol/L]	2.48	0.16	1.24	0.04	0.22	0.02	0.10	0.02	0.28	0.01	0.20	0.02
Urea [mmol/L]	2.65	0.05	3.50	0.10	8.40	0.60						
AST [U/L]	65.00	1.00	2648.50	333.50	4339.00	634.00	6398.00	1904.00	6769.00	1481.00	7497.50	1284.50
LDH [U/L]	885.00	515.00	2500.00	300.00	3500.00	100.00	246.50	78.50	240.50	74.50		
Ammonia [µmol/L]	480.00	120.00	695.00	25.00	530.00	125.00						
Lactate [mmol/L]	6.72	1.26	9.79	1.71	22.80	5.20						
Portal vein pressure [mmHg]	3.95	0.25	5.50	0.30	7.81	0.71	9.00	0.10	9.00	0.10	9.15	0.25
Hepatic artery pressure [mmHg]	31.25	5.75	47.75	2.75	84.00	3.00	78.90	3.00	79.70	1.50	79.95	0.85
Portal vein Flow [ml/min]	175.50	94.50	545.00	43.00	700.00	6.00	572.00	39.00	591.00	39.00	560.00	28.00
Hepatic artery flow [ml/min]	95.00	0.00	101.00	37.00	302.50	38.50	505.00	23.00	541.50	11.50	548.00	10.00
pH	7.36	0.02	7.36	0.00	7.30	0.03	7.25	0.02	7.28	0.05	7.31	0.02
Glucose [mmol/L]	3.95	0.75	18.40	4.90	16.75	5.65	15.05	7.25	9.90	1.40	7.85	0.35
Hct [%]	25.50	4.50	19.00	6.00	23.00	0.00	26.00	0.00	23.50	0.50	23.00	1.00
Hb [g/dL]	8.65	1.55	6.80	1.70	7.80	0.00	8.80	0.00	8.00	0.20	7.85	0.35
Bile [g]			1.40	0.00	14.15	2.85	2.19	0.83	17.70	2.10	21.54	0.66
Weight [g]	2563.50	38.50			2939.50	100.50	2255.35	216.05			2241.00	0.00

Table S4: Hematology parameters and weight for APAP_155 and APAP_300 treated livers as mean and SD for n = 3 livers over 5 h of perfusion.

	APAP_150						APAP_300					
	0		60		300		0		60		300	
Timepoints [min]												
Analyte	Mean	SD	Mean	SD	Mean	SD	Mean	SD	Mean	SD	Mean	SD
Glucose [mmol/L]	16.23	13.28	10.57	10.74	8.35	5.85	6.60	1.00	5.80	0.75	5.37	0.61
Urea [mmol/L]	4.03	0.49	8.43	0.92	10.50	1.41						
AST [U/L]	3208.67	827.97	5189.00	1618.25	6056.33	1800.64	5965.00	2727.25			8768.67	2830.80
ALT [U/L]	193.33	42.32	266.33	79.32	292.67	85.19	232.67	76.04			289.33	74.00
Ammonia [µmol/L]	273.67	16.03	228.00	41.79	224.33	38.47						
Lactate [mmol/L]	14.43	2.11	20.50	2.46	23.60	5.61						
Albumin [g/L]	26.67	2.87	24.67	3.30	26.00	3.27						
Portal vein pressure [mmHg]	6.20	1.98	8.80	0.99	9.93	0.38	8.53	2.05	7.10	3.00	8.23	2.27
Hepatic artery pressure [mmHg]	73.30	2.62	74.97	6.82	63.57	22.49	81.90	3.81	82.13	3.11	82.20	3.27
Portal vein Flow [mL/min]	648.67	122.50	660.00	83.22	538.33	184.92	527.33	91.23	528.00	87.55	512.67	85.99
Hepatic artery flow [mL/min]	331.67	17.75	384.00	32.78	299.00	180.73	201.77	104.98	229.93	122.25	225.00	123.26
pH	7.33	0.01	7.28	0.08	7.18	0.19	7.25	0.03	7.29	0.05	7.29	0.05
Hct [%]	21.00	2.16	19.67	1.70	19.67	2.62	25.67	3.30	24.67	3.40	24.67	3.30
Hb [g/dL]	7.17	0.74	6.70	0.59	6.67	0.91	8.70	1.13	8.37	1.14	8.40	1.13
Bile [g]	11.40	0.00	27.00	0.00	24.17	4.88	5.45	5.69	7.10	5.87	7.83	5.78
Weight [g]	2480.47	178.29			2911.17	67.13	2168.17	152.42			2579.47	379.14

7 General Discussion

Recreating a model that encompasses all the liver functions and can mimic the pathogenesis of liver disease remains one of the key challenges in the field of hepatology. The liver has a high level of complexity and heterogeneity, and liver injury can be caused by a plethora of infectious agents and compounds either biological or chemical. The lack of knowledge in modeling liver diseases is causing an increased burden on the healthcare system and more representative liver models, both healthy and diseased, could impact the field by providing superior liver models. This knowledge deficit is partly caused by suboptimal *in vitro* and *ex vivo* models that do not mimic the complexity of the liver and therefore cannot recapitulate different types of liver injuries. As discussed in **part I** of this thesis, the discovery of 3-dimensional culture methods, combined with new hydrogels and bioreactor technology can push the field forward by recreating liver models with increased complexity in a standardised fashion. The journey of liver tissue engineering begins with the search for an ideal biomaterial for scaffolds that can promote tissue formation and be used in a clinical setting. Nanofibrillar cellulose (CNF) has emerged as a promising option due to its biocompatibility, shear thinning behavior, and tunable

chemical definition. However, it is not degradable in animals and humans, limiting its clinical application. To overcome this shortcoming, in **chapter 3**, fibroblast spheroids were cultured under flow conditions within CNF hydrogels in a newly developed bioreactor, with and without the presence of cellulase for degradation. The results indicated that degradation combined with flow leads to more effective tissue production in CNF hydrogels compared to growth in undegraded scaffold, thereby making it a potent scaffold material for tissue engineering.

To utilize these novel biomaterials for creating liver models, the correct cells are vital. For replicating functional liver tissue for drug testing or transplantation, liver organoids have gained much interest due to their genetic stability, expansion potential, and ability to differentiate toward a hepatocyte-like fate. The current standard for culturing these organoids is a basement membrane hydrogel, which possesses an undefined composition and is therefore not clinically applicable. CNF hydrogel was investigated in **chapter 4** as a viable alternative to basement membrane hydrogel, and it was found that it can serve as a suitable clinical grade scaffold for differentiating liver organoids as it is of defined, non-animal derived composition as opposed to for example

Matrigel™. Furthermore, the CNF hydrogel not only has this tunable chemical definition but also possesses suitable mechanical properties for differentiation, making it a promising option for liver tissue engineering.

Part II of this thesis, focused on *ex vivo* liver models, which are larger and more complex tissue system with increased complexity. These models are used to study liver function during health and disease but can also be used to finally engineer whole organs. Whole organ engineering utilizing decellularized liver scaffolds repopulated with autologous cells, is an attractive alternative to increase the pool of available organs for transplantation. However, the development of this technology is hampered by a lack of a suitable models based on large animals that are representative of the human physiology and a reliable and continuous cell source. In an attempt to develop such a model, porcine intrahepatic cholangiocyte organoids were generated from adult stem cells and it was demonstrated that these cultures remained stable over multiple passages while retaining the ability to differentiate into hepatocyte- and cholangiocyte-like cells in **chapter 5**. Recellularization onto porcine scaffolds was efficient, and the organoids homogeneously differentiated, even showing polarization. This porcine intrahepatic cholangiocyte system combined

with a porcine liver scaffold paves the way for developing whole liver engineering in a relevant large animal model.

Metabolic and toxic liver disorders are highly prevalent and potentially life-threatening. To allow studying these disorders without the use of experimental animals, we have harvested porcine livers in a slaughterhouse and perfused these livers normothermically. The perfused slaughterhouse livers maintained viable and functional over five hours of perfusion, demonstrating their versatility to study different liver disorders. This platform offers an accessible system to perform research in a functional, relevant large animal model while avoiding the use of experimental animals.

Overall, the thesis has comprehensively addressed and met its multifaceted aims, advancing our understanding of tissue engineering and liver organoid culture.

7.1 Animal testing for liver function

Already in 1959, Russel and Burch developed the so-called "3R Principle": *replacement*, *reduction*, and *refinement*, with the aim of improving the quality of science while humanizing the treatment of laboratory animals[1,2]. The interpretation of these principles has slightly adapted since, where not only the infliction of pain, stress, fear, and other unpleasant feelings for the animals

should be avoided, but the use of animals in general. Today, these methods have become known as "alternatives"[2] that have found application in international policies and programmes such as the Policy #12 "Consideration of Alternatives to Painful/Distressful Procedures" of the United States Department of Agriculture[3] and The European Partnership for Alternative Approaches to Animal Testing (EPAA)[4]. However, many regulations in the US as well as the EU still require test data obtained from animal experiments for the approval of medical devices and drugs for the safety and risk assessments.

The EPAA has recognized that problem as well and identified this challenge in their programme from 2021-2025: the gap between new non-animal model method development and their routine use needs to be bridged and regulators should be involved early on in the development and implementation of such approaches to gain trust in the usefulness and validity of such models[4].

In fact, validation of alternative models is one of the hurdles that needs to be overcome before they can achieve widespread acceptance. In general, validation requires the prove that a mechanism or effect of a disease or treatment work at leas as well in the to be validated

model (alternative) as in the target (human). However, in a lot of cases those details are unknown in human, which is why research in models is required in the first place (see Figure 1). Because of the vast data historically available in animals there is often sufficient knowledge to validate new alternative models against the animal proxys[5], however the translation from animals to human is also often not possible[6].
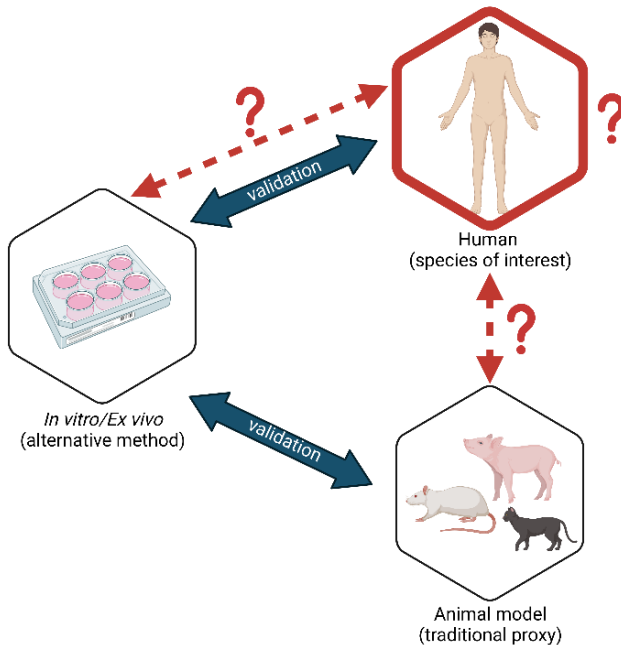
Figure 1: Adapted according to Griesinger et al.[5] Issues to overcome in validating alternative methods to research animal models. Often, the mechanistic details of the disease or treatment effect on the target species (human) is not known (unknowns in red color), only knowns are those details in the animal proxy models as well as the alternative models. This allows them to be validated against each other, but without direct correlation to the human itself.

7.2 New approach methodologies (NAMs)

New approach methodologies (NAMs) - or non-animal approaches - hold great promise in providing useful information for chemical hazard and risk assessment. Non-animal approaches, such as *in vitro* methods, computational modeling, and Adverse Outcome Pathways (AOP)-based assessments, are transforming toxicology[7]. Non-animal *in vitro* methods represent a pivotal shift away from traditional animal testing. These techniques involve the use of cultured cells as presented in chapter 3, tissues, and organoids as discussed in chapters 4 and 5 to simulate biological processes and assess toxicity. Such approaches offer the advantage of high-throughput screening, enabling researchers to evaluate a wide range of substances efficiently while reducing the ethical and logistical challenges associated with animal experimentation[8]. The incorporation of AOPs represents a significant breakthrough in the understanding of biological responses to chemical compounds. AOPs provide a structured framework to delineate the sequence of events from chemical exposure to adverse outcomes at various levels of biological organization. By elucidating these pathways, researchers gain insights into the mechanistic basis of toxicity as for example presented in **chapter 6**, enabling more targeted

and precise assessments without resorting to animal testing. These AOP-based assessments therefore contribute to a mechanistic understanding of toxicity, improving risk assessment and regulatory decision-making[9].

One of the further challenges with application of alternative models is that they are inherently a reduced version of the complex nature of the human body and thereby making it difficult to take every potential interaction into account[5]. Therefore, developing models that best mimic the anatomical and physiological organisation of the higher-level target system is essential as well as combining a suite of different model systems that can together address the different relevant properties[5].

A first step can be to already increase the level of complexity by using 3-dimensional *in vitro* models that have the potential to maintain cells, allow proliferation, differentiation, ECM production and signaling in order to develop functional tissues with the desired target functions[10–13]. In comparison, 2D-models; although mostly cheaper and easier to handle; lead to lower expression levels, less genetic stability, changes in cell morphology and artificial apical-basal polarity, making the obtained

data more unpredictable and less representative of the *in vivo* response[13,14]. Therefore, as shown in **chapter 3**, a 3-D system with an appropriate scaffold has the potential to be used for tissue engineering. ECM-derived scaffolds present the advantages of already providing a natural environment with good interactions with cells that contain needed biofunctional molecules, but they also have undefined compositions, a lot of variation between lots and possess the risk of unwanted interactions or interferences[15]. Hydrogels have many advantages such as their high water content and biocompatibility, mechanical tunability, low cost, high reproducibility and possibility for co-cultures[14,16] and as shown above even hydrogels that are not degradable in humans can be tailored and degraded through flow regimens[17]. On the other side, they can also possess variations between batches and be subject to structural changes over time[14]. The presented CNF hydrogel has shown its potential to serve as a scaffold for tissue engineering in general and for hepatocytes in particular as presented in **chapters 3 and 4***,* in particular because it is naturally biocompatible and of defined, non-animal derived composition.

For application as treatment in clinical practice, a whole host of requirements have to be met (see for example FDA's regulation 21 CFR Part 1271[18]). Biocompatibility is

a main requirement, as are sterility, non-toxicity, functional and mechanical properties, absence of diseases or cross-contaminations (sterility), durability/degradability, immunogenicity, tumorigenicity, stability during shelf-life, and many more. To achieve this, more research is necessary regarding hydrogel properties and functionality and unfortunately, as this material has only been used *in vitro* so far[16,19–21] and regulations still prescribe it, *in vivo* experiments will be necessary to prove its biocompatibility for example.

7.3 *Ex vivo* models

Acellular matrices as used in the **chapter 5** have the advantage of an already preserved native ECM and a natural high biocompatibility, but apart from being quite complex in protocols and culture, incomplete decellularization may cause adverse immune and inflammatory responses[22]. Translation to clinical applications is therefore connected to even more challenges than with synthetic or natural hydrogels.

Apart from the scaffold material itself, of course also the cells are of utmost importance in creating functional, representative alternative models and can also be differentiated into different levels of complexity. Not only the species is essential, but the often-used cell lines and

tumor cell lines are also less predictive and therefore less applicable than cells directly derived from human biospies[13]. In terms of culture protocols, spheroids as used in the **chapter 3** have the advantage of being simple, highly reproducible, can be tuned easily in size and are inexpensive. They are known to closely mimic the natural tissue architecture, providing a physiologically relevant environment for tissue construction[23]. Spheroids promote essential cell-cell interactions, supporting the differentiation of stem cells into specific lineages, a crucial aspect of tissue engineering[24]. They also serve as valuable platforms for studying angiogenesis and tissue development, processes integral to tissue engineering success[25]. However, their adoption in tissue engineering is not without challenges. Spheroids may exhibit variability in size, shape, and cell composition, posing challenges related to heterogeneity[23]. Scaling up spheroid production for large-scale tissue engineering applications can further be cost-prohibitive and logistically challenging[26] although high throughput creation of spheroids are under way[27,28]. Similarly, the spheroids as utilized in **chapter 3** are of murine origin and therefore not directly applicable to humans; moreover they are very simplified and hence have limited flexibility and size, lack vascularization and

matrix interaction[29,30], which makes them less suitable for more complex tissue engineering.

Organoids as used in **chapters 4 and 5** are already higher in complexity and can be directly extracted from a patient and therefore exhibit high biomimicking abilities[31]. But also in organoids a certain variability can be seen and it remains difficult to reach *in vivo* maturity with these cells[32]. Additionally, they also lack vascularization and most importantly, often lack key cell types that would be essential for full differentiation and functionality of the tissue[30]. Self-assembly of cells is another option where patient derived cells can produce their own ECM and can form tissue-mimicking organ-specific tissue depending on the used cell types. But this method requires quite long culture times, generates aggregates that are limited in size, lack vascularization and the mechanical properties could lead to incomplete differentiation which limits the biomimicking properties[33].

7.4 Regenerative hepatology

By recreating advanced *in vitro* models, we are mimicking the complexity of liver tissue and function. This also borders on the aim of the field of Regenerative Hepatology where novel technology is used to build an implantable liver mass for treating liver diseases and large bioengineered liver organs for transplantation, as substitutes to donor-organs[34]. There are, of course, some inherited hurdles to take to advance the findings in this thesis towards an implantable liver, but some lessons can be learned.

Ideally biomaterials, scaffolds and cells should together form a whole engineered liver for a replacement of the lacking donor organs by overcoming some of the shortcomings such as the dependence on matrices with animal components and lack of spatial organisation of cells and immature cell types[31]. As already mentioned, in moving forward, further studies that focus on improving the vascularization of engineered liver tissue will be important for the long-term viability and function of these tissues (see also Figure 2). In addition, research on the immune response to these engineered tissues will be necessary for successful transplantation[35].

Two of those significant immune-related hurdles are sterile inflammation and instant blood-mediated inflammatory reactions (IBMIR). Sterile inflammation arises due to the immune response initiated by the release of damage-associated molecular patterns (DAMPs) during cell death, a process triggered by ischemia-reperfusion injury during transplantation. This injury leads to the production of reactive oxygen and nitrogen species via mitochondrial pathways, resulting in uncontrolled cell death and the subsequent release of various DAMPs from the graft tissue[36]. IBMIR, on the other hand, occurs when blood interacts with the graft's cells which are promptly recognized by the innate immune system, leading to the rapid activation of both complement and coagulation pathways. Together with the activation of monocytes, granulocytes, Kupffer cells and natural killer cells this leads to cell lysis and therefore cell loss[37]. These inflammatory reactions can contribute to graft dysfunction, organ rejection, and early graft loss, emphasizing the need for strategies to mitigate their impact[36–39] (see Figure 2).

To prevent the rejection, transplant recipients often require immunosuppressive medications, which can have significant side effects[40]. Long-term immune suppression increases the risk of cytokine- release syndrome,

leukopenia, malignancies, and organ toxicity amongst others (see Figure 2)[41]. Balancing the need for immunosuppression to prevent graft rejection with the risk of these adverse effects is a critical challenge in liver transplantation[40,41].
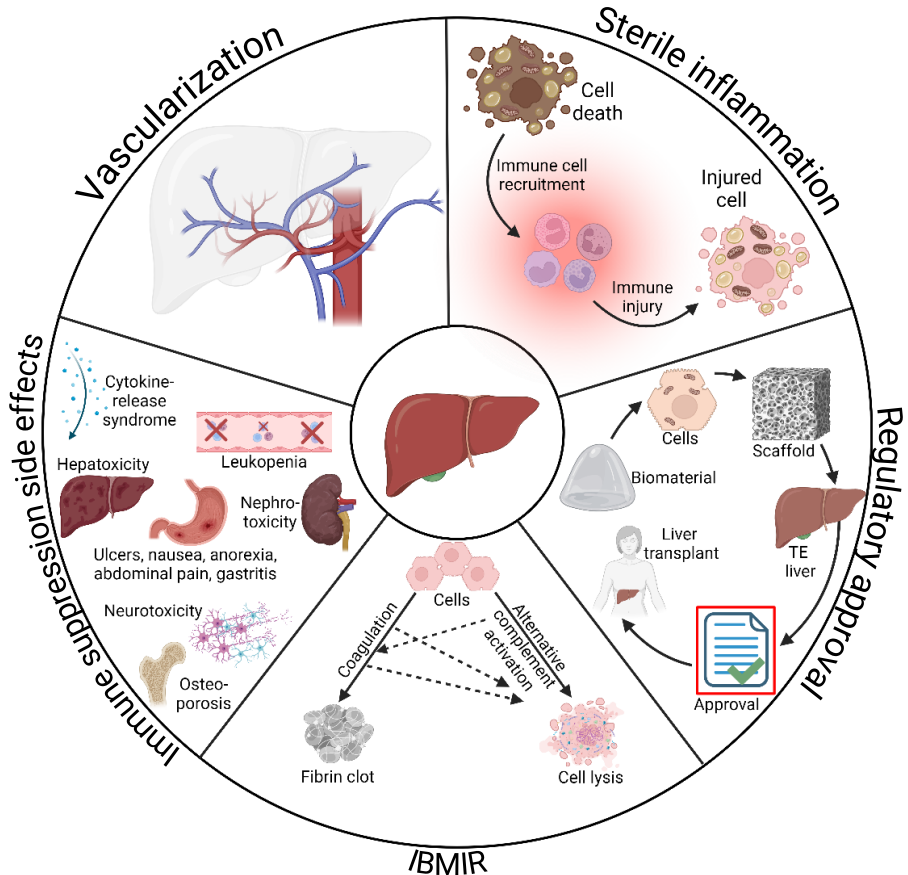

Figure 2: Adapted according to Wu et al. [39]. *Challenges in whole liver engineering and clinical applications. Proper vascularization, immune system responses such as sterile inflammation and instant blood-mediated inflammatory reaction (IBMIR), side effects of immune suppression and regulatory hurdles.*

Moreover, the path to realize a fully functional, vascularized, and transplantable liver tissue is laden with regulatory hurdles that can significantly extend the timeline for clinical implementation. The European Medicines Agency (EMA), the Food and Drug Administration (FDA) and similar regulatory bodies worldwide impose stringent guidelines and assessments for the approval of engineered tissues such as the liver. In the EU they are classified as Tissue Engineered Products (TEPs) and regulated as Advanced Therapy Medicinal Products (ATMPs). In the US, engineered tissues are regulated as "biological products", following the "tissue rules". These regulations ensure patient safety and efficacy but necessitate meticulous preclinical and clinical testing, adding years to the development process despite specific programs such as the Regenerative Medicine Advanced Therapy (RMAT) designation in the US and the Priorities Medicine scheme (PRIME) in the EU which intend to expedite the submission and review process[33].

Regulatory approval also requires the production of tissue-engineered liver constructs according to Good Manufacturing Practice (GMP) techniques, which poses its own set of challenges. GMP guidelines are essential in ensuring the quality and consistency of these advanced

therapy products, but adhering to them can be demanding[42].

Firstly, one of the primary challenges in GMP production is scalability. Moving from laboratory-scale production to large-scale manufacturing is a difficult task. Researchers and companies must optimize their processes to accommodate the larger volumes required for clinical trials and eventual commercialization[42]. This involves selecting appropriate bioreactor systems, developing scalable culture media, and ensuring the maintenance of consistent cell quality and differentiation throughout the production process[43]. Secondly, sourcing suitable cells for tissue engineering is critical. Obtaining a sufficient number of functional liver cells, such as hepatocytes, is a significant bottleneck. Human hepatocytes are primarily obtained from donated livers or derived from induced pluripotent stem cells (iPSCs). Both approaches have their challenges. The availability of donor organs is limited, and iPSC-derived hepatocytes must undergo rigorous characterization and differentiation protocols to ensure they exhibit proper liver functions[44,45]. Thirdly, maintaining the vascularization of the engineered liver tissue is crucial for its viability and functionality. Developing techniques to ensure the proper integration of blood vessels into the engineered tissue is a critical

aspect of GMP production[46]. Furthermore, ensuring the long-term stability and functionality of the engineered liver tissue presents ongoing challenges. As mentioned above, cells may lose their specialized functions or face immune rejection, necessitating immunosuppressive therapies that come with their own set of risks and complications[47]. Quality control and consistency in manufacturing are paramount in GMP production. Any variations in the production process or environment can lead to differences in the final product, affecting its safety and efficacy[48]. This requires rigorous testing, documentation, and monitoring throughout production, which can be resource-intensive and time-consuming[46].

In conclusion, while the concept of a fully functional, vascularized, and transplantable liver tissue holds immense promise and we have created liver tissue in **chapter 5** by decellularizing liver tissue and engrafting it with organoids, it will likely take years, if not decades, to overcome the regulatory hurdles, develop advanced biomaterials, achieve optimal spatial cell organization, improve vascularization, address immune response challenges and comply with GMP production requirements. These multifaceted complexities underscore the need for continued dedication and collaboration within the field of regenerative medicine,

ultimately bringing us closer to the realization of this medical advancement.

7.5 Normothermic machine perfusion

Next to Whole Organ Engineering, the use of *ex vivo* Normothermic Machine Perfusion has made a tremendous leap over the years. In fact, normothermic perfusion of marginal allografts allows for application of a variety of therapeutic interventions potentially enhancing organ quality before transplantation[49–52]. *Ex vivo* porcine perfusion models have not only found application for translational transplant research in liver perfusion but also for lung, heart, pancreas, small bowel, kidney or multiorgan perfusion[53]. Furthermore, *ex vivo* porcine perfusion models are increasingly utilized for studies in several other research topics as for example to investigate hemostatic products[54] and the arterial buffer response[55] in the liver, bacterial pathogenesis in the lung[56], reduction of ischemia reperfusion injury in the kindey[57,58], or mucoadhesion of microcontainers in the intestine[59] to only name a few. Hence, finally at the highest stage of complexity is the model described in the **chapter 6** where the whole porcine liver is utilized as a model. This retains the full natural ECM and cell diversity and structure as long as the liver can be kept viable and functional,

which is the biggest challenge in this approach, in particular over long time periods. Especially to avoid research animal models, slaughterhouse livers are used that are harvested in less-than-ideal circumstances and are damaged before even being kept alive. More specifically, the environment of this slaughterhouse is rather aseptic than sterile, and organs are harvested while cutting the carcass and dropped in a large collecting vessel which could cause trauma to the organ. Another major challenge is the need for the perfusion fluid, ideally autologous blood, which needs to be harvested and treated as well, if no alternatives such as polymerized oxygen carriers are used[60]. The protocol itself is also highly complex and therefore application of this model could be in conjunction with the previously described models in less high-throughput applications but more for the in-depth research that benefits from the presence of the full architecture of the liver after basic questions have already been previously answered. Once further developed this approach has high potential for use in human regenerative medicine for example by regeneration through decellularization and recellularization with organoids utilizing the existing vasculature, applying defatting or senolytic drugs, RNA interference or stem cell therapy[61].

7.6 Further perspectives

Overall, the advancements presented in this thesis represent every stage of liver tissue engineering, from simple to high tissue complexity. The findings indicate a promising future full of possibilities for novel treatment modalities of liver disease including the shortage of donor organs. This goal can be attained through individual approaches or a combination of models. For instance, one possibility would be the engineering of liver tissue using porcine organoids that have been expanded *in vitro* within a CNF hydrogel. Subsequently, this engineered tissue can be integrated into decellularized porcine liver scaffolds and transplanted into a diseased, perfused *ex vivo* liver for the purpose of regeneration. Biomaterials for liver tissue engineering are thereby utilized in the development of *ex vivo* models for disease modeling, organ transplantation and, ultimately, whole liver engineering, all while avoiding animal models. Further research on this topic is essential for advancing the field and improving the clinical translation of these models and establishing trust from the scientific community and regulatory authorities. This said, the advances described in this thesis might pave the way for safer and more effective treatments of liver disease patients all while avoiding the use of research animals.

7.7　References

1.　Russell WMS, Burch RL. The Principles of Humane Experimental Technique. Methuen & Co LTD; 1959.

2.　Tannenbaum J, Bennett BT. Russell and Burch's 3Rs then and now: the need for clarity in definition and purpose. J Am Assoc Lab Anim Sci. 2015;54(2):120-132.
http://www.ncbi.nlm.nih.gov/pubmed/25836957

3.　National Research Council (U.S.). Committee on Regulatory Issues in Animal Care and Use. Definition of Pain and Distress and Reporting Requirements for Laboratory Animals : Proceedings of the Workshop Held June 22, 2000. National Academy Press; 2000.

4.　European Commission. EPAA Action Programme 2021-2025.; 2020. Accessed April 2, 2023. https://ec.europa.eu/docsroom/documents/43242/ attachments/1/translations/en/renditions/native

5.　Griesinger C, Desprez B, Coecke S, Casey W, Zuang V. Validation of alternative In vitro methods to animal testing: Concepts, challenges, processes and tools. In: Advances in Experimental Medicine and Biology. Vol 856. Springer New York LLC; 2016:65-132. doi:10.1007/978-3-319-33826-2_4

6.　Van Norman GA. Limitations of Animal Studies for Predicting Toxicity in Clinical Trials: Is it Time to Rethink Our Current Approach? JACC Basic Transl Sci. 2019;4(7):845-854. doi:10.1016/j.jacbts.2019.10.008

7.　Parish ST, Aschner M, Casey W, et al. An evaluation framework for new approach methodologies (NAMs) for human health safety assessment. Regulatory Toxicology and

Pharmacology. 2020;112. doi:10.1016/j.yrtph.2020.104592

8.   Sewell F, Doe J, Gellatly N, Ragan I, Burden N. Steps towards the international regulatory acceptance of non-animal methodology in safety assessment. Regulatory Toxicology and Pharmacology. 2017;89:50-56. doi:10.1016/j.yrtph.2017.07.001

9.   ECHA. New Approach Methodologies in Regulatory Science. In: Proceedings of a Scientific Workshop Helsinki. ; 2016. doi:10.2823/543644

10. Iqbal N, Khan AS, Asif A, Yar M, Haycock JW, Rehman IU. Recent concepts in biodegradable polymers for tissue engineering paradigms: a critical review. International Materials Reviews. 2019;64(2):91-126.
doi:10.1080/09506608.2018.1460943

11. Salehi-Nik N, Ghassem Amoabediny BP, Tabesh H, et al. Engineering parameters in bioreactor's design: a critical aspect in tissue engineering. Biomed Res Int. 2013;2013(Article ID 762132):15. doi:10.1155/2013/762132

12. Janorkar A V., Harris LM, Murphey BS, Sowell BL. Use of three-dimensional spheroids of hepatocyte-derived reporter cells to study the effects of intracellular fat accumulation and subsequent cytokine exposure. Biotechnol Bioeng. 2011;108(5):1171-1180. doi:10.1002/bit.23025

13. Tutty MA, Movia D, Prina-Mello A. Three-dimensional (3D) liver cell models - a tool for bridging the gap between animal studies and clinical trials when screening liver accumulation and toxicity of nanobiomaterials. Drug Deliv Transl Res. 2022;12(9):2048-2074. doi:10.1007/s13346-

022-01147-0

14. Bédard P, Gauvin S, Ferland K, et al. Innovative human three-dimensional tissue-engineered models as an alternative to animal testing. Bioengineering. 2020;7(3):1-40. doi:10.3390/bioengineering7030115

15. Worthington P, Pochan DJ, Langhans SA. Peptide hydrogels - versatile matrices for 3D cell culture in cancer medicine. Front Oncol. 2015;5(APR). doi:10.3389/fonc.2015.00092

16. Torres-Rendon JG, Köpf M, Gehlen D, et al. Cellulose Nanofibril Hydrogel Tubes as Sacrificial Templates for Freestanding Tubular Cell Constructs. Biomacromolecules. 2016;17(3):905-913. doi:10.1021/acs.biomac.5b01593

17. Krüger M, Spee B, Walther A, De Laporte L, Kock LM. Nanofibrillar Cellulose as an Enzymatically and Flow Driven Degradable Scaffold for Three-Dimensional Tissue Engineering. J Eng Sci Med Diagn Ther. 2019;2(4):1-8. doi:10.1115/1.4044473

18. Food and Drug Administration. 21 CFR 1271. Published April 2, 2023. Accessed April 2, 2023. https://www.ecfr.gov/current/title-21/chapter-I/subchapter-L/part-1271

19. Lou YR, Kanninen L, Kuisma T, et al. The Use of Nanofibrillar Cellulose Hydrogel As a Flexible Three-Dimensional Model to Culture Human Pluripotent Stem Cells. Stem Cells Dev. 2013;23(4):380-392. doi:10.1089/scd.2013.0314

20. Bhattacharya M, Malinen MM, Lauren P, et al. Nanofibrillar cellulose hydrogel promotes three-dimensional liver cell culture. Journal of Controlled Release. 2012;164(3):291-298. doi:10.1016/j.jconrel.2012.06.039

21. Malinen MM, Kanninen LK, Corlu A, et al. Differentiation of liver progenitor cell line to functional organotypic cultures in 3D nanofibrillar cellulose and hyaluronan-gelatin hydrogels. Biomaterials. 2014;35(19):5110-5121. doi:10.1016/j.biomaterials.2014.03.020

22. Chaudhari AA, Vig K, Baganizi DR, et al. Future prospects for scaffolding methods and biomaterials in skin tissue engineering: A review. Int J Mol Sci. 2016;17(12). doi:10.3390/ijms17121974

23. Lin RZ, Chang HY. Recent advances in three-dimensional multicellular spheroid culture for biomedical research. Biotechnol J. 2008;3(9-10):1172-1184. doi:10.1002/biot.200700228

24. Semino CE, Merok JR, Gracy ¡, et al. Functional Differentiation of Hepatocyte-like Spheroid Structures from Putative Liver Progenitor Cells in Three-Dimensional Peptide Scaffolds. Vol 71. Blackwell Verlag; 2003. www.synpep.com,

25. Laschke MW, Menger MD. Spheroids as vascularization units: From angiogenesis research to tissue engineering applications. Biotechnol Adv. 2017;35(6):782-791. doi:10.1016/j.biotechadv.2017.07.002

26. Fong ELS, Toh TB, Yu H, Chow EKH. 3D Culture as a Clinically Relevant Model for Personalized Medicine. SLAS Technol. 2017;22(3):245-253. doi:10.1177/2472630317697251

27. Cui X, Liu Y, Hartanto Y, Bi J, Dai S, Zhang H. Multicellular Spheroids Formation and Recovery in Microfluidics-generated Thermoresponsive Microgel Droplets. Colloids and Interface Science Communications. 2016;14. doi:10.1016/j.colcom.2016.09.001

28. Sabhachandani P, Motwani V, Cohen N, Sarkar S, Torchilin V, Konry T. Generation and functional assessment of 3D multicellular spheroids in droplet based microfluidics platform. Lab Chip. 2016;16(3). doi:10.1039/c5lc01139f

29. Chaicharoenaudomrung N, Kunhorm P, Noisa P. Three-dimensional cell culture systems as an in vitro platform for cancer and stem cell modeling. World J Stem Cells. 2019;11(12):1065-1083. doi:10.4252/wjsc.v11.i12.1065

30. Fang Y, Eglen RM. Three-Dimensional Cell Cultures in Drug Discovery and Development. SLAS Discovery. 2017;22(5):456-472. doi:10.1177/1087057117696795

31. Lam DTUH, Dan YY, Chan YS, Ng HH. Emerging liver organoid platforms and technologies. Cell Regeneration. 2021;10(1). doi:10.1186/s13619-021-00089-1

32. Hofer M, Lutolf MP. Engineering organoids. Nat Rev Mater. 2021;6(5):402-420. doi:10.1038/s41578-021-00279-y

33. Saba I, Jakubowska W, Bolduc S, Chabaud S. Engineering Tissues without the Use of a Synthetic Scaffold: A Twenty-Year History of the Self-Assembly Method. Biomed Res Int. 2018;2018. doi:10.1155/2018/5684679

34. Papatheodoridi M, Mazza G, Pinzani M. Regenerative hepatology: In the quest for a modern prometheus? Digestive and Liver Disease. 2020;52(10):1106-1114. doi:10.1016/J.DLD.2020.08.001

35. Wang Y, Bao J, Wu X, et al. Genipin crosslinking reduced the immunogenicity of xenogeneic decellularized porcine whole-liver matrices through

regulation of immune cell proliferation and polarization. Sci Rep. 2016;6(April):1-16. doi:10.1038/srep24779

36.   Kahan R, Cray PL, Abraham N, et al. Sterile inflammation in liver transplantation. Front Med (Lausanne). 2023;10. doi:10.3389/fmed.2023.1223224

37.   Lee CA, Dhawan A, Smith RA, Mitry RR, Fitzpatrick E. Instant blood-mediated inflammatory reaction in hepatocyte transplantation: Current status and future perspectives. Cell Transplant. 2016;25(7):1227-1236. doi:10.3727/096368916X691286

38.   Kanak MA, Takita M, Itoh T, et al. Alleviation of instant blood-mediated inflammatory reaction in autologous conditions through treatment of human islets with NF-κB inhibitors. Transplantation. 2014;98(5):578-584. doi:10.1097/TP.0000000000000107

39.   Wu S, Wang L, Fang Y, Huang H, You X, Wu J. Advances in Encapsulation and Delivery Strategies for Islet Transplantation. Adv Healthc Mater. 2021;10(20). doi:10.1002/adhm.202100965

40.   Di Maira T, Little EC, Berenguer M. Immunosuppression in liver transplant. Best Pract Res Clin Gastroenterol. 2020;46-47. doi:10.1016/j.bpg.2020.101681

41.   Claeys E, Vermeire K, Leuven KU. Immunosuppressive Drugs in Organ Transplantation to Prevent Allograft Rejection: Mode of Action and Side Effects.; 2019.

42.   Mansbridge J. Commercial considerations in tissue engineering. In: Journal of Anatomy. Vol 209. ; 2006:527-532. doi:10.1111/j.1469-

7580.2006.00631.x

43. Verbarendse M, Snyder R, Lakshmipathy U. Mini-review: Equipment evaluation for process scalability and readiness for current Good Manufacturing Practices in cell therapy workflows. Cytotherapy. Published online 2023. doi:10.1016/j.jcyt.2023.05.005

44. Nadi A, Moradi L, Ai J, Asadpour S. Stem Cells and Hydrogels for Liver Tissue Engineering: Synergistic Cure for Liver Regeneration. Stem Cell Rev Rep. 2020;16(6):1092-1104. doi:10.1007/s12015-020-10060-3

45. Ozawa H, Matsumoto T, Nakagawa M. Culturing human pluripotent stem cells for regenerative medicine. Expert Opin Biol Ther. 2023;23(6):479-489. doi:10.1080/14712598.2023.2225701

46. Yang GH, Kang D, An SH, et al. Advances in the development of tubular structures using extrusion-based 3D cell-printing technology for vascular tissue regenerative applications. Biomater Res. 2022;26(1). doi:10.1186/s40824-022-00321-2

47. Reza H Al, Okabe R, Takebe T. Organoid transplant approaches for the liver. Transplant International. 2021;34(11). doi:10.1111/tri.14128

48. Burger SR. Current regulatory issues in cell and tissue therapy. Cytotherapy. 2003;5(4):289-298. doi:10.1080/14653240310002324

49. van Beekum CJ, Vilz TO, Glowka TR, von Websky MW, Kalff JC, Manekeller S. Normothermic machine perfusion (NMP) of the liver – current status and future perspectives. Ann Transplant. 2021;26. doi:10.12659/AOT.931664

50. Schön MR, Kollmar O, Wolf S, et al. Liver

transplantation after organ preservation with normothermic extracorporeal perfusion. Ann Surg. 2001;233(1):114-123. doi:10.1097/00000658-200101000-00017

51. Clavien PA, Dutkowski P, Mueller M, et al. Transplantation of a human liver following 3 days of ex situ normothermic preservation. Nature Biotechnology 2022 40:11. 2022;40(11):1610-1616. doi:10.1038/s41587-022-01354-7

52. Mueller M, Hefti M, Eshmuminov D, et al. Long-term Normothermic Machine Preservation of Partial Livers: First Experience With 21 Human Hemi-livers. Ann Surg. 2021;274(5). doi:10.1097/SLA.0000000000005102

53. Kumar R, Chung WY, Dennison AR, Garcea G. Ex Vivo Porcine Organ Perfusion Models as a Suitable Platform for Translational Transplant Research. Artif Organs. 2017;41(9):E69-E79. doi:10.1111/aor.12865

54. Roozen EA, Lomme RMLM, Calon NUB, Warlé MC, Van Goor H. Validity of a novel ex vivo porcine liver perfusion model for studying haemostatic products. Lab Anim. Published online 2022. doi:10.1177/00236772221138398

55. Becker D, Hefti M, Schuler MJ, et al. Model assisted analysis of the hepatic arterial buffer response during ex vivo porcine liver perfusion. Transactions on Biomedical Engineering. 2019;PP(c):in revision. doi:10.1109/TBME.2019.2919413

56. Dumigan A, Fitzgerald M, Santos JSPG, et al. A porcine ex vivo lung perfusion model to investigate bacterial pathogenesis. mBio. 2019;10(6). doi:10.1128/mBio.02802-19

57. Huijink TM, Venema LH, Posma RA, et al. Metformin Preconditioning and Postconditioning to Reduce Ischemia Reperfusion Injury in an Isolated Ex Vivo Rat and Porcine Kidney Normothermic Machine Perfusion Model. Clin Transl Sci. 2021;14(1):222-230. doi:10.1111/cts.12846

58. Jassem W, Xystrakis E, Ghnewa YG, et al. Normothermic Machine Perfusion (NMP) Inhibits Proinflammatory Responses in the Liver and Promotes Regeneration. Hepatology. 2019;0(0):1-14. doi:10.1002/hep.30475

59. Dalskov Mosgaard M, Strindberg S, Abid Z, et al. Ex vivo intestinal perfusion model for investigating mucoadhesion of microcontainers. Int J Pharm. 2019;570. doi:10.1016/j.ijpharm.2019.118658

60. Matton APM, Burlage LC, van Rijn R, et al. Normothermic machine perfusion of donor livers without the need for human blood products. Liver Transplantation. 2018;24(4):528-538. doi:10.1002/lt.25005

61. Lascaris B, de Meijer VE, Porte RJ. Normothermic liver machine perfusion as a dynamic platform for regenerative purposes: What does the future have in store for us? J Hepatol. 2022;77(3):825-836. doi:10.1016/j.jhep.2022.04.033

8 Summary

Understanding the critical importance of reducing reliance on traditional research animal models in liver disease research, this thesis focused on advancing the development of more sophisticated, physiologically relevant, and ethically aligned models. These alternatives aimed to effectively simulate the complexities of liver disease, fostering the exploration of novel therapeutic strategies and a more comprehensive understanding of liver pathophysiology without compromising ethical standards.

In **chapter 3**, the study offered critical insights into the use of nanofibrillar cellulose as an effective scaffold material for tissue engineering, providing a viable alternative to animal-based models. By shedding light on the interplay between cellulase enzyme concentration, flow conditions, and fibroblast spheroid cultures within nanocellulose hydrogels, the research enhanced our understanding of the cell microenvironment and contributed to the advancement of ethical and effective alternatives to animal-based disease modeling.

Furthermore, **chapter 4** addressed the pressing need for reliable and clinically applicable liver disease models. Through a systematic assessment of cellulose nanofibril

271

hydrogels as a viable alternative to traditional Matrigel, the research presented a pathway for the development of more standardized and ethically sound liver disease models, fostering a more responsible approach to liver disease research and therapeutic development.

Chapter 5 represented a crucial step forward in the quest for advanced large-animal models that closely mimicked human liver physiology. By successfully generating and integrating porcine intrahepatic cholangiocyte organoids into porcine liver scaffolds, the research provided a promising animal-free platform for studying complex liver pathologies and advancing therapeutic interventions, ultimately reducing the reliance on traditional research animal models.

Lastly, **chapter 6** introduced a practical and ethical alternative to animal-based studies, emphasizing the importance of developing comprehensive research alternatives. By accurately replicating biochemical markers of liver damage, the platform served as a promising solution for studying metabolic and toxic liver disorders without the need for traditional research animal models, contributing to the establishment of a more ethical and effective paradigm in liver disease research.

In conclusion, these endeavors mark significant progress in the field of liver tissue engineering and disease modeling, emphasizing the importance of advancing sophisticated and ethically aligned research alternatives. Through the development of these innovative models, the research not only furthers our understanding of liver disease mechanisms but also significantly contributes to the ongoing effort to reduce the dependence on traditional research animal models in liver disease research.

8.1 Samenvatting

Vanwege het grote belang van het verminderen van de afhankelijkheid van proefdieren in het onderzoek naar leverziekten, richtte dit proefschrift zich op de ontwikkeling van geavanceerde, fysiologisch relevante en ethisch verantwoorde modellen. Een randvoorwaarde van deze alternatieve modellen was dat ze een goede benadering waren van de complexiteit van leverziekten, waardoor betrouwbaar nieuwe therapeutische strategieën kunnen worden ontwikkeld en meer kennis van leverpathofysiologie kan worden opgebouwd, zonder ethische normen te schaden.

De studie beschreven in **Hoofdstuk 3** biedt belangrijke nieuwe inzichten in het gebruik van nanofibrillair cellulose als een effectief scaffold-materiaal voor "tissue engineering", waarmee een bruikbaar alternatief voor modellen op basis van proefdieren wordt geboden. Onderzoek naar de wisselwerking tussen de concentratie van het enzym cellulase, de weefseldoorstroming, en de fibroblast-sferoïden in de nanocellulose-hydrogels verbeterde het inzicht in de processen die op weefselniveau spelen en droeg bij aan het ontwikkelen van ethisch verantwoorde en werkzame alternatieven voor proefdieren.

De basis van **Hoofdstuk 4** is de dringende behoefte aan betrouwbare en klinisch toepasbare leverziekte-modellen. Door een systematische beoordeling van hydrogelen van nanofibrillair cellulose als een werkzaam alternatief voor het traditioneel gebruikte Matrigel, kon een routekaart worden opgesteld voor de ontwikkeling van meer gestandaardiseerde en ethisch verantwoorde leverziekte-modellen, hetgeen bij kan dragen aan een meer verantwoorde benadering van leverziekte-onderzoek en de ontwikkeling van therapeutische mogelijkheden bij leveraandoeningen.

Hoofdstuk 5 beschrijft een cruciale stap voorwaarts in de zoektocht naar geavanceerde grootschalige modellen die nauwkeurig de menselijke leverfysiologie nabootsen. Door met succes intrahepatische cholangiocyt-organoïden van het varken te ontwikkelen en te integreren in gedecellulariseerde varkenslever-scaffolds, biedt het onderzoek een veelbelovend proefdiervrij-platform voor het bestuderen van complexe leverziekten en het bevorderen van therapeutische interventies, waarmee uiteindelijk de afhankelijkheid van proefdieren kan worden verminderd.

In **Hoofdstuk 6** wordt een praktisch en ethisch alternatief voor op proefdieren gebaseerde studies naar leverziekten

gepresenteerd. Onderzoek naar de effecten van de inductie van leverschade liet zien dat het ontwikkelde platform zeer bruikbaar is voor het bestuderen van metabole en toxische leveraandoeningen zonder de noodzaak om proefdieren te gebruiken, hetgeen bijdraagt aan het creëren van ethisch verantwoorde en effectievere modellen in het onderzoek naar leverziekten.

Samenvattend kan gesteld worden dat de onderzoeken beschreven in dit proefschrift een significante vooruitgang markeren op het gebied van lever-tissue engineering en het ontwikkelen van modellen voor leverziekten, waarbij het belang van het bevorderen van geavanceerde en ethisch verantwoorde onderzoeksalternatieven, zonder het gebruik van proefdieren, wordt benadrukt. Door de ontwikkeling van deze innovatieve modellen is de weg vrij om ons begrip van de mechanismen van leverziekten te vergroten, terwijl het gebruik van proefdieren bij het onderzoek naar leveraandoeningen aanzienlijk kan worden verminderd.

9 Addendum

9.1 **Acknowledgements**

Getting to this point has been a marathon, not a sprint. After the initial years of intense commitment to research, it became increasingly challenging to maintain the same level of dedication while managing full-time jobs and building a career. Therefore, I want to express my deepest gratitude to everyone who persevered alongside me and never lost trust and confidence in me, even during times when I doubted myself. I was frequently asked, "So, when will you be done? How much longer will it take?" and my response was often, "Almost done, not much longer." Now that the end is finally in sight, I am immensely thankful for all the people in my life who never left my side and patiently checked in on me time and time again.

First and foremost, I want to extend my heartfelt thanks to Bart Spee. After many attempts, I am incredibly happy that you finally became my academic supervisor and promoter, making this research and PhD possible in the first place. I couldn't have asked for a better supervisor; your positivity and encouragement were unwavering, even when you needed to muster the most patience. I have learned so much from you, both personally and

scientifically. You are truly an inspiring person in every aspect.

To Linda Kock, you were the one who hired me for LifeTec and the BIOGEL project, setting everything into motion. I am deeply grateful for that! I also learned a great deal from you, and we shared many memorable moments, especially during our BIOGEL travels, where you effortlessly connected with everyone and made us feel like a cohesive team. You always encouraged me to explore my own methods and try out new ideas, both in my research and in our work environment, which was incredibly valuable for my development.

Hans Kooistra, like Bart, you are a very positive and encouraging person who always provided constructive and appreciative feedback. I'm very grateful that you took me on as a PhD student and supported me throughout this journey.

I would also like to express my sincere gratitude to my reading committee: Prof. dr. de Bruin, Dr. Levato, Prof. Rasponi, Prof. dr. Ritskes-Hoitinga, and Prof. dr. Salvatori for dedicating your time and effort to reading and evaluating this thesis. I'm looking forward to a meaningful discussion with each of you and the opportunity to learn from your diverse expertise.

In addition to Linda, I would like to extend my thanks to all of my former colleagues at LifeTec: Jurgen, Marco, Sjoerd, Bart, Janneke, Mattia, Anke, Elke, Marcel, Naudia, Bertus, and many others. I look back on my time at LifeTec with great fondness, and I grew significantly during that period, thanks to all of you!

Special thanks go to my LifeTec Marie-Curie fellows, with whom I went through "thick and thin," as we say in German: Noemi, my good friend, with whom I still consult on all sorts of questions; Ben, who made significant contributions to the *ex vivo* liver platform; and, of course, my lovely friend Martina, who made work so much more enjoyable and continues to be a close friend.

Big thanks also go to the students who worked alongside me: Dave, with whom I spent countless late nights in the lab; Sharon, with whom I cleaned up the odd blood bath; and of course, my dear Alicia, the brilliant and kind PhD student who not only finished before me but also improved on everything I did.

I would also like to thank the BIOGEL students and friends who were part of my journey: Arturo, Marcel, Irene, Jenny, Sitara, Paula, Max, Filippo, Nestor, Leander, Dominik, Luis, and Daria. We shared so many beautiful trips and fun times, and I count myself very lucky to have been part

of such an awesome group. The scientific exchanges we had contributed greatly to my eventual success. I think I'm the last one of us, but we all made it in the end!

A special acknowledgment goes to Laura DeLaporte for her role in the BIOGEL organization, enabling my secondment, and providing some of the novel materials and many ideas. And to everyone in Bart's group — Loes, Kerstin, Monique, Roos-Anne — thank you for your support and collaboration.

Finally, I want to express my deep appreciation to my family for their unwavering support and to my friends for their friendship and encouragement throughout this journey.

I would also like to acknowledge my colleagues and friends at Protembis, who have been part of the latest and most difficult phase of this journey.

Of course, there were many more people and organizations that played a role in the past few years and contributed to this thesis in some shape or form. Even if not named individually, I'm deeply thankful for everything!

9.2 Curriculum vitae

<u>Education</u>

PHD Candidate

University Utrecht, Regenerative medicine. 09/2018 – present

Alternatives to animal research: from *in vitro* to *ex vivo* liver models

Marie-Sklodowska-Curie funded EU project BIOGEL

Biochemical engineering (Diploma Degree Grade 2.4)

Technical University Dortmund, Germany. 05/2006 – 11/2014

- Research Paper at the Leibniz- Institute for Analytical Sciences – ISAS – E.V.: Characterization and storage stability of cell repellent surfaces (Grade: 1.3)
- Research Paper in the Group Bioprocess Technology: Extension and optimization of a model for the description of an enzyme catalyzed esterification (Grade: 1.8)
- Diploma Thesis at ThyssenKrupp Electrolysis GmbH in cooperation with the Working Group Bioprocess Technology of TU Dortmund and the Working Group Bioprocess Technology of TU Wien: Total organic carbon reduction in a biologically pretreated waste salt brine for reuse in an electrolysis process (Grade: 1.1)

Physics

University of Wuppertal. 04/2005 – 05/2006

<u>Work Experience</u>

Director Regulatory Affairs

Protembis GmbH, Germany 07/2023 – present

Member of the management team, contributing to strategic decision-making and overseeing regulatory compliance. Lead regulatory submissions and ensure adherence to regulatory standards.

Manager Regulatory Affairs International

Protembis GmbH, Germany 06/2022 – 06/2023

Development of regulatory strategies for market entry on mainly the EU and US market, communication with competent authorities and notified bodies, interface to R&D and QM departments as well as CROs to ensure completeness of respective technical files. Responsible for development and initiation of necessary clinical studies including respective application processes and scientific evaluation of protocols and results.

R&D Engineer

Protembis GmbH, Germany 01/2021 – 05/2022

Development of non-active class III cerebral protection device with incorporated medicinal substance, assurance of regulatory compliance with a focus on but not limited to pre-clinical activities regarding risk management, design control, creation of technical file, verification testing, process validation. Involvement in clinical validation data evaluation and reporting. SCM representative.

R&D Engineer

LifeTec Group B.V., The Netherlands. 09/2015 – 12/2020

Development, and application of *ex vivo* mock loops for pre-clinical medical device and drug testing (mainly hepatic and cardiac field), bioreactor development, leadership of EU projects, communication and marketing, intrapreneurship, business development for new platforms.

9.3   Conflict of interest statement

The author was employed by two commercial entities (LifeTec Group BV and Protembis GmbH) during the finalization of her thesis and declares that there are no conflicts of interest regarding the publication of this thesis.

9.4 List of publications

1. Alwast H, Baumann W, Birnstengel B, Fleischhauer M, **Krüger M**, Warzecha OB. Abfallmengen und Recyclingpotenziale in der Europäischen Union. MÜLL und ABFALL. 2008;(10):3. doi:10.37307/j.1863-9763.2008.10.03

2. Cipriani F, **Krüger M**, De Torre IG, et al. Cartilage Regeneration in Preannealed Silk Elastin-Like Co-Recombinamers Injectable Hydrogel Embedded with Mature Chondrocytes in an Ex Vivo Culture Platform. Biomacromolecules.2018;19(11):4333-4347. doi:10.1021/acs. biomac.8b01211

3. **Krüger M**, Spee B, Walther A, De Laporte L, Kock LM. Nanofibrillar Cellulose as an Enzymatically and Flow Driven Degradable Scaffold for Three-Dimensional Tissue Engineering. J Eng Sci Med Diagn Ther. 2019;2(4):1-8. doi:10.1115/1.4044473

4. **Krüger M**, Oosterhoff LA, van Wolferen ME, et al. Cellulose Nanofibril Hydrogel Promotes Hepatic Differentiation of Human Liver Organoids. Adv Healthc Mater. 2020;9(6):1901658. doi:10.1002/adhm. 201901658

5. Tsanaktsidou E, Kammona O, Labude N, Neuss S, **Krüger M**, Kock L, Kiparissides C. Biomimetic cell-laden meha hydrogels for the regeneration of cartilage tissue. Polymers (Basel). 2020;12(7). doi:10.3390/polym12071598

6. **Krüger M**, Samsom RA, Oosterhoff LA, et al. High level of polarized engraftment of porcine intrahepatic cholangiocyte organoids in decellularized liver scaffolds. J Cell Mol Med. 2022;(May):1-10. doi:10.1111/jcmm.17510

7. **Krüger M**, Ruppelt A, Kappler B, et al. Normothermic Ex Vivo Liver Platform Using Porcine Slaughterhouse Livers for Disease Modeling. Bioengineering. 2022;9(9). doi:10.3390/bioengineering9090471

9.5   PhD Portfolio

Name of PhD student: Melanie Krüger

PhD period: 2015-2024

Name of PhD supervisors: Prof. dr. H.S. Kooistra, Dr. B. Spee

Name of PhD co-supervisors: Dr. L. Kock

	Organising Institute	Year	Work-load (ECTS)
1. General Courses			
- Introduction to RM (mandatory)	RMUtrecht	2018	1
- Introduction to Stem Cells	RMUtrecht	2018	1
- Perspectives in RM (mandatory)	RMUtrecht	2018	1
- Bench to Bedside	RMUtrecht	2018	2
- Cardiovascular RM	RMUtrecht	2018	1.2
- Enabling Technologies	RMUtrecht	2018	1.5
- Theme Day: Musculoskeletal	RMUtrecht	2018	0.3
- Theme Day: Cardiovascular	RMUtrecht	2018	0.3

		Organising Institute	Year	Work-load (ECTS)
-	Theme Day: Stem Cell-based Therapies	RMUtrecht	2018	0.3
-	RM Lunch Seminar Series	RMUtrecht	2018	0.6/yr
-	PhD Retreat	RMUtrecht	2018	0.5
-	Workshop transferable skills	TBNBT Valladolid, Spain	2015	1
-	Workshop hydrogel synthesis	CERTH, Thessaloniki, Greece	2015	1
-	Mechanical characterization	RU, Nijmegen, Netherlands	2016	1
-	Biomimetic hydrogels	UVa, Valladolid, Spain	2016	1
-	Summerschool: transferable skills	CERTH, Thessaloniki, Greece	2017	3
-	Workshop coatings and sensors	NovioSense, Nijmegen, Netherlands	2017	1
-	Workshop *in vitro*, *ex vivo*, and *in vivo* models	DWI, RWTH Aachen, Germany	2017	2
-	Workshop Imaging	AIT, Vienna, Austria	2018	1

		Organising Institute	Year	Work-load (ECTS)
-	International BIOGEL conference	DWI, RWTH Aachen, Germany	2018	1
-	Course: Performance Skills: Master Class	TU/e, Eindhoven, Netherlands	2016	1
-	Course: Scientific Writing	TU/e, Eindhoven, Netherlands	2017	1
-	Course: Entrepreneurship	RWTH Aachen, Germany	2018	1

2. Conferences and presentations

-	Karman Conference	DWI, RWTH Aachen, Germany	2015	1
-	Hydrozones Workshop	LifeTec Group, Eindhoven, Netherlands	2015	1
-	NBTE Annual Meeting	NBTE	2015	1
-	Ambassador Day	RU, Nijmegen, Netherlands	2016	1
-	Dutch liver retreat	NVH	2016	1
-	Deutsche Arbeitsgemeinschaft zum Studium der	GASL	2017	1

		Organising Institute	Year	Work-load (ECTS)
	Leber Jahrestagung 2017			
-	Research Day Biomedical Engineering	TU/e, Eindhoven, Netherlands	2017	1
		TOTAL		**34.5**

3. Supervision of research projects

-	Supervision graduate student Dave Wanders "Optimization and validation of mechanical loading and test system"	LifeTecGroup/ TU/e Eindhoven	2016	2
-	Supervision of graduate student Sharon Linders "Extending *ex vivo* liver culture with normothermic machine perfusion"	LifeTecGroup/ TU/e Eindhoven	2019	2
-	Partial supervision of PhD student Alicia Ruppelt "Maintaining liver functionality *ex vivo:* from platform design to application"	LifeTecGroup/ Politecnico di Milano	2020	2
		TOTAL		**40.5**